

# ASHRAE Research Project Report

## 1458-RP

### Modeling Person-to-Person Contaminant Transport in Mechanical Ventilation Space

**Approval:** January 2014

**Contractor:** Building Energy and Environment Engineering LLP  
Lafayette, IN 47905-7600

**Principal Investigator:** Zheng Jiang  
**Authors:** Qingyan Chen

Author Affiliations, Purdue University

**Sponsoring Committee:** TC 4.10 (Indoor Environmental Modeling)

**Co-Sponsoring Committee:** N/A

**Co-Sponsoring Organizations:** N/A



Shaping Tomorrow's  
Built Environment Today

## **ASHRAE Research Project (RP-1458)**

### **Executive Summary**

It is essential to investigate person-to-person contaminant transport in enclosed environments to improve air distribution design and reduce the infection risk from airborne infectious diseases. The objective of this ASHRAE research was to develop various models for quickly predicting person-to-person contaminant transport in enclosed environments and to investigate the effect of different ventilation factors on the contaminant transport. The research scope and main findings can be summarized as follows:

- (1). This investigation first conducted a literature review on modeling person-to-person contaminant transport in enclosed environments. By collecting available literature on physical and biological emission data from human with different activities, this study critically reviewed different modeling methods for predicting person-to-person contaminant transport in enclosed environments. The investigation has identified several major problems which were solved later in this project.
- (2). This study developed a hybrid DES-Lagrangian and RANS-Eulerian model for investigating transient particle transport in enclosed environments, which can ensure accuracy and reduce computing costs for predicting particle transport. This study proposed and verified the estimation methods of two key time constants for the model. This investigation also conducted experimental measurements in the first-class cabin of an MD-82 aircraft cabin to validate the hybrid model, which was found to be reasonably accurate.
- (3). This research developed a combined CFD and Markov chain method for predicting transient particle transport in enclosed environments, which can provide faster-than-real-time information. The method first calculated a transition probability matrix using CFD simulations. Next, the Markov chain technique was applied to calculate the transient particle concentration distributions. The method was validated by three experimental measurement cases and the simulated results agree with the measured data.
- (4). This research conducted a systematic study of the effects of ventilation mode, ventilation rate, and person-to-person distance on person-to-person contaminant transport in enclosed environments. The study was completed by developing a database with a large amount of cases from the literature and with additional CFD simulations. The investigation found that person-to-person distance was more important than ventilation mode and ventilation rate in controlling person-to-person contaminant transport.
- (5). This research further developed simplified models for predicting the airflow from a cough with the mouth covered. By using smoke to visualize the airflow exhaled by 16 human subjects, the flow characteristics was identified when their mouths were covered by a tissue, a cupped hand, a fist, and an elbow with and without a sleeve. With the models, this investigation can perform numerical simulations to assess the influence of mouth coverings on the receptor's exposure to exhaled airflow.

# **MODELING PERSON-TO-PERSON CONTAMINANT TRANSPORT IN A MECHANICAL VENTILATION SPACE**

Final Report Submitted to

ASHRAE  
1791 Tullie Circle, NE  
Atlanta, GA 30329

For

ASHRAE Research Project (RP-1458)

Principal Investigators: Zheng Jiang and Qingyan Chen  
Research Assistant: Chun Chen

Building Energy and Environment Engineering LLP  
1401 Castle Dr, Lafayette, IN 47905-7600  
Phone: (450)465-6561, Email: [zjjane@gmail.com](mailto:zjjane@gmail.com)

And

School of Mechanical Engineering, Purdue University  
585 Purdue Mall, West Lafayette, IN 47907-2088  
Phone: (765)496-7562, Email: [yanchen@purdue.edu](mailto:yanchen@purdue.edu)

October 30, 2013

## ABSTRACT

It is essential to investigate person-to-person contaminant transport in enclosed environments to improve air distribution design and reduce the infection risk from airborne infectious diseases. This study aims to develop various models for quickly predicting person-to-person contaminant transport in enclosed environments and investigate the effect of influencing factors on the contaminant transport.

Firstly, this study introduces a hybrid DES-Lagrangian and RANS-Eulerian model for simulating transient particle transport in enclosed environments; this hybrid model can ensure the accuracy and reduce the computing cost. Our investigation estimated two key time constants for the model that are important parameters for reducing the computing costs. The two time constants estimated were verified by airflow data from both an office and an aircraft cabin case. This study also conducted experiments in the first-class cabin of an MD-82 commercial airliner with heated manikins to validate the hybrid model. A pulse particle source was applied at the mouth of an index manikin to simulate a cough. The particle concentrations versus time were measured at the breathing zone of the other manikins. The trend of particle concentrations versus time predicted by the hybrid model agrees with the experimental data. The proposed hybrid DES-Lagrangian and RANS-Eulerian model can be used for investigating transient particle transport in enclosed environments with relatively high accuracy, while the computing time can be reduced by 80%.

This study further developed a combined Computational Fluid Dynamics (CFD) and Markov chain method for quickly predicting transient particle transport in enclosed environments. The method first calculated a transition probability matrix using CFD simulations. Next, the Markov chain technique was applied to calculate the transient particle concentration distributions. This investigation used three cases, particle transport in an isothermal clean room, an office with an Under-Floor Air-Distribution (UFAD) system, and the first-class cabin of an MD-82 airliner, to validate the combined CFD and Markov chain method. The general trends of the particle concentrations versus time predicted by the Markov chain method agreed with the CFD simulations for these cases. The proposed Markov chain method can provide faster-than-real-time information about particle transport in enclosed environments. Furthermore, for a fixed airflow field, when the source location is changed, the Markov chain method can be used to avoid recalculation of the particle transport equation and thus reduce computing costs.

In addition, this study investigated the effect of influencing factors on person-to-person contaminant transport in enclosed environments. This study first collected available cases of person-to-person contaminant transport from the literature to create a database. Then this investigation identified the limitations of the existing data and added a number of cases to complete the database. The additional cases were generated by using a RANS-Eulerian model that was validated by experimental data from an occupied office with under-floor air-distribution (UFAD) systems. The database shows that the overall performance of displacement ventilation and the UFAD systems was better than that of mixing ventilation. A higher ventilation rate was beneficial in reducing person-to-person contaminant transport to some extent. Person-to-person contaminant exposure increased rapidly with a decrease in person-to-person distance when the

distance was smaller than 1.1 m. Generally speaking, person-to-person distance is an important parameter when compared with ventilation mode and ventilation rate.

Finally, this study developed simplified models for predicting the airflow by a cough with a mouth covering. This investigation firstly conducted smoke tests to visualize exhaled airflow by a cough with a mouth covering by 16 human subjects. Then this study developed and verified simplified models for predicting the airflow by a cough with a mouth covering based on the experimental data. It was found that covering a cough with a tissue, a cupped hand and an elbow can significantly reduce the horizontal velocity and make the droplets move upward with the human thermal plume. Furthermore, covering a cough or turning head can avoid the receptor's direct exposure at the first stage. In term of inhaled dose, it is reasonable to use the zero momentum assumption for covering a cough with a mouth covering. In addition, based on the available emission data in the literature and theoretical analysis, the mouth coverings can remove about 60% of total number of coughed droplets.

The models developed in this study can be used for quickly predicting person-to-person contaminant transport in enclosed environments. The correlations between the influencing factors and person-to-person contaminant transport can be used as general guidance on how to design ventilation systems to minimize inter-personal infection in a mechanically ventilated space.

## TABLE OF CONTENTS

	Page
ABSTRACT.....	ii
1. INTRODUCTION.....	1
1.1 Background and significance .....	1
1.2 Objectives.....	2
1.3 Outline of this report .....	4
2. LITERATURE REVIEW .....	6
2.1 Emission data from humans with different activities.....	6
2.1.1 Exhaled airflow .....	6
2.1.2 Droplet size distribution and concentration .....	9
2.1.3 Evaporation of droplets.....	15
2.1.4 Virus in droplets.....	15
2.2 Modeling person-to-person contaminant transport in enclosed spaces.....	16
2.3 Influencing factors on person-to-person contaminant transport .....	19
2.4 Effectiveness of a mouth covering.....	19
3. A HYBRID MODEL FOR PREDICTING TRANSIENT PARTICLE TRANSPORT .....	22
3.1 Model Determination .....	22
3.1.1 Steady-state airflow conditions.....	22
3.1.2 Unsteady-state airflow conditions.....	23
3.1.3 Calculation procedure .....	25
3.2 Verification of the Two Time Constants Used in the Hybrid Model.....	29
3.2.1 Verification of $t_1$ .....	29
3.2.2 Verification of $t_2$ .....	32
3.3 Validation of the Hybrid Model.....	34

3.3.1	Experimental setup.....	34
3.3.2	Validation.....	36
3.4	Discussion .....	39
3.5	Conclusions .....	40
4.	A COMBINED CFD AND MARKOV CHAIN METHOD FOR PREDICTING TRANSIENT PARTICLE TRANSPORT .....	41
4.1	Development of the Method.....	41
4.1.1	Markov chain model .....	41
4.1.2	Calculating the transition probability matrix using CFD.....	43
4.2	Validation .....	44
4.2.1	Particle transport in an isothermal clean room .....	44
4.2.2	Particle transport in a room with a UFAD system.....	47
4.2.3	Particle transport in an MD-82 aircraft cabin .....	51
4.3	Discussion .....	54
4.4	Conclusions .....	57
5.	SYSTEMATIC STUDY OF PERSON-TO-PERSON CONTAMINANT TRANSPORT ...	58
5.1	Methods.....	58
5.1.1	Developing a database from the literature .....	58
5.1.2	Adding necessary cases to the database.....	59
5.1.3	Obtaining person-to-person contaminant exposure data.....	60
5.2	Validation of the CFD Model.....	62
5.3	Results .....	66
5.3.1	Effect of ventilation mode .....	66
5.3.2	Effect of ventilation rate .....	67
5.3.3	Effect of person-to-person distance .....	69
5.4	Discussion .....	70
5.5	Conclusions .....	71

6.	SIMPLIFIED MODELS FOR PREDICTING THE EXHALED AIRFLOW BY A COUGH WITH A MOUTH COVERING.....	72
6.1	Visualization of exhaled airflow by a cough with a mouth covering.....	72
6.1.1	Experimental methods .....	72
6.1.2	Characterizing exhaled airflow by a cough with a mouth covering .....	72
6.2	Simplified models for the airflow by a cough with a mouth covering.....	78
6.2.1	Methods for determining the jet velocity, direction and flow ratio .....	78
6.2.2	Verification of the jet velocity .....	79
6.2.3	Results of the jet velocity, direction and flow ratio .....	80
6.2.4	Simplified models .....	82
6.3	Model verification and case study.....	82
6.3.1	Case setup .....	83
6.3.2	Simulation models .....	83
6.3.3	Verification of the simplified models .....	84
6.3.4	Influence of mouth coverings on droplet dispersion and receptor's exposure.....	85
6.3.5	Influence of turning head on receptor's exposure.....	87
6.3.6	Possibility in further simplifying the model .....	89
6.4	Estimation of droplet removal by mouth coverings.....	90
6.4.1	Droplet removal due to diffusion and gravitational settling .....	90
6.4.2	Droplet removal due to inertial impaction.....	90
6.5	Conclusions .....	92
7.	CONCLUSIONS AND FUTURE DIRECTION .....	93
7.1	Conclusions .....	93
7.2	Future direction .....	94
	REFERENCES .....	95

# 1. INTRODUCTION

## 1.1 Background and significance

Researchers from both the medical and engineering disciplines have been collectively addressing the issue of transmission of airborne infectious diseases (Mangili and Gendreau, 2005). Airborne infectious diseases include cold, influenza, avian flu, tuberculosis (TB) and Severe Acute Respiratory Syndrome (SARS). Viboud et al. (2004) reported that about 47,200 deaths were caused by influenza epidemics every year in the United States. The Spanish flu of 1918-19 (H1N1) was found as the most lethal flu pandemic of the 20th century, which infected about one-quarter of the global population and killed more than 40 million people (WHO, 2002). The World Bank (2005) concluded that a pandemic of avian flu among humans could cost the global economy \$800 billion a year. The evaluation of the global burden of TB showed that TB infections were found in about 22 countries and cause a total of 1.87 million deaths (Dye et al., 1999). The World Health Organization (WHO) (2002) reported that there were 8098 people all over the world infected by SARS and 774 of them lost their lives. These airborne diseases cause endless social and economic disruptions. Thus, it is important to understand and control the transmission of airborne disease to reduce its influence on human health.

Enclosed spaces such as buildings and transport vehicles are more susceptible to the transmission of airborne infectious diseases than the outdoors due to the low air exchange rate (Mangili and Gendreau, 2005). For instance, among enclosed spaces, a greater risk of infection is possible in aircraft cabins due to the high occupant density and long exposure time. Some of the outbreaks of TB (Kenyon et al., 1996), influenza (Moser et al., 1979), SARS (Olsen et al., 2003), and norovirus transmission (Kirking et al., 2010) are alleged to have happened during air travel. The swine flu epidemic in 2009 also created a panic among air travelers and caught the attention of researchers (Khan et al., 2010). These transmissions could have happened through direct contact, indirect contact, droplets or airborne route. The infection spread to rows away from the infected person indicated the transmission to these places may have happened through airborne route (Olsen et al., 2003 and Kirking et al., 2010). Due to the rapidly growing number of air passengers (800 million air passengers in 2010, US DOT 2011), the transmission of airborne infectious diseases in aircraft cabins becomes more and more important. Furthermore, people spend roughly 90% of their life time indoors (Klepeis et al., 2001). Thus, it is essential to predict and control the transmission of airborne infectious disease in enclosed environments.

The airborne disease transmission process starts from droplets carrying the infectious agents. These droplets are exhaled by an infected person through various respiratory exhalations (Cole and Cook, 1998). They then disperse in the enclosed environment and can be inhaled by susceptible fellow occupants. The droplet dispersion depends on the airflow in the enclosed environment and the exhalation process. The airflow in enclosed environments is normally not uniform (Chen, 2009). The pulse release of infectious agents by the index passenger through coughing, breathing, or talking exhalations is transient (Gupta et al., 2009 and 2010). Therefore, the expiratory droplet distribution and the risk of infection in enclosed environments are inhomogeneous and temporal.

To predict such complex airborne infectious diseases transmission, the computational methods are widely used since they are inexpensive, fast and flexible. The main computational methods include well-mixed model, multi-zone models, and computational fluid dynamics (CFD). Walkinshaw (2010) predicted the risk of infection from influenza in an aircraft cabin. He quantified the amount of influenza virus ribonucleic (RNA) particles inhaled by the passengers assuming perfectly mixed and transient conditions. Ko et al. (2004) and Jones et al. (2009) used multi-zone models to quantify the risks based on the dose response model under steady and unsteady scenarios, respectively. In recent years, CFD has been widely used in modeling person-to-person contaminant transport in enclosed environments, since it can provide more detailed and accurate information than well-mixed and multi-zone models. For instance, Wan et al. (2009) performed detailed steady-state CFD simulations and quantified the risk of infection from influenza in an aircraft cabin. Gupta et al. (2011) investigated a fully occupied seven-row section of a twin aisle cabin for the transmission of expiratory droplets using the CFD simulations. The transport of droplets exhaled from the coughing, breathing and talking of the infected passenger was studied. Detailed boundary conditions for the coughing, breathing and talking flow were used in the simulation. Thus, the CFD models can effectively predict airborne contaminant transport in commercial aircraft cabins and associated non-uniformities. However, current CFD simulations are very time consuming. For example, the simulation of the temporal distributions of expiratory droplets in a fully occupied seven-row section of a twin aisle cabin for four minutes of real time by Gupta et al. (2011) took four weeks of computational time on an 8-parallel-processor computer cluster (total of two 2.33 GHz Quad-Core Intel processors and 16 GB memory). Thus, it is necessary to develop methods to quickly predict person-to-person contaminant transport in enclosed environments.

Understanding how the influencing factors affect the person-to-person contaminant transport is essential for controlling the transmission of airborne infectious diseases. Ventilation mode, ventilation rate, and person-to-person distance are among the factors that may influence person-to-person contaminant transport in enclosed spaces. A number of studies have focused on these influencing factors. The first factor, ventilation mode, was investigated by Qian et al. (2006), Lai and Wong (2010, 2011), Yin et al. (2011) and Olmedo et al. (2012). However, fewer studies are available in the literature for another commonly used ventilation mode, the Under-Floor Air-Distribution (UFAD) system (He et al., 2011; Li et al., 2011). The second factor, ventilation rate, was studied by Qian et al. (2006), Nielsen et al. (2010) and Yin et al. (2011). However, in most of these cases, the patients were lying in beds, which may not be representative of normal scenarios such as working in an office. The third factor, person-to-person distance, was investigated by Qian et al. (2006) and Olmedo et al. (2012). However, the effect of person-to-person distance on exhaled contaminant transport under high ventilation rates has not been well understood. Therefore, additional cases of person-to-person contaminant transport are needed to in order to address the limitations discussed above.

## 1.2 Objectives

To identify the appropriate CFD models for predicting particle transport, Wang et al. (2012) tested different combinations of the airflow and particle models for steady- and unsteady-state cases. For steady-state airflow conditions, they preferred the RANS model with the Eulerian method due to its reasonable accuracy and low computing cost. For unsteady-state airflow

conditions, Wang et al. recommended the DES model with the Lagrangian method due to its relatively high accuracy. However, if the DES with Lagrangian model is applied for studying the whole period of transient exhaled particle transport by coughing, sneezing, or talking among persons, it requires considerable computing cost. It should be noticed that coughing, sneezing, or talking may have a significant impact on airflow distribution only in the first few seconds. But after the effect of the coughing, talking, and sneezing on the airflow is damped, the airflow can be regarded as steady-state. Then RANS with the Eulerian model can be applied to reduce the computing cost (Wang et al., 2012). Thus, this study develops a hybrid DES-Lagrangian and RANS-Eulerian model for simulating transient particle transport in enclosed environments, which can ensure the accuracy and reduce the computing cost.

Although CFD models have been widely used, when the source location is changed, even for a fixed airflow field, all of these models require recalculation of the particle equations, which requires considerable computing effort. Moreover, CFD models may not be able to provide fast-than-real-time information of particle transport, which is extremely important for controlling emergent infectious disease transmissions. Thus, it is worthwhile to develop an approach that can solve this problem. Nicas (2000) has demonstrated the capability of the combined multi-zone model and Markov chain method in providing fast-than-real-time information of spatial and temporal particle concentrations. However, the multi-zone model cannot account for most of the particle dispersion mechanisms such as drag force, gravitational settling, and turbulent dispersion, which can be easily modeled by CFD simulation. Thus, this study develops a combination of CFD with the Markov chain technique to provide more accurate and fast-than-real-time information of spatial and temporal particle concentrations.

Furthermore, it is important to fully understand the effect of major influencing factors on person-to-person contaminant transport in mechanically ventilated spaces. Thus, this study provides a systematic study of the effects of ventilation mode, ventilation rate, and person-to-person distance on person-to-person contaminant transport. This study first collected available cases of person-to-person contaminant transport from the literature to create a database. Then this investigation identified the limitations of the existing data and added a number of cases to complete the database. The additional cases were generated by using a RANS-Eulerian model that was validated by experimental data from an occupied office with under-floor air-distribution (UFAD) systems. Then, influence of ventilation mode, ventilation rate and person-to-person distance was investigated.

It should be noticed that most people attempt to cover their mouth with their hand or a tissue when they cough or sneeze. Moreover, ill people may wear masks to reduce the possibility of transmitting infectious diseases to others. For masks which are equipped with filters that can purify the air passing through, there are numerous studies focusing on the effectiveness of masks on removing exhaled droplets. For example, Gupta (2010) conducted a systematic review on the performance of N95 masks on removing exhaled droplets and concluded that the penetration rate including the face seal leakages to be 10%. In addition to the removal of exhaled droplets, mouth coverings can also reduce the horizontal transport of exhaled air. Tang et al. (2009) roughly visualized the exhaled airflow by a cough with various mouth coverings, including covering with a tissue, cupped hand, fist, surgical mask and N95 mask. The existing studies provided some ideas of the characteristics of exhaled airflow by a cough with mouth covering. However, there

are no valid approaches for modeling mouth covering available in the literature. Since coughing with mouth covering is quite common in civilized societies, it is critical to develop a valid modeling approach for mouth covering when investigating person-to-person contaminant transport in enclosed environments. This study conducts smoke tests to visualize the exhaled airflow by a cough with a mouth covering by 16 human subjects. Based on the experimental results, this investigation then develops simplified models for predicting the airflow by a cough with a mouth covering.

### **1.3 Outline of this report**

To achieve these objectives, this study has performed five tasks corresponding to the following chapters:

#### Chapter 2 (Task 1): Literature review

Chapter 2 presents a literature review on modeling person-to-person contaminant transport in enclosed environments. The review firstly collects the available literature on physical and biological emission data from human with different activities. Then this chapter discusses the available literature on the modeling methods applied for predicting person-to-person contaminant transport in various enclosed environments and identifies the major problems of the current studies. The final part of the review explores the effectiveness of mouth coverings on reducing person-to-person contaminant transport as well as the existing modeling approaches for mouth coverings.

#### Chapter 3 (Task 2): A hybrid DES-Lagrangian and RANS-Eulerian model

Chapter 3 presents a hybrid DES-Lagrangian and RANS-Eulerian model for investigating transient particle transport in enclosed environments, which can ensure the accuracy and reduce the computing cost. Then, the estimation methods of two key time constants for the model and their verifications are discussed. Finally, the validation of the hybrid model by the experimental measurements in the first-class cabin of an MD-82 aircraft cabin is presented.

#### Chapter 4 (Task 3): A combined CFD and Markov chain method

Chapter 4 presents a combined CFD and Markov chain method for predicting transient particle transport in enclosed environments, which can provide faster-than-real-time information. The validation of the method by three experimental measurement cases is then discussed.

#### Chapter 5 (Task 4): Systematic study on person-to-person contaminant transport

Chapter 5 provides a systematic study of the effects of ventilation mode, ventilation rate, and person-to-person distance on person-to-person contaminant transport. This study first developed a database with a large amount of cases from the literature as well as additional CFD simulations. Based on the database, influence of ventilation mode, ventilation rate and person-to-person distance was investigated.

#### Chapter 6 (Task 5): Simplified models for a cough with a mouth covering

Chapter 6 presents simplified models for predicting the airflow by a cough with a mouth covering. Firstly, the visualizations of exhaled airflow by a cough with a mouth covering are presented. Then, simplified models for predicting the airflow by a cough with a mouth covering is developed. Finally, the influence of mouth coverings on the dispersion of coughed droplets and receptor's exposure was discussed.

#### Chapter 7: Conclusions

Chapter 7 summarizes the major findings of this investigation.

## 2. LITERATURE REVIEW

This chapter firstly collects the available literature on physical and biological emission data from human with different activities. Then, this chapter reviews the available literature on modeling methods applied for predicting person-to-person contaminant transport in various enclosed environments. Moreover, the major problems of current studies are identified. The final part of the review explores the effectiveness of mouth covering on controlling person-to-person contaminant transport as well as the existing modeling approaches for mouth coverings.

### 2.1 Emission data from humans with different activities

#### 2.1.1 Exhaled airflow

##### 2.1.1.1. Cough

There are several parameters that can be used to characterize cough flow rate, such as Cough Peak Flow Rate (CPFR), Cough Expired Volume (CEV), and Peak Velocity Time (PVT). Mahajan et al. (1994) used 10 subjects to perform voluntary cough manoeuvres, and the CPFR, PVT and CEV were measured during each manoeuvre. They found highly significant correlations between CPFR and PVT, CPFR and CEV, and PVT and CEV. Zhu et al. (2006) measured the total cough expired volume to be in the range of 0.8 to 2.2 liters with an average of 1.4 liters. However, Mahajan et al. (1994) observed a variation of up to 5 liters with an average of about 3 liters, which was higher compared to the results by Zhu et al. (2006). Recently, Chao et al. (2009) used Particle Image Velocimetry (PIV) to capture and visualize the flow field of a cough. Although these studies provided some information on coughs, the dynamics of the cough profile has not been quantified. Without this information, the boundary conditions in computational fluid dynamics (CFD) modeling of person-to-person contaminant transport are incomplete.

Gupta et al. (2009) used 25 human subjects to measure flow rates, flow directions, and mouth opening areas of coughs. A spirometer was used to measure the flow rates versus time with a frequency of 330 Hz. The flow directions were visualized using cigarette smoke as seeding fluid through moderate-speed photography (120Hz) with 1 Mega Pixel resolution. Figure 2-1 shows the cough flow rates versus time for the 25 subjects. It was found that the mouth opening area was almost constant to be  $4.00 \text{ cm}^2$  for males and  $3.37 \text{ cm}^2$  for females. The flow direction did not vary substantially among the subjects and can be determined by two angles as shown in Figure 2-2. The average  $\theta_1$  and  $\theta_2$  was  $15^\circ$  and  $40^\circ$ , respectively. The information provided in this paper can be used as boundary conditions in modeling coughing cases.

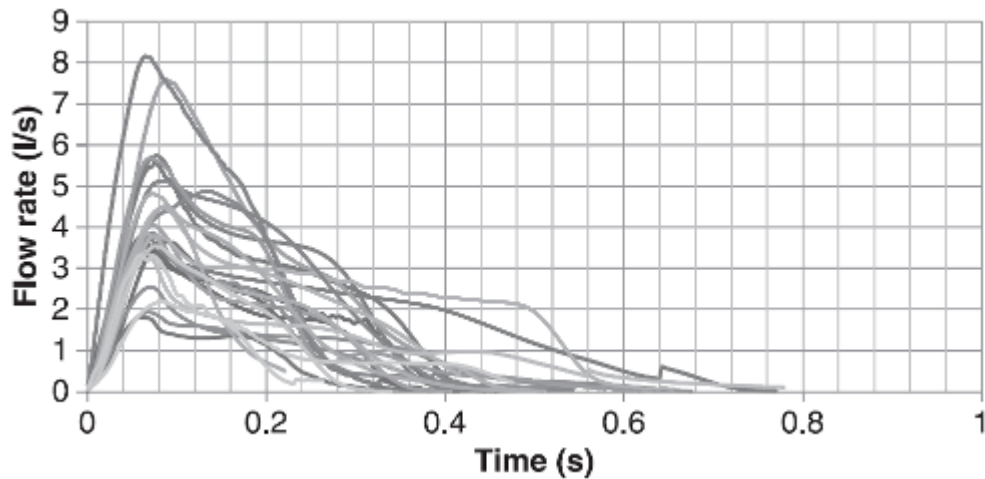


Figure 2-1 Cough flow rates for the 25 subjects (Gupta et al., 2009).

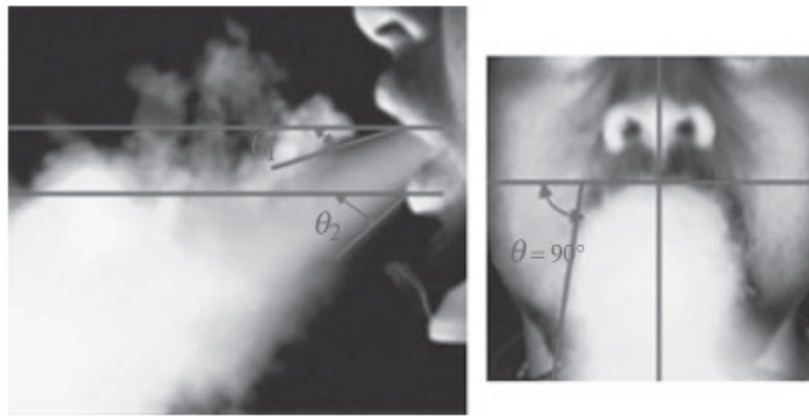


Figure 2-2 Cough jet direction from the side and front views (Gupta et al., 2009).

#### 2.1.1.2. Breath

Gupta et al. (2010) used the same approach to that used in measuring coughs to characterize flow rates, flow directions, and mouth opening areas of breaths. Figure 2-3 shows the breath flow rates versus time for a subject. It can be seen that a sine wave can represent the normal breathing flow rate versus time. It was found that the average nose opening area during breathing was  $0.71 \text{ cm}^2$  for males and  $0.56 \text{ cm}^2$  for females, respectively. For mouth opening, the average area during breathing was  $1.20 \text{ cm}^2$  for males and  $1.16 \text{ cm}^2$  for females, respectively. The flow direction from the nose can be determined by four angles as shown in Figure 2-4. The average  $\theta_m$ ,  $\phi_m$ ,  $\theta_s$  and  $\phi_s$  was  $60^\circ$ ,  $69^\circ$ ,  $23^\circ$ , and  $21^\circ$ , respectively. Figure 2-5 shows a mouth breathing jet which was discharged in the horizontal direction with a spreading angle of  $30^\circ$ . The information can be used as boundary conditions in modeling breathing cases.

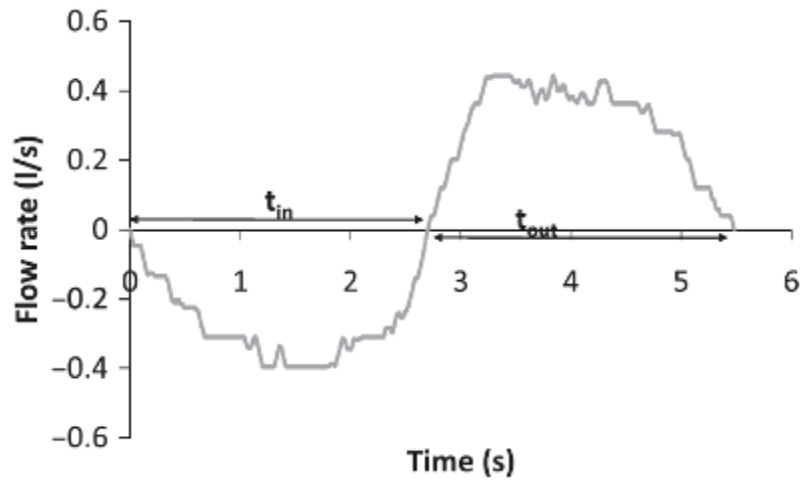


Figure 2-3 Flow generated over time for a subject for normal breathing (Gupta et al., 2010).

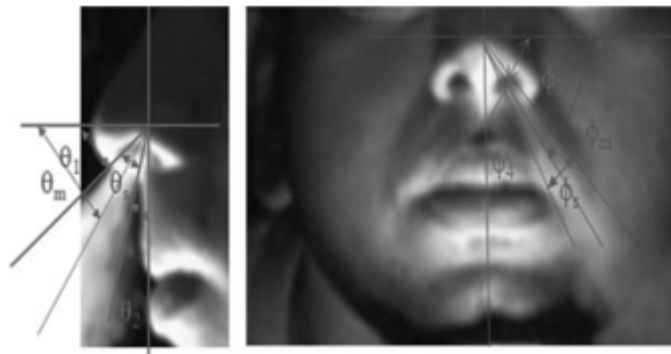


Figure 2-4 Angles needed to define the direction of a nose breathing jet (Gupta et al., 2010).

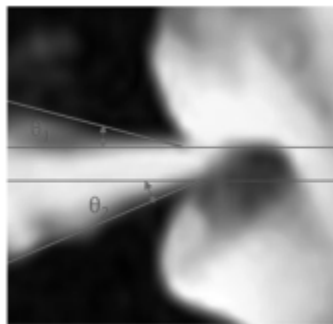


Figure 2-5 Visualization of a mouth breathing jet (Gupta et al., 2010).

### 2.1.1.3. Talk

Applying the same approach to the above, Gupta et al. (2010) characterized flow rates and mouth opening areas when the subjects were talking. Figure 2-6 shows the flow rates versus time when

the subjects were talking. It can be seen that the flow rate versus time was irregular. By integrating the positive and negative flow rates over time, the exhaled and inhaled volume was obtained. Most of the exhalation took place through mouth, while most of the inhalation took place from the nose. The total volume exhaled/inhaled during talking was about 27 liters in 2 minutes. It was found that the average nose opening area during talking was  $1.8 \text{ cm}^2$  for males and females. The information can be used as boundary conditions in modeling talking cases.

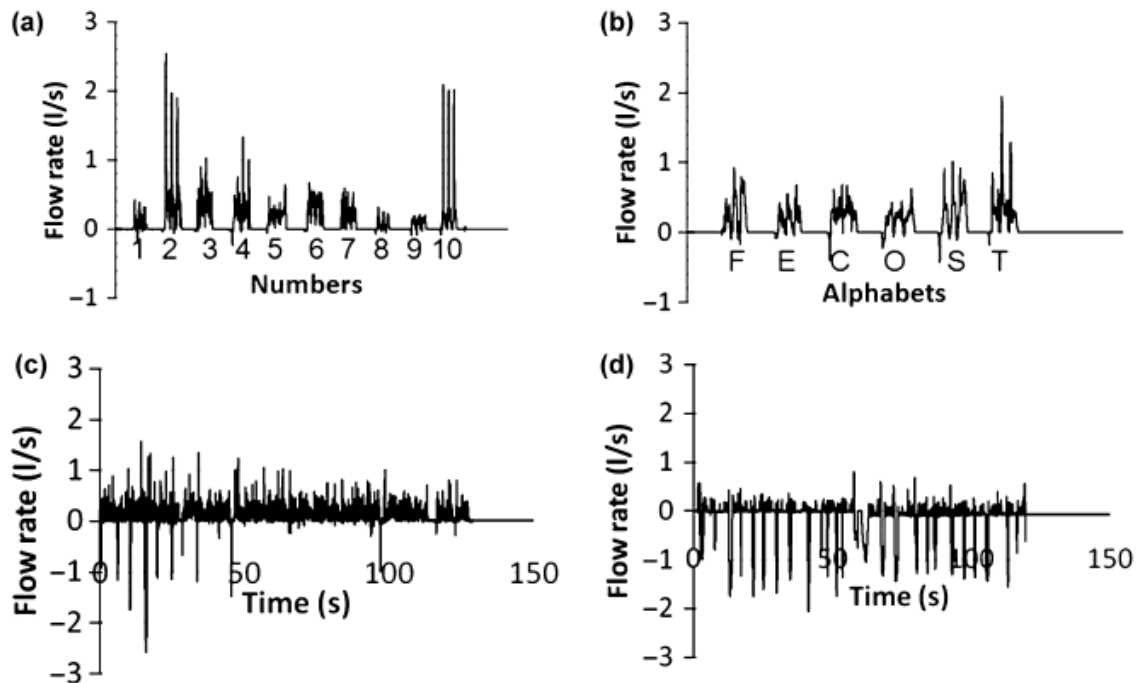


Figure 2-6 Flow rate measured for a subject: (a) from the mouth by counting the numbers three times consecutively, (b) from the mouth by pronouncing the alphabets three times consecutively, (c) from the mouth for reading the passage, and (d) from the nose for reading the passage (Gupta et al., 2010).

## 2.1.2 Droplet size distribution and concentration

### 2.1.2.1. Cough

There have been a number of studies and excellent reviews (Nicas et al., 2005; Morawska, 2006) on the size distribution of coughed droplets. Early studies suggested that the majority of droplets generated through coughs are in the super-micrometer size (Duguid, 1945; Loudon and Roberts, 1967). Chao et al. (2009) also reported that the coughed droplets in close proximity to the mouths are in the super-micrometer size. Yang et al. (2007) reported that droplet size spans from  $0.6$  to  $16 \mu\text{m}$ , with the average at  $8.35 \mu\text{m}$  during coughing. However, some other studies

indicated that the majority of coughed droplets are within the sub-micrometer size range (Papineni and Rosenthal, 1997; Morawska et al., 2009). The discrepancy of these studies on the size distribution of droplets is more because of the instrument and measurement methodology (Chen and Zhao, 2010). Table 2-1 summarizes the representative diameter, concentration, measurement technique and limitations of the previous studies. It can be found that the studies before 2009 had certain limitations including not considering the effect of evaporation, nucleation and water partitioning onto sample media. Furthermore, when using microscopic technique after collection of droplets on a media, the sub-micrometer droplets cannot be captured. On the other hand, when using modern aerodynamic particle sizers, the accuracy of super-micrometer droplets is a major issue. Considering the measurement accuracy, the size distribution and concentration of sub-micrometer droplets measured by Morawska et al. (2009) tends to be the most reliable. The representative diameter is less than  $0.8 \mu\text{m}$  and the average total number concentration for sub-micrometer droplets is  $0.64 \text{ cm}^{-3}$ . For super-micrometer droplets, the size distribution measured by Chao et al. (2009) tends to be the most reliable. The results show that the geometric mean diameter of super-micrometer droplets by coughs is  $13.5 \mu\text{m}$ . Although their technique cannot measure the actual concentrations, they roughly estimated the droplet concentration using four different methods based on some unverified assumptions. The first method was to convert the size-dependent droplet numbers measured by Duguid (1946) to the total volume of droplets. Then the total volume of droplets and the size distribution were used to estimate the concentrations. The second method was analogous to the first one but using the data by Loudon and Roberts (1967). The third method was to directly use the total volume of droplets reported by Zhu et al. (2006). The fourth method was to divide the total number of droplets captured by the total laser measurement volume. However, they acknowledged that significant uncertainties existed for all the methods. Figure 2-7 shows the combination of the size distribution obtained by Morawska et al. (2009) and Chao et al. (2009) (the first method in their study) for the entire size range. There are two peaks in the size distribution for the entire size range. The total concentration including sub-micrometer and super-micrometer droplets is  $2.91 \text{ cm}^{-3}$ . It should be noticed that the considerable uncertainty in the concentration of super-micrometer droplets may lead to significant error of the size distribution for the entire size range.

Table 2-1 Summary of the previous studies on coughed droplets.

Reference	Representative diameter ( $\mu\text{m}$ )	Concen. ( $\text{cm}^{-3}$ )	Technique	Limitations
Duguid (1946)	14	$5^a$	Count of large droplets using microscopy after collection on a slide	Sampling losses for submicron droplets, evaporation, nucleation, water partitioning NOT considered
Loudon & Roberts (1967)	12	$0.47^a$	Count of large droplets using microscopy after collection on a filter	Sampling losses for submicron droplets, evaporation, nucleation,

				water partitioning NOT considered
Fairchild & Stamper (1987)		0.6	Sample aerosol from a respirator mask using a laser aerosol spectrometer	Sampling losses for submicron droplets, evaporation, nucleation, water partitioning NOT considered
Papineni & Rosenthal (1997)	<0.6	0.024–0.22	A subject coughed into a funnel connected to an OPC <sup>b</sup>	Sampling losses for supermicron droplets, evaporation, nucleation NOT considered
Yang et al. (2007)	8.35	881–2355	Measure size distribution and concentration using APS <sup>c</sup> after collection in an air bag	Sampling losses for supermicron droplets, evaporation, nucleation, water partitioning NOT considered
Chao et al. (2009)	13.5	2.368–5.212 <sup>d</sup>	Measure size distribution immediately at mouth opening using IMI <sup>e</sup>	Sampling losses for submicron droplets NOT considered
Morawska et al. (2009)	<0.8	0.64	Measure size distribution and concentration using APS immediately at the mouth opening	Sampling losses for supermicron droplets NOT considered

<sup>a</sup> Assuming the Cough Expired Volume (CEV) to 1.0 L (Gupta et al., 2009)

<sup>b</sup> OPC: Optical Particle Counter

<sup>c</sup> APS: Aerodynamic Particle Sizer

<sup>d</sup> Concentration estimated based on four different methods

<sup>e</sup> IMI: Interferometric Mie Imaging

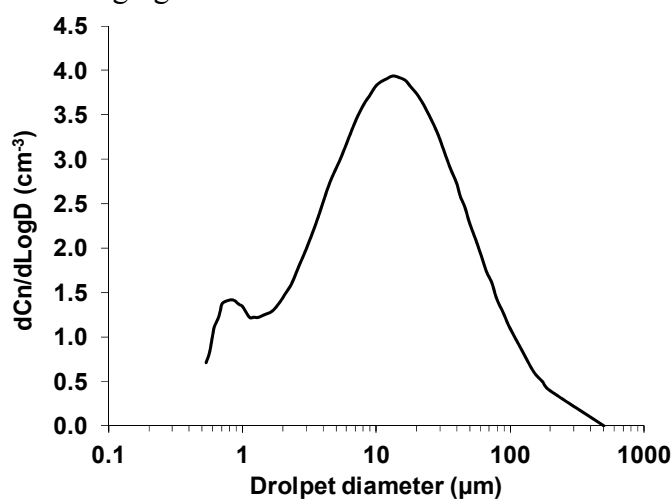


Figure 2-7 Size distribution and concentration of coughed droplets combined from Morawska et al. (2009) and Chao et al. (2009) (the first method in their study).

### 2.1.2.2. Breath

Most of the previous studies suggested that the exhaled droplets through normal breathing are in the sub-micrometer size. Table 2-2 summarizes the representative diameter, concentration, measurement technique and limitations of the previous studies on breathing droplets. Considering the measurement accuracy, the size distribution and concentration of breathed droplets measured by Morawska et al. (2009) tends to be the most reliable, as shown in Figure 2-8. The representative diameter is less than 0.8  $\mu\text{m}$  and the average total number concentration of breathed droplets is 0.092  $\text{cm}^{-3}$ .

Table 2-2 Summary of the previous studies on breathed droplets.

Reference	Representative diameter ( $\mu\text{m}$ )	Concen. ( $\text{cm}^{-3}$ )	Technique	Limitations
Fairchild & Stamper (1987)		0.1	Sample aerosol from a respirator mask using a laser aerosol spectrometer	Evaporation, nucleation, water partitioning NOT considered
Papineni & Rosenthal (1997)	<0.6	0.0027–0.033	A subject breathed into a funnel connected to an OPC <sup>a</sup>	Evaporation, nucleation NOT considered
Edwards et al. (2004)		0.014–0.32	Subjects breathed into a pneumotachograph connected to an OPC <sup>a</sup>	Evaporation, nucleation NOT considered
Fabian et al. (2008)	0.3–0.5	0.724	Measure size distribution and concentration using an OPC <sup>a</sup> after collection on Teflon filters	Evaporation, nucleation, water partitioning NOT considered
Morawska et al. (2009)	<0.8	0.092	Measure size distribution and concentration using APS <sup>b</sup> immediately at the mouth opening	

<sup>a</sup> OPC: Optical Particle Counter

<sup>b</sup> APS: Aerodynamic Particle Sizer

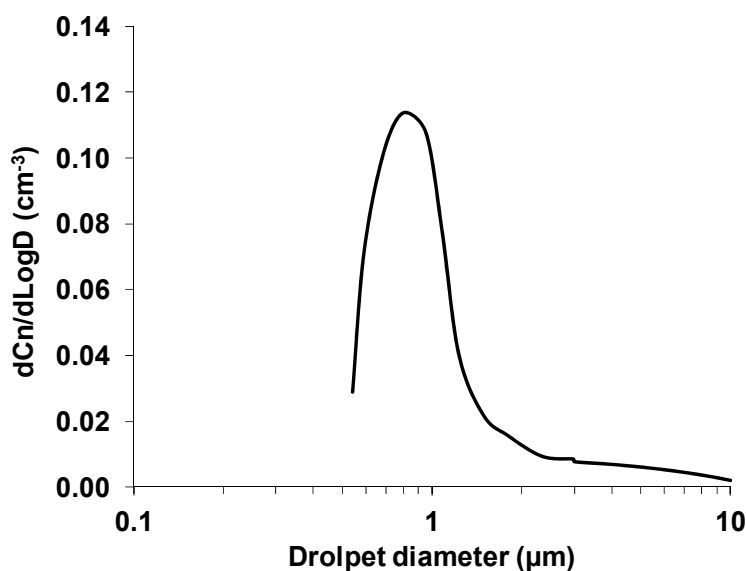


Figure 2-8 Size distribution and concentration of breathed droplets (Morawska et al., 2009).

### 2.1.2.3. Talk

Some studies indicated that most of the droplets generated during talking are within the super-micrometer size (Duguid, 1945; Loudon and Roberts, 1967; Chao et al., 2009). However, some other studies suggested that the majority of droplets exhaled during talking are in the sub-micrometer size range (Papineni and Rosenthal, 1997; Morawska et al., 2009). The discrepancy of these studies is again owing to the instrument and measurement methodology. Table 2-3 summarizes the representative diameter, concentration, measurement technique and limitations of the previous studies. The limitations associated with the measurement techniques are similar to that for coughs. Figure 2-9 shows the combination of size distribution and concentration of droplets generated during talking by Morawska et al. (2009) and Chao et al. (2009), which tends to be the most reliable data. The representative droplet diameter is less than  $0.8 \mu\text{m}$  and the average total number concentration is  $0.46 \text{ cm}^{-3}$ . Again, since the uncertainty of the concentration estimated by Chao et al. (2009) is considerable, the size distribution for the entire size range may not be accurate.

Table 2-3 Summary of the previous studies on droplets during talking.

Reference	Representative diameter ( $\mu\text{m}$ )	Concen. ( $\text{cm}^{-3}$ )	Technique	Limitations
Duguid (1946)	10.7		Count of large droplets using microscopy after collection on a slide	Sampling losses for submicron droplets, evaporation, nucleation, water partitioning NOT considered

Loudon & Roberts (1967)	90		Count of large droplets using microscopy after collection on a filter	Sampling losses for submicron droplets, evaporation, nucleation, water partitioning NOT considered
Fairchild & Stamper (1987)		0.6	Sample aerosol from a respirator mask using a laser aerosol spectrometer	Sampling losses for submicron droplets, evaporation, nucleation, water partitioning NOT considered
Papineni & Rosenthal (1997)	<0.6	0.0063–0.0355	A subject talked into a funnel connected to an OPC <sup>a</sup>	Sampling losses for supermicron droplets, evaporation, nucleation NOT considered
Chao et al. (2009)	16	0.004–0.223 <sup>b</sup>	Measure size distribution immediately at mouth opening using IMI <sup>c</sup>	Sampling losses for submicron droplets NOT considered
Morawska et al. (2009)	<0.8	0.307	Measure size distribution and concentration using APS <sup>d</sup> immediately at the mouth opening	Sampling losses for supermicron droplets NOT considered

<sup>a</sup> OPC: Optical Particle Counter

<sup>b</sup> Concentration estimated based on four different methods

<sup>c</sup> IMI: Interferometric Mie Imaging

<sup>d</sup> APS: Aerodynamic Particle Sizer

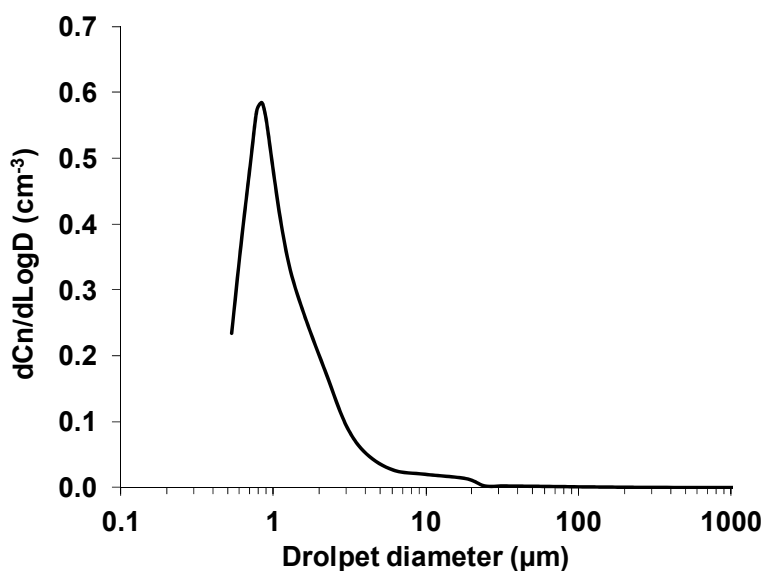


Figure 2-9 Size distribution and concentration of droplets generated during talking combined from Morawska et al. (2009) and Chao et al. (2009) (the first method).

### 2.1.3 Evaporation of droplets

Droplet evaporation is related to the composition of the droplets. There have been different opinions on defining the size of droplet nuclei, which relates to the component of the droplets. Some researchers adopted the solid matter content of 1.8% to define the size of droplet nuclei (Duguid, 1945; Chao and Wan, 2006; Wan and Chao, 2007). However, some other researchers considered that the solution of the droplets should be assumed to be 0.9% NaCl as the physiological solution (Wang et al., 2005; Xie et al., 2007). Nicas et al. (2005) summarized that respiratory droplets are composed of an aqueous solution containing inorganic and organic ions, glycoprotein and protein, and the equilibrium diameter of the completely evaporated particle ( $d_{ep}$ ) is related to the initial diameter ( $d_0$ ) by:

$$d_{ep} = 0.44d_0 \quad (2.1)$$

Wan et al. (2007) and Chao et al. (2008) adopted the droplet component summarized by Nicas et al. (2005) in their studies. Although there have been different opinions on defining the size of droplet nuclei, the fact that evaporation process is very rapid was found by different researchers (Chen and Zhao, 2010; Morawska et al., 2009; Parienta et al., 2011). Chen and Zhao (2010) suggested that modeling the transient process from a droplet to a droplet nucleus due to evaporation can be neglected for droplets with a diameter larger than 10  $\mu\text{m}$ . Morawska et al. (2009) indicated that the evaporation from the original droplets to droplet nuclei occurred within 0.8 s.

### 2.1.4 Virus in droplets

#### 2.1.4.1. Virus RNA particle amount

The virus RNA particles can be a representative of virus in droplets. Fabian et al. (2009) and Milton et al. (2010) measured the amount of influenza virus RNA particles generated through coughs and breaths of influenza infected patients. It was observed that an influenza infected subject can generate 0.01 to 2 influenza virus RNA particles per minute with a geometric mean of 0.1 through breathing. The amount of such influenza virus RNA particles for a cough combined with one minute of breathing ranged from 0.1 to 20000 per minute with a geometric mean of 3.1 for coarse particles. For fine particles, the amount ranges from 0.1 to 100000 per minute with a geometric mean of 5.

#### 2.1.4.2. Virus survival

There are several environmental influencing factors that can affect the survival of virus, such as humidity and temperature, ultraviolet (UV) radiation and ozone. For humidity and temperature, a recent study by Shaman and Kohn (2009) found that 50% of influenza virus transmission (IVT) variability and 90% of influenza virus survival (IVS) variability were explained by AH, whereas,

respectively, only 12% and 36% were explained by relative humidity (RH). The virus survival rate decreases with the increase of AH, as shown in Figure 2-10.

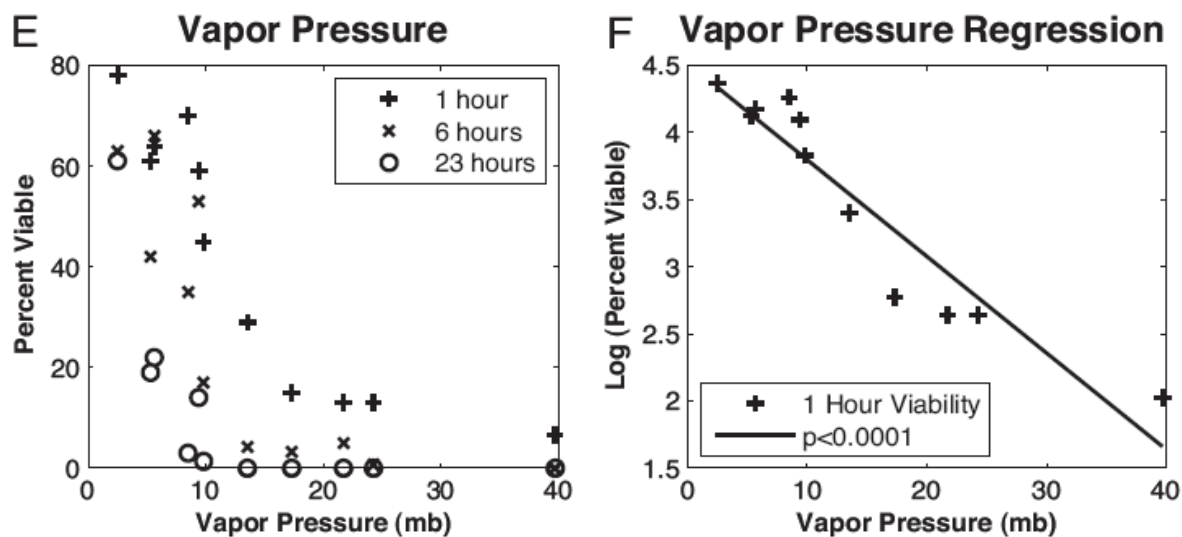


Figure 2-10 Correlation between absolute humidity and influenza virus survival (Shaman and Kohn, 2009).

For UV radiation in the sunlight, it is a major natural virucidal agent outdoors. However, if there is no sunlight indoors, this factor can be ignored (Weber and Stilianakis, 2008). Furthermore, ozone can be a potent inactivator of viruses and appears to be especially effective if the fluids to be treated are nebulized (Weber and Stilianakis, 2008). However, the effectiveness of inactivating exhaled viruses by ozone in indoor environments has not yet been well studied.

This section collects the available literature on physical and biological emission data during coughing, breathing and talking. The data include the time-dependent flow rate and direction of exhaled airflow, mouth opening area, droplet size distribution and concentration, evaporation, virus RNA particle amount and influencing factors on virus survival. These data can be used as the boundary conditions in modeling person-to-person contaminant transport in ventilated spaces.

## 2.2 Modeling person-to-person contaminant transport in enclosed spaces

To model person-to-person contaminant transport in enclosed environments, various computational methods, including well-mixed model, multi-zone models, CFD models, can be applied. Walkinshaw (2010) applied a well-mixed model to predict the risk of infection from influenza in an aircraft cabin. Ko et al. (2004) and Jones et al. (2009) used multi-zone models to calculate the risks based on dose response models. Chen et al. (2011) applied an improved multi-

zone model to investigate the influence of two-way airflow due to temperature difference on the transmission of SARS in a hospital ward in Hong Kong. However, the assumption of the well-mixed and multi-zone models that air temperature and contaminant concentration in a zone is uniform may not be valid.

On the other hand, CFD models can provide more detailed and accurate information than well-mixed and multi-zone models. Thus, in recent years, CFD models have been widely used in modeling person-to-person contaminant transport in various enclosed environments. Zhao et al. (2005) applied a zero equation turbulence model with an Eulerian method to investigate exhaled particle transport during breathing, coughing, and sneezing in a ventilated room. Zhang and Chen (2006) used the standard k- $\epsilon$  model with a Lagrangian method to calculate particle transport in a chamber with under-floor air-distribution system. Zhang and Chen (2007) compared the Eulerian and Lagrangian methods for predicting respiratory particle transport from a single cough in a four-row aircraft cabin. Gupta et al. (2011), Zhang and Li (2012) and Gao et al. (2012a) used the RNG k- $\epsilon$  model with a Lagrangian method to calculate droplet transport in an aircraft cabin, a fully-occupied high-speed rail cabin and an office, respectively. Li et al. (2011) and Seepana and Lai (2012) investigated person-to-person particle transport under various ventilation modes using an Eulerian drift flux model. Memarzadeh and Xu (2012) assessed the role of air changes per hour (ACH) in possible transmission of airborne infections using an Eulerian model. Wan et al. (2009) and Zhang et al. (2009) performed detailed steady-state CFD simulations and quantified the exhaled contaminant transport in aircraft cabins. The numerous studies discussed above can demonstrate the popularity of CFD models in modeling person-to-person contaminant transport.

There are two parts of CFD modeling on person-to-person contaminant transport: airflow modeling and particle modeling. For airflow modeling, there are several turbulence models such as Reynolds-Averaged Navier-Stokes (RANS) models, Large Eddy Simulation (LES), and Detached Eddy Simulation (DES), which have that has been reviewed and tested by Zhang et al. (2007), Wang and Chen (2009). For particle modeling, Eulerian and Lagrangian are two popular methods. The Eulerian method often uses the drift flux model for considering the slippage between particle phase and fluid (air) phase. This model performed well in modeling indoor particle dispersion as reported by Murakami et al. (1992), Chen et al. (2006), and Zhao et al. (2009a). The Lagrangian method with the Discrete Random Walk (DRW) model has also performed very well in modeling and analyzing the particle transport and dispersion as shown by Zhang and Chen (2006), Zhang et al. (2009), and Chen and Zhao (2010). Most of the studies mentioned above focused on steady-state particle transport processes. However, particle transport processes can be in an unsteady state. Wang et al. (2012) have tested different combinations of the airflow and particle models for steady- and unsteady-state cases. For steady-state airflow conditions, they preferred the RANS model with the Eulerian method due to the reasonable accuracy and low computing cost associated with the model. For unsteady-state airflow conditions, Wang et al. recommended the DES model with the Lagrangian method due to its relatively high accuracy. The reason for using DES rather than RANS model is that RANS

model fails to predict correct transient airflow (Wang and Chen, 2009). Moreover, when the airflow field is still developing, the Lagrangian method may have better accuracy than the Eulerian method since it accounts for more physics of airflow and particle motion (Wang et al., 2012). But if the DES with Lagrangian model is applied for studying coughing, talking, and sneezing among persons in an enclosed environment, it requires considerable computing cost.

Therefore, it is worthwhile to develop a model that can not only ensure the accuracy but also reduce the computing cost. It should be noticed that coughing, sneezing, or talking are unsteady-state and may have a significant impact on airflow distribution only in the first few seconds. But after the effect of the coughing, talking, and sneezing on the airflow is damped, the airflow can be regarded as steady-state. Then RANS with the Eulerian model can be applied to reduce the computing cost (Wang et al., 2012). Thus, it may be possible to develop a hybrid DES-Lagrangian and RANS-Eulerian model for simulating transient particle transport in enclosed environments, which can ensure the accuracy and reduce the computing cost.

Although CFD models have been widely used, when the source location is changed, even for a fixed airflow field, all of these models require recalculation of the particle equations, which requires considerable computing effort. Thus, it is worthwhile to develop an approach that can solve this problem. Nicas (2000) applied the Markov chain technique in a multi-zone model to further quickly assess transient particle transport. That study demonstrated the capability of the Markov chain technique in providing fast-than-real-time information of spatial and temporal particle concentrations. However, this simple model failed to account for most of the particle dispersion mechanisms such as drag force, gravitational settling, and turbulent dispersion. As shown in the literature mentioned above, CFD simulation can easily take these influencing factors into account. Thus, a combination of CFD with the Markov chain technique has the potential to provide more accurate and fast-than-real-time information of spatial and temporal particle concentrations.

In summary of the review, the following work may significantly improve the simulation speed of person-to-person contaminant transport in enclosed environments:

- 1) Develop a hybrid DES-Lagrangian and RANS-Eulerian model for simulating transient particle transport in enclosed environments, which can ensure the accuracy and reduce the computing cost;
- 2) Develop a combination of CFD with the Markov chain technique to provide accurate and fast-than-real-time information of transient particle transport in enclosed environments;

### **2.3 Influencing factors on person-to-person contaminant transport**

Ventilation mode, ventilation rate, and person-to-person distance are among the factors that may influence person-to-person contaminant transport in enclosed spaces. A number of studies have focused on these influencing factors. The first factor, ventilation mode, was investigated by Qian et al. (2006) and Yin et al. (2011), they compared the effectiveness of mixing and displacement ventilation in controlling person-to-person contaminant transport in hospital wards. Lai and Wong (2010, 2011) and Olmedo et al. (2012) experimentally investigated person-to-person contaminant transport in laboratory chambers with mixing and displacement ventilation. There are more than 30 cases comparing the effect of mixing and displacement ventilation on person-to-person contaminant transport available in these studies. However, fewer studies are available in the literature for another commonly used ventilation mode, the Under-Floor Air-Distribution (UFAD) system (He et al., 2011; Li et al., 2011).

In regard to the second factor, ventilation rate, Qian et al. (2006) experimentally investigated its effect on person-to-person contaminant transport in a hospital ward with a displacement ventilation system. Nielsen et al. (2010) compared the person-to-person contaminant exposure in a hospital ward with ventilation rates of 6, 9, and 10 ACH. In addition, Yin et al. (2011) compared the person-to-person contaminant exposure in an inpatient room with ventilation rates of 4 and 6 ACH. However, in most of these cases, the patients were lying in beds, which may not be representative of normal scenarios such as working in an office.

The third factor, person-to-person distance, was investigated by Qian et al. (2006); they assessed its effect on person-to-person contaminant transport in a hospital ward with a ventilation rate of 4 ACH. Recently, Olmedo et al. (2012) experimentally investigated the effect of person-to-person distance on exhaled contaminant transport in a room with a ventilation rate of 5.6 ACH. However, the effect of person-to-person distance on exhaled contaminant transport under high ventilation rates has not been well understood.

The review of existing studies shows that additional cases of person-to-person contaminant transport are needed in order to address the limitations discussed above. Thus, this study aims to develop a database and systematically investigate the general effect of ventilation mode, ventilation rate, and person-to-person distance on person-to-person contaminant transport in mechanically ventilated spaces.

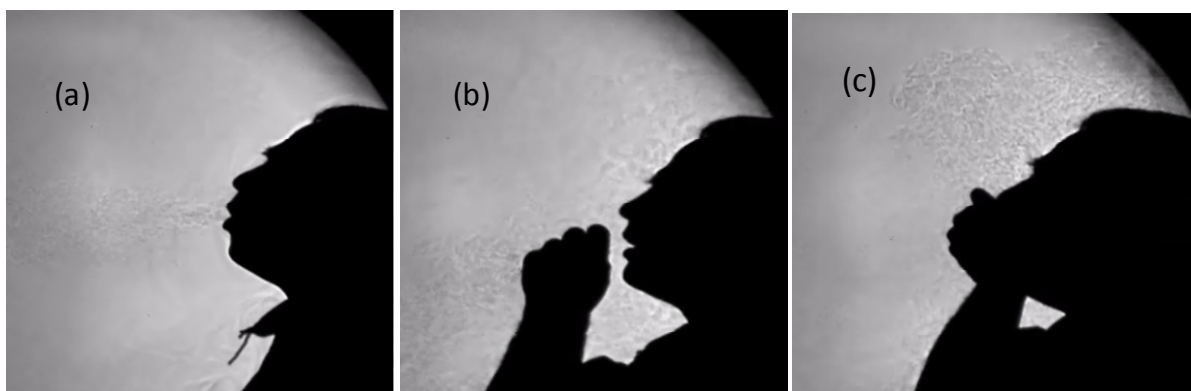
### **2.4 Effectiveness of a mouth covering**

Note that a lot of people attempt to cover their mouth with their hand or a tissue when they cough or sneeze. Moreover, ill people may wear masks to reduce the possibility of transmitting

infectious diseases to others. Thus, it is essential to investigate the effectiveness of mouth covering on person-to-person contaminant transport in enclosed environments and its modeling approaches.

Since masks are equipped with filters that can purify the air passing through, there are numerous studies focusing on the effectiveness of masks on removing exhaled droplets. Surgical mask and N95 mask are among the most popular and widely available masks. For the surgical masks, Grinshpun et al. (2009), Lee et al. (2008) and Oberg and Brosseau (2008) found that the total penetration rate ranges from 10 to 50%. For N95 masks, Balazy et al. (2006) concluded that the penetration rate was less than 7% for virus particles with a diameter from 10 to 80 nm. Qian et al., (1998) and Willeke and Qian, (1998) found that the penetration rate of particles of size 0.1 to 1  $\mu\text{m}$  through the N95 masks was well below 5%. Coffey et al., (1999) indicated that the penetration rate of ambient particles through the N95 masks was lower than 16%. Furthermore, the exhaled droplets can escape from the gaps between the face and the masks (Coffey et al., 1999) in addition to through the filter. Gupta (2010) conducted a systematic review on the performance of N95 masks on removing exhaled droplets and concluded that the penetration from the N95 masks including the face seal leakages to be 10%.

In addition to the removal of exhaled droplets, mouth coverings can also reduce the horizontal transport of exhaled air. Tang et al. (2009) roughly visualized the exhaled airflow by a cough with various mouth coverings, including covering with a tissue, cupped hand, fist, surgical mask and N95 mask. As shown in the following figures that were captured from their videos, the velocity of exhaled airflow can be reduced. However, there was still airflow penetrating the leakages of the coverings. In general, the recorded videos can provide some ideas of the characteristics of exhaled airflow by a cough with mouth covering.



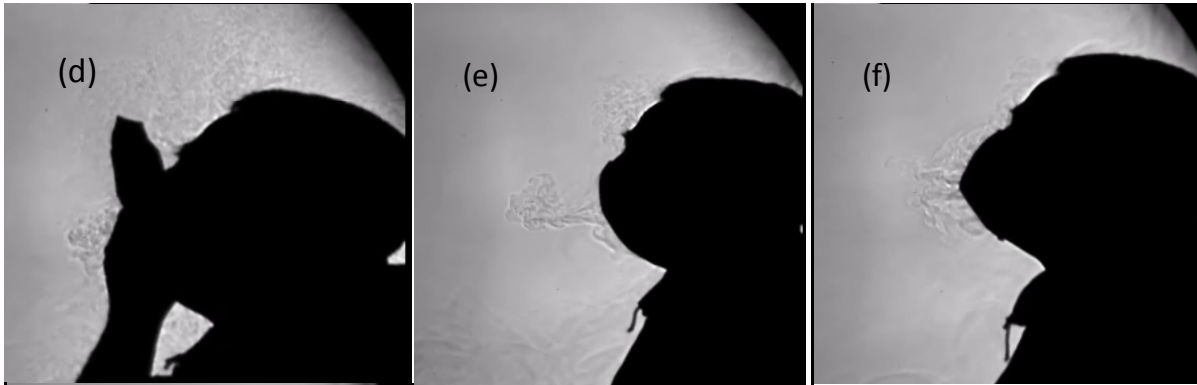


Figure 2-11 Visualization of exhaled airflow by a cough with mouth covering (a) uncovered, (b) fist, (c) cupped hand, (d) tissue, (e) surgical mask, (f) N95 mask.

Li et al. (2012) further investigated the effects of mouth covering on the co-occupant's exposure under three commonly employed ventilation systems using CFD approaches. They simplified the mouth covering as a solid rectangle (0.20 m in length  $\times$  0.12 m in height) located in front of the infector's mouth. The results show that the use of mouth covering can reduce the horizontal exhaled air velocity to protect the co-occupant from direct exposure to the coughed droplets. Furthermore, the exhaled air velocity can only influence the co-occupant's direct exposure. The indirect exposure at the later stage is mainly associated with the specific ventilation mode. This study provided important information on the effects of mouth covering on the co-occupant's exposure, however, the approach for modeling mouth covering was arbitrarily simplified without validation.

The review of existing studies shows that there are no valid approaches for modeling mouth covering available in the literature. To model the airflow by a cough with a mouth covering, one option is to directly build the realistic geometry of the mouth coverings, such as a tissue, a cupped hand, a fist or an elbow. However, it would be highly difficult to identify the air leakages between the face and the mouth covering. Furthermore, the complicated geometry and the associated large amount of grids in and around the mouth covering could result in significant consumption of computing cost. Thus, it is critical to develop simplified models for predicting the airflow by a cough with a mouth covering.

### 3. A HYBRID MODEL FOR PREDICTING TRANSIENT PARTICLE TRANSPORT

The review in Chapter 2 shows that it is possible to develop a hybrid DES-Lagrangian and RANS-Eulerian model for simulating transient particle transport in enclosed environments, which can ensure the accuracy and reduce the computing cost. To further reduce the computing cost, one solution is to use a RANS model as the initial field for a DES model. Then the DES model can be used to calculate accurate results within a very short period of time. Now the question is how long the DES simulations should be performed in order to completely eliminate the effects of RANS modeling. In addition, if the DES is applied to study coughing, how short should the transient simulation be so that the steady-state modeling afterwards will still give accurate results? This chapter set out to identify the two time constants and test the hybrid model for transient particle distributions in an airliner cabin.

#### 3.1 Model Determination

To identify the two time constants, this study used the RANS model for steady-state flows and the DES model for unsteady-state flows. Similar to in previous research, we used the Eulerian and Lagrangian methods for particle transport under steady-state and unsteady-state, respectively. This section details the flow and particle models used as well as the procedure to determine the two time constants.

##### 3.1.1 Steady-state airflow conditions

###### 3.1.1.1. Airflow and turbulence model

For steady-state flows, the renormalization group (RNG) k- $\epsilon$  model (Choudhury, 1993) is applied to calculate the airflow and turbulence. It has the best overall performance among all RANS models for enclosed environments (Zhang et al., 2007). This model calculates the turbulence kinetic energy by:

$$\frac{\partial}{\partial t}(\rho k) + \frac{\partial}{\partial x_i}(\rho k u_i) = \frac{\partial}{\partial x_j} \left[ \alpha_k \mu_{eff} \frac{\partial k}{\partial x_j} \right] + G_k + G_b - \rho \epsilon - Y_M \quad (3.1)$$

where  $\alpha_k$  is the inverse effective Prandtl number for  $k$ ;  $\mu_{eff}$  is the effective viscosity;  $G_k$  and  $G_b$  are the turbulence generation due to the mean velocity gradient and buoyancy, respectively; and  $Y_M$  is the contribution of the fluctuating dilatation in compressible turbulence to the overall dissipation rate.

This model calculates the turbulence dissipation rate by:

$$\frac{\partial}{\partial t}(\rho \epsilon) + \frac{\partial}{\partial x_i}(\rho \epsilon u_i) = \frac{\partial}{\partial x_j} \left[ \alpha_\epsilon \mu_{eff} \frac{\partial \epsilon}{\partial x_j} \right] + C_{1\epsilon} \frac{\epsilon}{k} (G_k + C_{3\epsilon} G_b) - C_{2\epsilon} \rho \frac{\epsilon^2}{k} - R_\epsilon \quad (3.2)$$

where  $\alpha_\varepsilon$  is the inverse effective Prandtl number for  $\varepsilon$ ; and  $C_{1\varepsilon}$ ,  $C_{2\varepsilon}$  and  $C_{3\varepsilon}$  are constants. The equations for term,  $R_\varepsilon$ , can be found in the Fluent manual (Fluent Inc., 2005).

### 3.1.1.2. Particle transport model

For steady-state flows, the Eulerian drift flux model is applied to calculate the particle dispersion. The drift flux model considers the slippage between particle phase and fluid (air) phase, which takes the effect of the gravitational settling into consideration:

$$\frac{\partial[(u_j + u_{sj})C]}{\partial x_j} = \frac{\partial}{\partial x_j} \cdot \left( \frac{\nu_t}{\sigma_c} \frac{\partial C}{\partial x_j} \right) + S_c \quad (3.3)$$

where  $u_j$  is the averaged fluid (air) velocity;  $\nu_t$  the turbulent kinetic viscosity;  $\sigma_c$  the turbulent Schmit number, which is usually equal to 1.0 (Murakami et al., 1992); and  $S_c$  the generating rate of the particle source. The  $u_{sj}$  in the equation is the gravitational settling velocity of the particles, which can be calculated by:

$$u_{sj} = \tau_p g_j \quad (3.4)$$

where  $\tau_p$  is the particle relaxation time. The  $\tau_p$  can be calculated by:

$$\tau_p = \frac{C_c \rho_p d_p^2}{18\mu} \quad (3.5)$$

where  $C_c$  is the Cunningham coefficient caused by slippage. The  $C_c$  can be calculated by (Hinds, 1999):

$$C_c = 1 + \frac{\lambda}{d_p} (2.514 + 0.8 \times \exp(-0.55 \frac{d_p}{\lambda})) \quad (3.6)$$

where  $\lambda$  is the mean free path of the air molecules.

## 3.1.2 Unsteady-state airflow conditions

### 3.1.2.1. Airflow and turbulence model

For unsteady-state flows, the DES Realizable k- $\varepsilon$  model (Shur et al., 1999) is applied to predict the airflow and turbulence. The reason for using DES rather than RANS model for unsteady-state flows is that RANS model fails to predict correct transient airflow (Wang et al., 2012). This model calculates the turbulence kinetic energy by:

$$\frac{\partial}{\partial t}(\rho k) + \frac{\partial}{\partial x_j}(\rho k u_j) = \frac{\partial}{\partial x_j} \left[ \left( \mu + \frac{\mu_t}{\sigma_k} \right) \frac{\partial k}{\partial x_j} \right] + G_k + G_b - Y_k \quad (3.7)$$

The dissipation term,  $Y_k$ , is modeled by:

$$Y_k = \frac{\rho k^{3/2}}{l_{DES}} \quad (3.8)$$

where:

$$l_{DES} = \min(l_{rke}, l_{LES}) = \min\left(\frac{k^{3/2}}{\varepsilon}, C_{DES} \Delta_{max}\right) \quad (3.9)$$

The  $C_{DES}$  in the above equation is a constant and  $\Delta_{max}$  is the maximum local grid spacing,  $max(\Delta x, \Delta y, \Delta z)$ .

The model calculates the turbulence dissipation rate by:

$$\frac{\partial}{\partial t}(\rho\varepsilon) + \frac{\partial}{\partial x_j}(\rho\varepsilon u_j) = \frac{\partial}{\partial x_j} \left[ \left( \mu + \frac{\mu_t}{\sigma_\varepsilon} \right) \frac{\partial \varepsilon}{\partial x_j} \right] + \rho C_1 S \varepsilon - \rho C_2 \frac{\varepsilon^2}{k + \sqrt{\nu \varepsilon}} + C_{1\varepsilon} \frac{\varepsilon}{k} C_{3\varepsilon} G_b \quad (3.10)$$

where  $C_1$ ,  $C_2$ ,  $C_{1\varepsilon}$ , and  $C_{2\varepsilon}$  are constants.

### 3.1.2.2. Particle transport model

For unsteady-state flows, the Lagrangian model is applied to calculate the particle dispersion. Using the momentum equation based on Newton's law, the trajectory of each particle can be calculated by:

$$\frac{d\vec{u}_p}{dt} = F_D(\vec{u}_a - \vec{u}_p) + \frac{\vec{g}(\rho_p - \rho_a)}{\rho_p} + \vec{F}_a \quad (3.11)$$

where  $\vec{u}_p$  is the velocity vector of the particle;  $\vec{u}_a$  the velocity vector of air;  $\vec{g}$  the gravitational acceleration vector;  $\rho_p$  and  $\rho_a$  the particle and air density, respectively; and  $\vec{F}_a$  Brownian motion and Saffman lift force. The Brownian motion was included in the model since it is a typical characteristic of fine particles. Furthermore, the Saffman lift force may be relatively large near a room's wall for sub-micro particles (Zhao et al., 2004). Thus, we included the Saffman lift force in our study. The drag force is calculated by:

$$F_D(\vec{u}_a - \vec{u}_p) = \frac{18\mu}{\rho_p d_p^2} \frac{C_D Re}{24} (\vec{u}_a - \vec{u}_p) \quad (3.12)$$

where  $\mu$  is fluid viscosity,  $C_D$  the drag coefficient,  $Re$  Reynolds number, and  $d_p$  particle diameter.

The Discrete Random Walk (DRW) model (Fluent Inc., 2005) is used to model the turbulence dispersion:

$$u_i' = \zeta_i \sqrt{2k/3} \quad (3.13)$$

where  $\zeta_i$  is a normal random number, and  $k$  is turbulence kinetic energy.

### 3.1.3 Calculation procedure

#### 3.1.3.1. Overall calculation procedure

In order to reduce the computing cost, this study introduces a hybrid DES-Lagrangian and RANS-Eulerian model to calculate the transient particle transport in enclosed environments. The key point of this model is to determine a suitable calculation procedure to keep the DES simulations as short as possible without sacrificing the accuracy.

Figure 3-1 shows the overall calculation procedure for using the hybrid DES-Lagrangian and RANS-Eulerian models, taking coughing as an example. It consists of three steps:

- (1). The RNG k- $\epsilon$  model is used to calculate the initial field of airflow under steady-state conditions. Then the DES Realizable k- $\epsilon$  model is used to calculate for a period of time,  $t_1$ , as shown in Figure 3-1 to obtain the time-dependent flow distribution under steady-state boundary conditions;
- (2). The DES-Lagrangian model is applied to calculate for another period of time,  $t_2$ , also shown in the figure for the unsteady-state boundary conditions due to coughing;
- (3). The RANS-Eulerian model is used again to calculate flow fields under the steady-state boundary conditions, by assuming the effect of the coughing on the airflow distribution being fully damped.

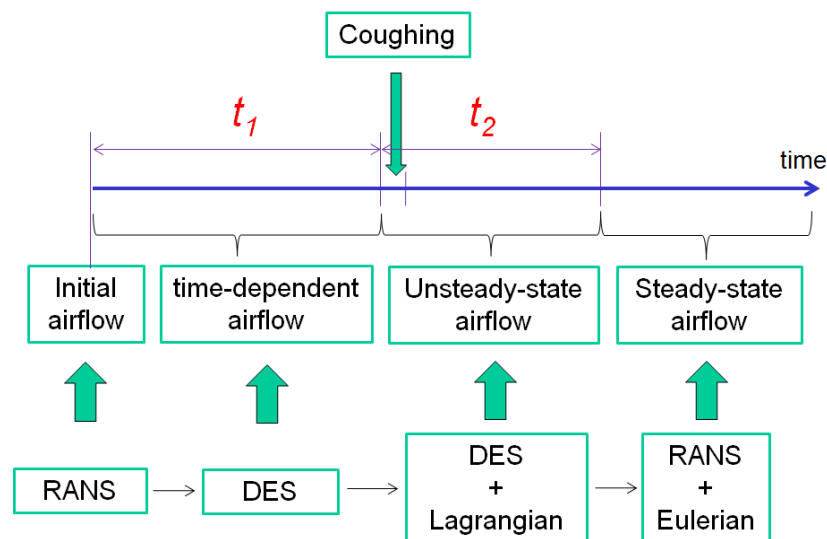


Figure 3-1 Overall calculation procedure.

The above procedure shows that the computing effort depends very much on the  $t_1$  and  $t_2$ . The shorter of the  $t_1$  and  $t_2$  are, the less the computing effort should be since transient DES-Lagrangian calculations are very computationally intensive. The following subsection describes our effort in estimating the  $t_1$  and  $t_2$ .

### 3.1.3.2. Estimation for $t_1$

The estimation of  $t_1$  started from the room time constant,  $\tau$ . Normally, a flow will become stable again after the corresponding boundary conditions have been changed and stabilized for  $2\tau$  (Wang and Chen, 2009). Therefore, if we start to simulate room airflow with a uniform initial field by using the DES model, the results of the first  $2\tau$  period are considered to be transient from its initial field to a stable one. However, this study did not use the DES model with a uniform initial field, but rather a flow field obtained from the RANS model. Although the flow field may not be accurate, it should be close to reality,  $t=t^*$ , as shown in Figure 3-2. Then the DES model should only be used for the  $t_1 = 2\tau - t^*$  period to reach a stable airflow field.

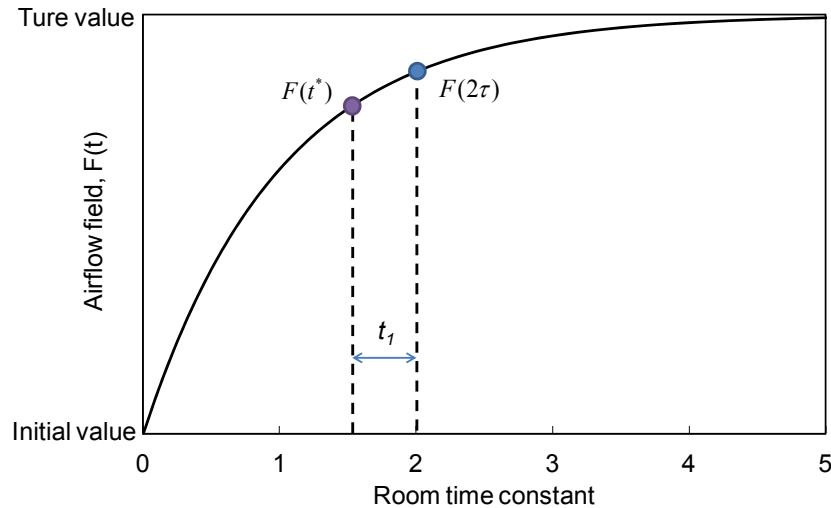


Figure 3-2 Airflow field versus room time constant for estimating  $t_1$ .

Let us define an error between  $F(t^*)$  and  $F(2\tau)$  as  $\eta$ , then the following equation can be obtained:

$$\frac{F(t^*)}{F(2\tau)} = \frac{(1 - e^{-\frac{t^*}{\tau}})}{(1 - e^{-\frac{2\tau}{\tau}})} = 1 - \eta \quad (3.13)$$

Therefore, the  $t_1$  can be calculated by:

$$t_1 = 2\tau - t^* = \left[ 2 - \ln \frac{1}{1 - (1 - \eta)(1 - e^{-2})} \right] \tau \quad (3.14)$$

If we use the typical error between the RANS and DES model,  $\eta$ , to be 10% as suggested by Wang (2011), the  $t_1$  is obtained as,

$$t_1 = 0.5\tau \quad (3.15)$$

### 3.1.3.3. Estimation for $t_2$

The  $t_2$  is the time period when a cough can affect the room airflow distribution and the flow is considered to be unsteady. It should be noted that the time-dependent air velocity varies along the traveling path of the coughing jet. To estimate the overall process, this study averaged the coughing jet peak velocity along the traveling path,  $\overline{U}_m$ , and investigated its decay process.

Figure 3-3 shows an example of the air velocity versus time at position  $s_{\overline{U}_m}$ .  $s_{\overline{U}_m}$  is the corresponding distance from the mouth to  $\overline{U}_m$ . As shown in the figure, the  $t_2$  is affected by:

- (1). The duration of the coughing ( $t_{release}$ );
- (2). The traveling time needed for the coughing jet peak to travel to position  $s_{\overline{U}_m}$  ( $t_{travel}$ ).
- (3). The decay time when the  $\overline{U}_m$  decreases to the surrounding value ( $t_{decay}$ );

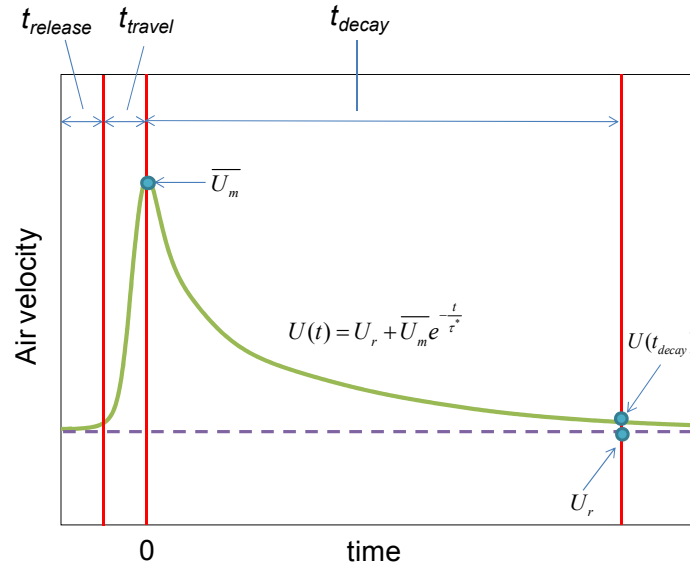


Figure 3-3 An example of the air velocity versus time at position  $s_{\overline{U}_m}$ .

The duration of coughing,  $t_{release}$ , has been studied by many researchers. For example, Gupta et al. (2009) found the time to be

$$t_{release} = 0.4 \text{ s} \quad (3.16)$$

by measuring it from 25 human subjects.

To estimate the  $\overline{U}_m$ , this study referred to the jet equation (Xie et al., 2007):

$$U_m(s) = \begin{cases} U_0, & s < 6.8d_0 \\ \frac{6.8U_0d_0}{s}, & s \geq 6.8d_0 \end{cases} \quad (3.17)$$

where  $U_m(s)$  is the jet velocity at distance  $s$ ,  $U_0$  the coughing initial velocity,  $d_0$  the diameter of the mouth, and  $s$  the distance from the mouth. It should be noted that the above jet equation is for steady-state, while the coughing jet is unsteady with a decay process. The  $U_m(s)$  in the jet equation can be regarded as the coughing jet peak at distance  $s$ . Then the  $\overline{U}_m$  can be determined via:

$$\overline{U}_m = \frac{1}{s^*} \int_0^{s^*} U_m(s) ds = \frac{6.8U_0d_0}{s^*} \left(1 + \ln \frac{s^*}{6.8d_0}\right) \quad (3.18)$$

where  $s^*$  is the distance that a cough can travel. This study assumed that when the centerline velocity decays to a reference room air velocity, the effect of the coughing is damped. The reference room air velocity,  $U_r$ , was set as 0.25 m/s, which is a recommended limit value for thermal comfort (ISO, 2005). Then, the  $s^*$  can be calculated using the jet equation. However, in many enclosed environments, the jet is not a free one but an impinging one. The distance from the mouth to the wall is  $L$  and  $L < s^*$ , then the  $s^*$  should be set as  $L$ , namely:

$$s^* = \min\left(\frac{6.8U_0d_0}{U_r}, L\right) \quad (3.19)$$

Based on Eq. (3.17), the distance from the mouth corresponding to  $\overline{U}_m$  can be calculated by:

$$s_{\overline{U}_m} = \frac{6.8U_0d_0}{\overline{U}_m} \quad (3.20)$$

Based on Eqs. (3.17) and (3.20), the traveling time,  $t_{travel}$ , can be calculated by integrating the coughing jet peak traveling time from the mouth to the position  $s_{\overline{U}_m}$ :

$$t_{travel} = \int_0^{s_{\overline{U}_m}} \frac{1}{U_m(s)} ds = \frac{6.8d_0}{U_0} + \frac{s_{\overline{U}_m}^2 - (6.8d_0)^2}{13.6U_0d_0} \quad (3.21)$$

The decay time,  $t_{decay}$ , is the time needed for the  $\overline{U}_m$  to diminish to the surrounding velocity. The jet velocity at position  $s_{\overline{U}_m}$  during the decay process can be described by:

$$U(t) = U_r + \overline{U_m} \cdot e^{-\frac{t}{\tau^*}} \quad (3.22)$$

where  $U_r$  is the reference room air velocity,  $\tau^*$  is the average local time constant. This study simply considered the local time constant as the time needed for the coughing jet peak to diminish along its traveling path. Based on Eqs (3.17) and (3.19), the  $\tau^*$  can be determined by:

$$\tau^* = \int_0^{s^*} \frac{1}{U_m(s)} ds = \frac{6.8d_0}{U_0} + \frac{s^{*2} - (6.8d_0)^2}{13.6U_0d_0} \quad (3.23)$$

As shown in Figure 3-3, if the average coughing jet peak velocity decreases to a value  $U(t_{decay})$  that is very close to the reference room air velocity,  $U_r$ , the decay process is considered to be completed. Let us define an error between  $U(t_{decay})$  and  $U_r$  as  $\eta$ , then the following equation can be obtained:

$$\eta = \frac{U(t_{decay}) - U_r}{U_r} = \frac{\overline{U_m}}{U_r} e^{-\frac{t_{decay}}{\tau^*}} \quad (3.24)$$

Reformatting Eq. (3.24), the decay time can be obtained:

$$t_{decay} = \ln\left(\frac{\overline{U_m}}{\eta U_r}\right) \tau^* \quad (3.25)$$

Then the  $t_2$  can be roughly estimated by combining Eqs. (3.16), (3.21) and (3.25):

$$t_2 = t_{release} + t_{travel} + t_{decay} \quad (3.26)$$

## 3.2 Verification of the Two Time Constants Used in the Hybrid Model

### 3.2.1 Verification of $t_1$

This study used two cases to verify the  $t_1$  proposed in the previous section. The first case was in an office with an Under-Floor Air-Distribution (UFAD) system (Zhang and Chen, 2006), as shown in Figure 3-4. The room had four heated human simulators. The air was supplied from the two floor inlets and exhausted from the ceiling. The air velocity was measured at the seven poles (V1 to V7) as shown in the figure. The second one was in a four-row aircraft cabin mockup (Zhang et al., 2009), as shown in Figure 3-5. The cabin mockup had 28 seats, 14 of which were occupied by heated human simulators. The air was supplied from two groups of linear diffusers located near the center of the ceiling. The air velocity vectors were measured in the cross-section through the third row and the mid-section along the longitudinal direction. The air change rates of the office and the cabin were 5.5 and 24 ACH, respectively. The corresponding room time constants were 655 and 150 s, respectively. Since the estimation of the  $t_1$  is directly associated with the room time constant, the two cases with quite different room time constants are useful to verify the  $t_1$  estimated in the previous section.

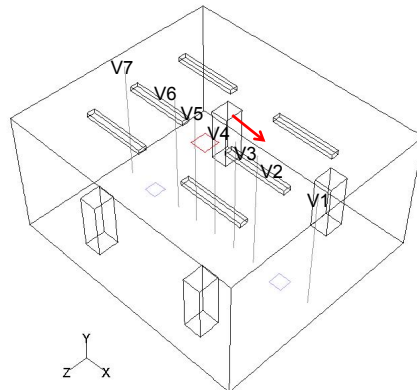


Figure 3-4 Schematic of the office with UFAD system where air velocity was measured at the seven poles (Zhang and Chen, 2006).

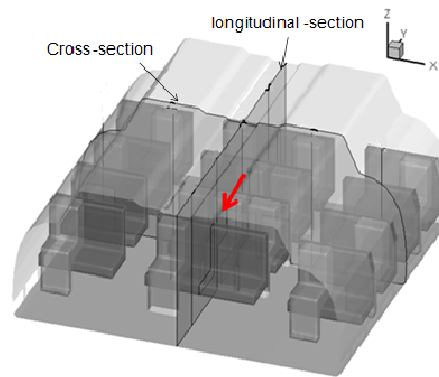


Figure 3-5 Schematic of the four-row aircraft cabin mockup (Zhang et al., 2009).

Since the  $t_I$  was associated with both the RANS and DES models, this study used the following four approaches to calculate the airflow fields of these two cases:

- (1). Approach\_1: only RANS model,
- (2). Approach\_2a: combined RANS and DES with  $t_I=0.5\tau$ ,
- (3). Approach\_2b: combined RANS and DES with  $t_I=2\tau$ ,
- (4). Approach\_3: only DES model,

Approach\_2a averaged the results between  $0.5\tau$  and  $1.5\tau$  as the mean flow field, which was the approach proposed in the previous section. Similarly, Approach\_2b averaged the results between  $2\tau$  and  $3\tau$  as the mean flow field. When Approach\_3 was used, the investigation calculated the airflow fields for  $2\tau$  with a uniform initial flow field and then averaged the results between  $2\tau$  and  $3\tau$  to obtain the mean flow field. Since normally a flow will become stable again after the corresponding boundary conditions have been changed for  $2\tau$ , we expected that both Approach\_2b and Approach\_3 could provide an accurate airflow field as a benchmark.

Figure 3-6 compares the air velocities obtained by the different approaches with the experimental data from Zhang and Chen (2006) for the office case. Approach\_1 and Approach\_3 performed

similarly at poles V3 to V6. Approach\_1 matched better with the experimental data in the middle part of pole V1, but worse at the lower part of pole V1 and middle part of pole V2 than in Approach\_3. At pole V7, both the approaches showed significant discrepancies from the experimental data. Therefore, it is difficult to say which approach is better for predicting the airflow field in this case. Since the DES model can provide detailed information on transitional flows, this study used Approach\_3 as the benchmark. As shown in the figure, Approach\_2b agreed very well with Approach\_3. This further confirms that Approach\_3 can be used as the benchmark. To verify the  $t_l$  proposed in the previous section, this investigation compared Approach\_2a with Approach\_3. The results show that they matched very well for the whole field. Although Approach\_2a still showed significant discrepancies from the experimental data, it can at least achieve the similar accuracy to Approach\_3. Hence,  $t_l=0.5\tau$  was long enough to obtain the accurate time-dependent flow distribution under steady-state boundary conditions. This study has correctly estimated the  $t_l$  for the office case.

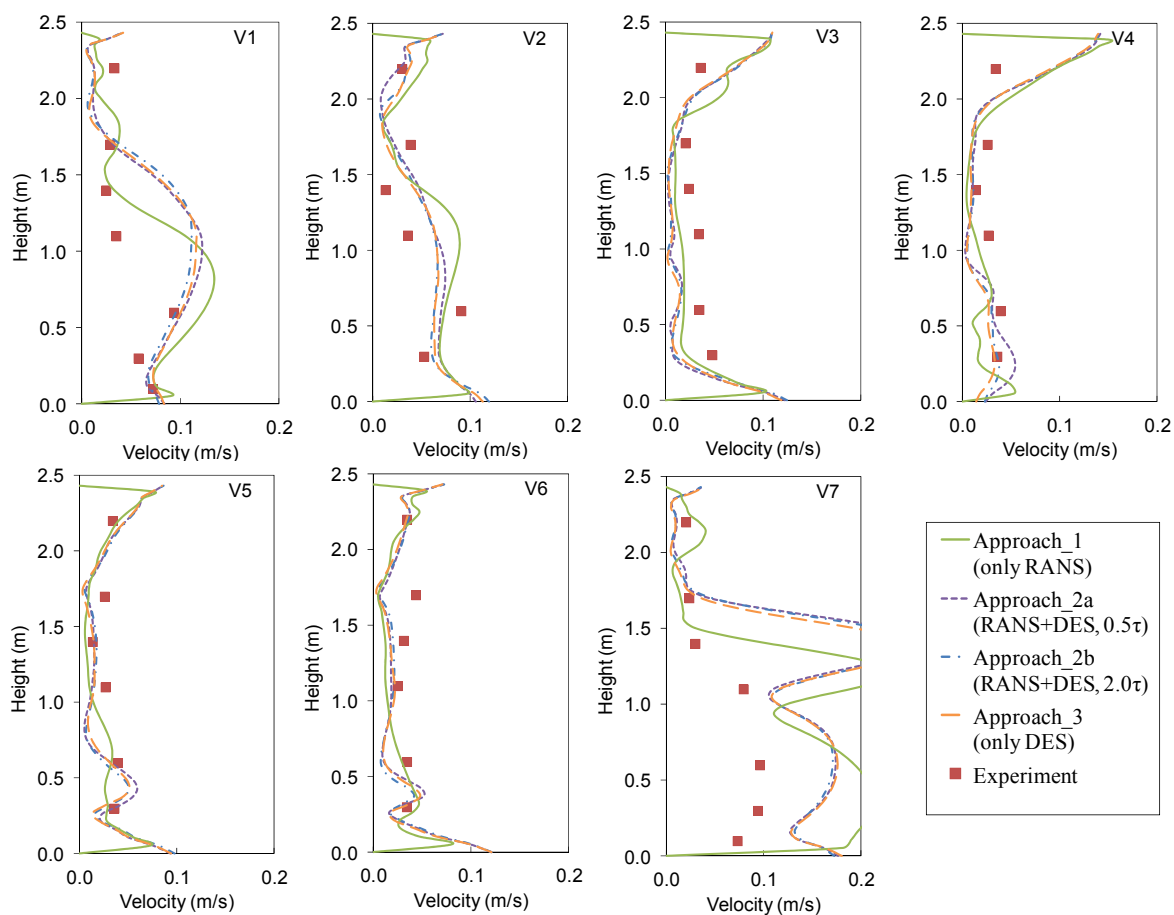


Figure 3-6 Comparison of air velocities obtained by the different approaches with the experimental data from Zhang and Chen (2006).

Figure 3-7 compares the airflow fields obtained by the different approaches with the experimental data from Zhang et al. (2009) for the cabin case. For easy observation, only Approach\_2a and Approach\_3 were shown in the Figure. It can be seen that Approach\_3 showed

significant discrepancies from the experimental data. Zhang et al. (2009) also reported this phenomenon and concluded that the modeling results were very sensitive to the accuracy of the boundary conditions. It should be noted that the velocity directions at the inlets were not measured in the experiments, which may generate errors for quantitative comparison. Nevertheless, the experimental data still preserved the qualitative character of the airflow field. Similar to in the office case, this investigation used Approach\_3 as the benchmark. To verify the  $t_1$  proposed in the previous section, this study compared Approach\_2a with Approach\_3. In the mid-section along the longitudinal direction, both the approaches predicted an upward motion of the airflow field. The quantitative comparison also showed very good agreement in this section. In the cross-section through the third row, both the approaches again matched well with each other for most of the positions. Although differences can be found at some positions at the upper left side of this section, the general airflow pattern was similar between the two approaches. Generally speaking, Approach\_2a agreed well with Approach\_3. Thus,  $t_1=0.5\tau$  is a reasonable estimate for the cabin case.

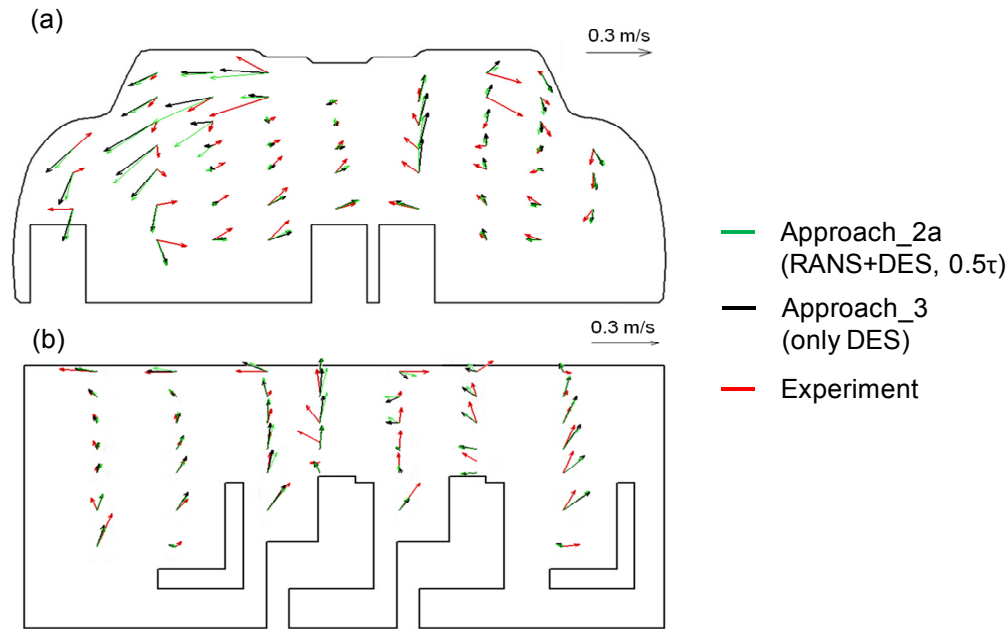


Figure 3-7 Comparison of airflow field obtained by the different approaches with the experimental data from Zhang et al. (2009): (a) cross-section through the third row, (b) mid-section along the longitudinal direction.

The two cases with different room time constants show that the  $t_1$  estimated by Eq. (3.15) is acceptable. The  $t_1$  can be used as the minimum time for obtaining an accurate flow field by DES if the calculation starts from a RANS result.

### 3.2.2 Verification of $t_2$

This investigation again used the office and the aircraft cabin cases to verify  $t_2$ . Different from  $t_1$ ,  $t_2$  was only associated with the DES model. Sub-section 3.2.1 has shown that the DES model can

be used as a benchmark. Hence, the DES model was used to calculate the jet velocity versus time at different positions. Then the time needed for the jet velocity decreased to the surrounding value can be obtained from the DES results as a benchmark to verify the  $t_2$  proposed. The arrows in Figures 3-4 and 3-5, respectively, show the mouth location and coughing direction. Table 3-1 lists the input parameters and the estimated  $t_2$ . According to Eq. (3.17), the jet was associated with the coughing velocity ( $U_0$ ) and the diameter of the mouth ( $d_0$ ). The  $U_0$  was set as 8 m/s for both cases, while the  $d_0$  was set as 4 and 1 cm for the office and cabin cases, respectively, to create jets with different characteristics. The two cases with different jet characteristics are useful to verify the  $t_2$  estimated in the previous section.

Table 3-1 Input parameters and the  $t_2$  estimated.

Case	$U_0$	$d_0$	$L$	$\eta$	$t_{release}$	$t_{travel}$	$t_{decay}$	$t_2$
	m/s	m	m	--	s	s	s	s
Office (UFAD)	8	0.04	2.10	5%	0.4	0.13	5.70	6.22
Aircraft Cabin	8	0.01	0.65	5%	0.4	0.04	2.11	2.55

Figure 3-8 shows the results of the jet velocity versus time at different positions from the DES model for both the office and cabin cases. It can be seen from the table that the influence of the  $t_{decay}$  on the  $t_2$  was dominating for both the office and cabin cases. This was supported by the DES model calculation as shown in Figure 3-8. The  $t_2$  was estimated to be 6.22 and 2.55 s through Eq. (3.26) for the office and cabin cases, respectively. The estimated  $t_2$  for the office case was larger than the cabin case, which was also supported by the DES modeling results. As shown in Figure 3-8(a), after the estimated  $t_2$ , 6.22 s, the air velocity had decreased to the surrounding value for the office case. Similarly, after the estimated  $t_2$ , 2.55 s, the air velocity had decreased to the surrounding value for the cabin case, as shown in Figure 3-8(b). The two cases with different jet characteristics show that the  $t_2$  estimated by Eq. (3.26) is acceptable. Hence, the  $t_2$  can be used as the minimum time in which a cough can affect the room airflow distribution.

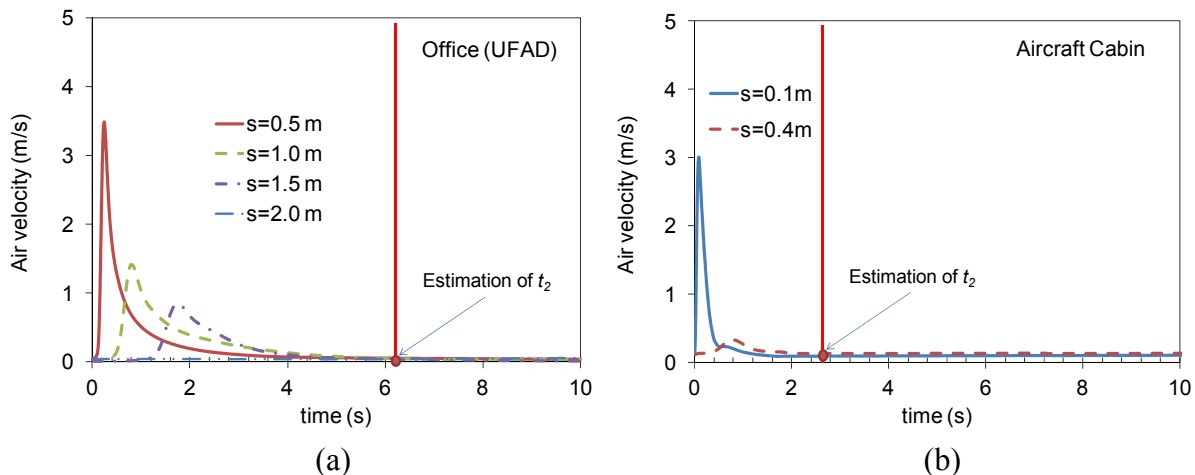


Figure 3-8 Jet velocity versus time from DES model and estimated  $t_2$  for (a) office and (b) aircraft cabin case.

### 3.3 Validation of the Hybrid Model

With the calculation procedure as shown in Figure 3-1 and the two time constants as determined by Eqs. (3.15) and (3.26), this investigation used the hybrid model for predicting the transient particle concentration distribution in the first-class cabin of an MD-82 aircraft cabin. The cabin was fully-occupied by manikins and mechanically ventilated. The case was an ideal one for studying person-to-person transient particle transport in a mechanical ventilated space. Since we have conducted experimental measurements of transient particle distribution in the cabin, the data can be used to validate the hybrid model. This section details our effort in the model validation.

#### 3.3.1 Experimental setup

Figure 3-9(a) shows the schematic model of the fully-occupied first-class cabin of the MD-82 aircraft. The cabin contained three rows of seats, and each row had four seats as numbered in Figure 3-9(b). A detailed description of the cabin can be found in Liu et al. (2012). The heated manikins were built by wrapping solid manikins with nickel-chromium wires. The sensible heat production of the manikin was 75 W (2013). The airflow and thermal boundary conditions of the first-class cabin were measured previously by Liu et al. (2012, 2013).

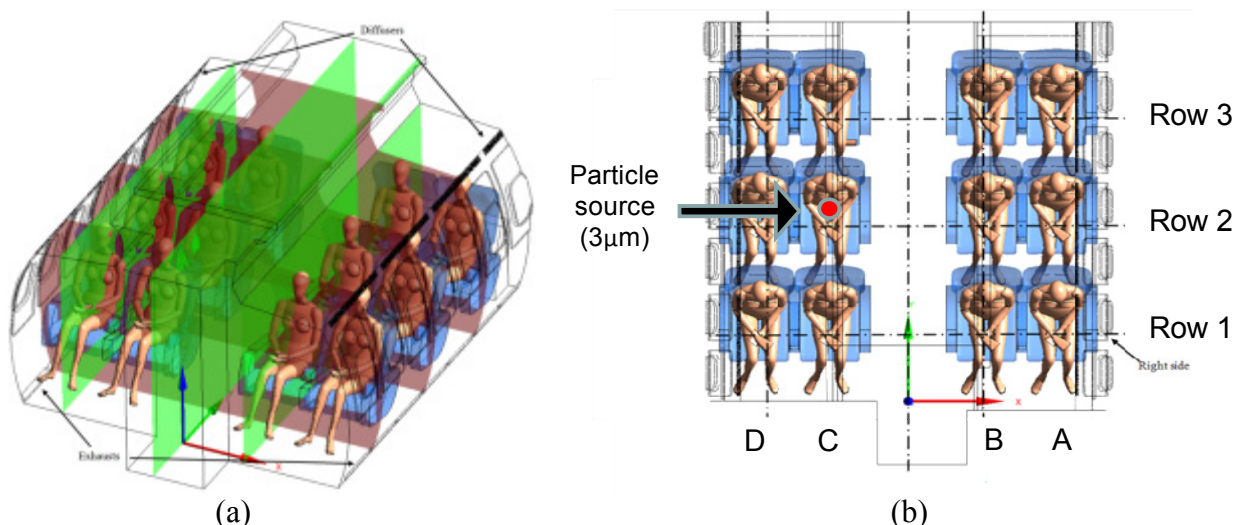


Figure 3-9 Schematic of the fully-occupied first-class cabin: (a) perspective view and (b) plane view (Liu et al., 2013).

The manikin 2C was set as the index passenger with a particle source. At the mouth, particles were released to the cabin air through a tube of 0.01 m in diameter at a speed of  $1.03 \pm 0.02$  m/s. Although the speed was different from a real cough, the experiment was still meaningful since the aim of this study was to provide reliable experimental data to validate the hybrid model. To simulate a cough, an electromagnetic valve was installed in the tube. Then the particle release time could be controlled. A MAG 3000 PALAS particle generator was used to generate Di-Ethyl-Hexyl-Sebacat (DEHS) mono-size particles with a diameter of  $3 \mu\text{m}$ . DEHS is a non-soluble liquid with a low evaporation rate and a density of  $912 \text{ kg/m}^3$ .

The particle concentrations versus time at the breathing zones were measured in front of each passenger's mouth. An aerodynamic particle sizer (APS 3321, TSI Inc., St. Paul, MN) spectrometer was used to measure the particle concentration. To measure the transient particle concentration in a location, the sampling time should be larger than the response time of the aerodynamic particle sizer but should also be as short as possible. The response time of the instrument was 1 s so it was used in the experiment. Since only one particle sizer spectrometer was available, the particle concentrations versus time were measured for one passenger at a time. The measurement time for each passenger was set as 500 s, so the entire experiment for measuring 11 passengers took about 2 hours. The complete experiment was repeated 3 times on different days. Since the experimental data quality is related to the repeatability of the experiment, Figure 3-10 compares the three independent measurements of particle concentration versus time, taking 1B and 2A as examples. It can be seen that the three independent measurements matched very well with each other. Hence, the repeatability of the experiment is acceptable.

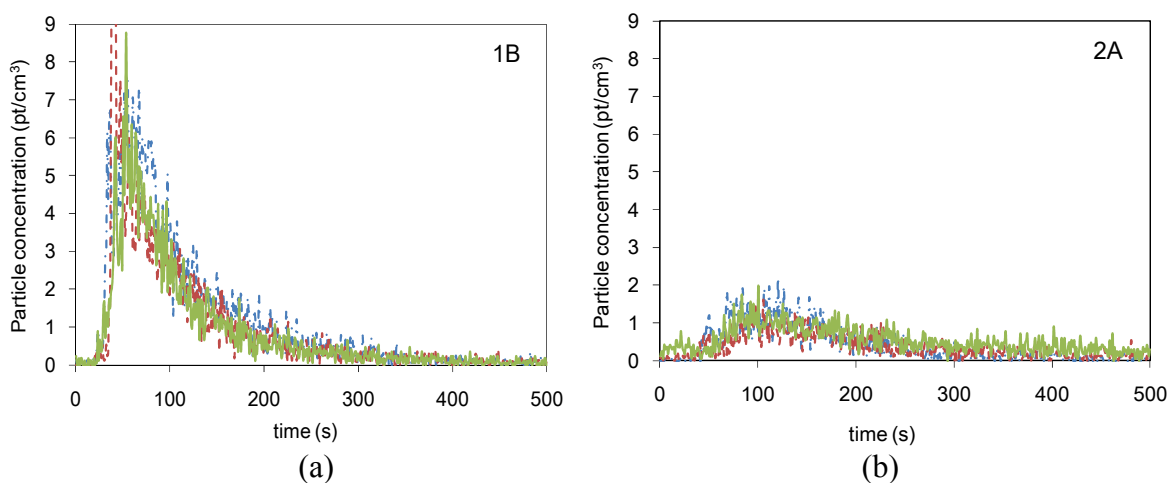


Figure 3-10 Comparison of three independent measurements of particle concentration versus time for (a) 1B and (b) 2A.

The source release time is also an important factor of experimental data quality. A single cough lasts for less than 1 s (Gupta et al., 2009). With such a short source release time in the experiment, the particle concentrations in the cabin may be too low to be detected by the aerodynamic particle sizer, so the data quality would be poor. Therefore, the source release time should be increased to some extent. Although the increased source release time was different from the real coughing case, the experiment was still meaningful since the aim of this study was to provide reliable experimental data to validate the hybrid model. If the source release time had been too long, the experiment might have become a steady-state case. Hence, the source release time still needs to be as short as possible to meet the purpose of this study, while the particle concentrations at the breathing zone of other manikins should be detectable with the aerodynamic particle sizer. This investigation compared the particle concentration versus time at 1A and 2A under three different source release times: 5, 20, and 60 s, as shown in Figure 3-11. It can be seen that a 5 s source release time cannot result in obvious particle concentration peaks. A 20 s source release time can generate a peak concentration that is more than 5 times the

background concentration. Although a 60 s source release time can result in even higher peaks, this may be too long for a transient particle transport case. Hence, a 20 s source release time was applied in the experiment.

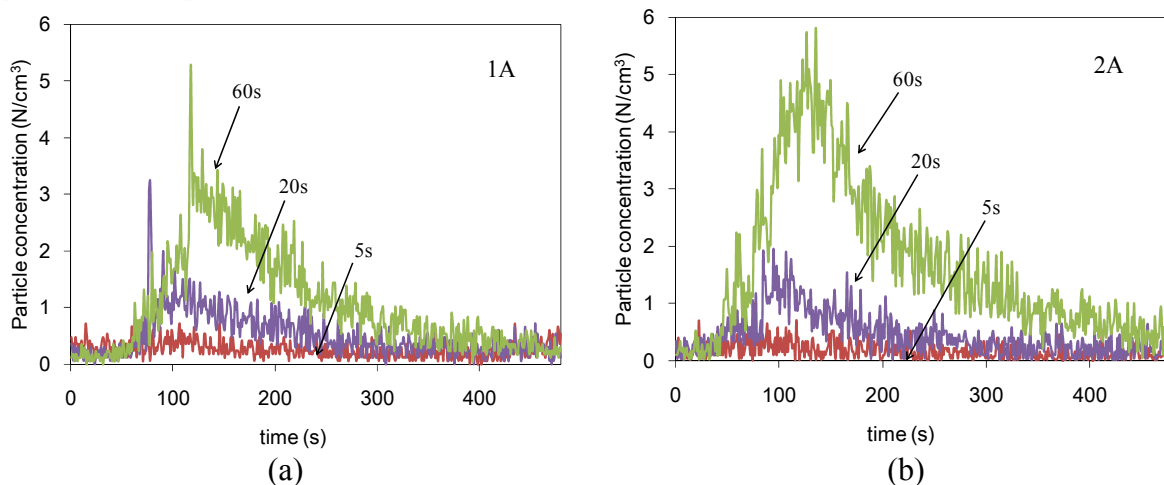
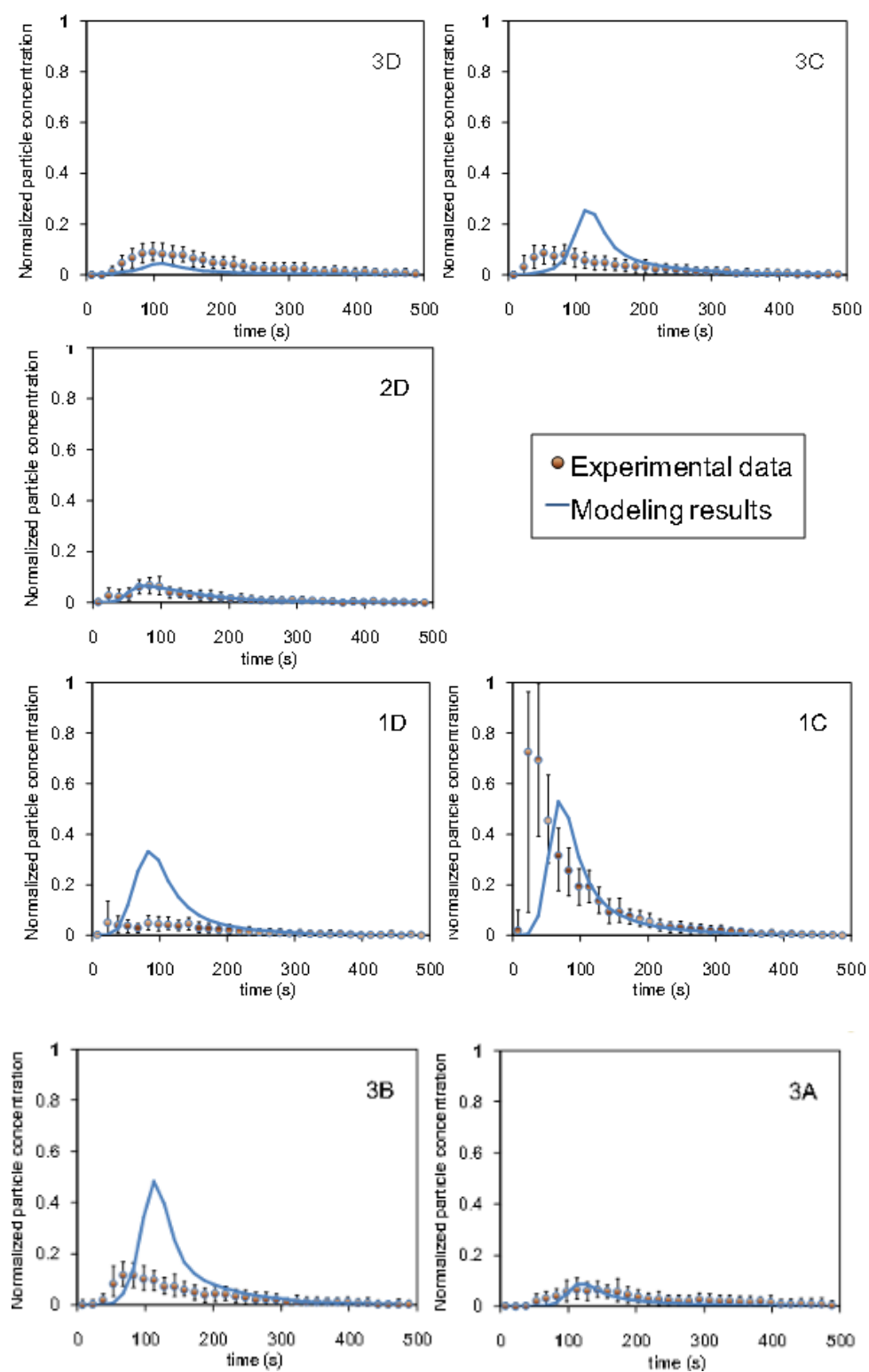


Figure 3-11 Comparison of the particle concentration levels when the source release time was 5, 20, and 60 s for (a) 1A and (b) 2A.

### 3.3.2 Validation

The hybrid model was then used to calculate the transient particle distribution in the first-class cabin of the MD-82 aircraft by using the digital geometry model as shown in Figure 3-9. The numerical simulation was conducted using the CFD code ANSYS Fluent 12.1. The user-defined function (UDF) was implemented to realize the Eulerian drift flux model. Three grid resolutions (6.4, 8.4, and 13 million) were tested for CFD grid independence. The 6.4 million grid resolution was sufficiently fine to capture such a flow. When using the Lagrangian method, 500,000 particles with a diameter of 3  $\mu\text{m}$  were generated during the 20 s source release time. The particle source in-cell (PSI-C) scheme (Zhang and Chen, 2006) was used to translate the trajectories into the concentrations. The time step was set at 0.02 s. The particle deposition was neglected in the simulations due to the large air change rate in the aircraft cabin (Gupta et al., 2011a). The  $t_1$  and  $t_2$  was estimated to be 51 and 22.3 s by using Eqs. (3.17) and (3.26), respectively, for the cabin.

Figure 3-12 compares the numerical results of the transient particle concentrations at the breathing zone of each passenger with the corresponding experimental data. For easy observation, the experimental data were averaged every 15 s. Since the experiment was repeated 3 times, each solid point in the figure represents the average value of the 45 data points ( $15 \times 3 = 45$ ). The lower and upper bound of the error bars represents the 10<sup>th</sup> and 90<sup>th</sup> percentile of the 45 data points, respectively. The experimental data and modeling results were normalized by the maximum concentration among the monitoring points for the entire experiment. The comparison in Figure 3-12 shows that the trend of the particle concentration variation versus time predicted by the hybrid model agrees with the experimental data.



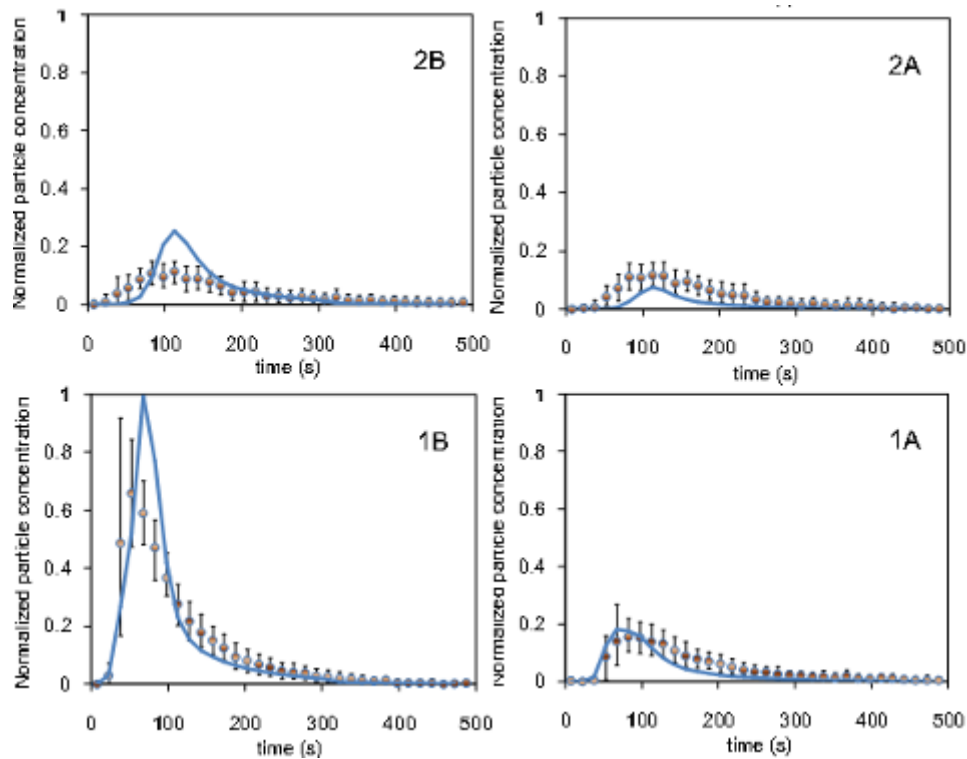


Figure 3-12 Comparison of the numerical results of transient particle concentrations at the breathing zone of each manikin with the corresponding experimental data. The experimental data and modeling results were normalized by the maximum concentration among the monitoring points for the entire experiment.

Note that a large portion of the released particles moved forward from 2C to 1B, and 1C and resulted in relatively high peak concentrations. The rest of the particles dispersed to other locations and also led to peaks but with lower concentrations. The hybrid model over-predicted the concentrations at 1D, 3B, and 3C and somewhat under-predicted at 1C. We suspected that the discrepancies were mainly attributed to the differences between the modeled and measured airflow fields, as shown in Figure 3-13. Observing the experimental data, very limited portion of particles moved backward, which indicated that the general direction of the airflow above 2C was pointing forward. However, the modeled airflow showed the existence of both the forward and backward directions. Therefore, the modeling results showed that a considerable portion of particles moved backward so that the concentrations at 3B and 3C increased. The airflow distribution in aircraft cabins is extremely complicated and difficult to model accurately (Zhang et al., 2009; Liu et al., 2012; 2013). Nevertheless, the hybrid model can predict the transient particle concentration distribution for engineering applications.

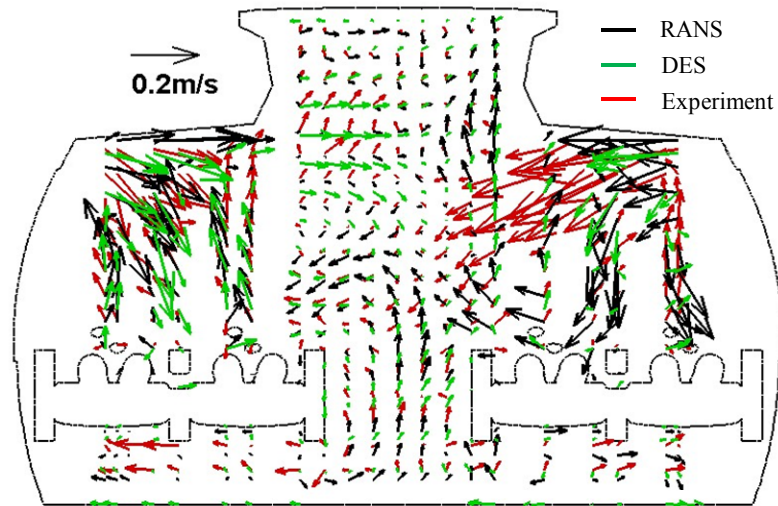


Figure 3-13 Comparison of the numerical results of the air velocity vectors with the experimental data from Liu et al. (2013) at the cross-section through the third row.

### 3.4 Discussion

The validation section has shown that the hybrid model is acceptable for engineering applications. In addition, the hybrid model can significantly reduce the computing cost in two aspects. First, the traditional approach for obtaining the time-dependent flow distribution using the DES model is Approach\_2b or Approach\_3. However, the hybrid model uses Approach\_2a, which can save about 75% of the computing time compared with Approach\_2b or Approach\_3. Secondly, Wang et al. (2012) recommended using the DES-Lagrangian model for transient particle transport simulations. The hybrid model uses the DES-Lagrangian model in the first few seconds of the flow time and the RANS-Eulerian model afterwards. The RANS-Eulerian model can save about 84% of the computing time compared with the DES-Lagrangian model (Wang et al., 2012). The ratio of the computing time by the hybrid model to the DES-Lagrangian model is:

$$\frac{T_{\text{hybrid}}}{T_{\text{DES-Lagrangian}}} = \frac{t_{\text{DES-Lagrangian}} + (1-84\%) \cdot t_{\text{RANS-Eulerian}}}{t_{\text{DES-Lagrangian}} + t_{\text{RANS-Eulerian}}} \quad (22)$$

where  $t_{\text{DES-Lagrangian}}$  and  $t_{\text{RANS-Eulerian}}$  is the computing time used by DES-Lagrangian and RANS-Eulerian, respectively, for the hybrid model. Taking the first-class cabin of the MD-82 aircraft as an example, the  $t_{\text{DES-Lagrangian}}$  and  $t_{\text{RANS-Eulerian}}$  were 22.3 and 477.7 s, respectively. Then  $T_{\text{hybrid}}/T_{\text{DES-Lagrangian}}$  was only 20%; that is, the hybrid model can save about 80% of the computing time compared with the DES-Lagrangian model. Therefore, the proposed hybrid model can significantly reduce the computing costs.

It should be noticed that a person who is very ill with a respiratory infection tends to cough more than just once. To take this factor into account, the super-imposition method proposed by Gupta et al. (2011b) can be used together with our experimental or modeling data to estimate the effect of multiple coughs. Furthermore, a lot of people attempt to cover their mouth with their hand or a

tissue when they cough. However, a model for predicting exhaled particle transport by coughs with covering the mouth with a hand or tissue is not available, which deserves further investigations. Our study simulated a scenario when a coughing passenger who was at sleep so he/she could not cover the mouth when coughing.

### 3.5 Conclusions

This chapter proposed a hybrid DES-Lagrangian and RANS-Eulerian model for investigating transient particle transport in enclosed environments. From the results presented in this chapter, the following conclusions can be made:

- (1). This study proposed how to estimate the two key time constants for the model,  $t_1$  and  $t_2$ . The estimated  $t_1$  and  $t_2$  were verified by an office and an aircraft cabin case.
- (2). This investigation conducted experimental measurements of transient particle distributions in the first-class cabin of an MD-82 aircraft cabin to validate the hybrid model. The results show that the model can predict the trend of the transient particle concentration distribution when compared with the experimental data.
- (3). The proposed hybrid DES-Lagrangian and RANS-Eulerian model can be used for investigating transient particle transport in enclosed environments with relatively high accuracy, while the computing time can be reduced by 80%.

## 4. A COMBINED CFD AND MARKOV CHAIN METHOD FOR PREDICTING TRANSIENT PARTICLE TRANSPORT

The review in Chapter 2 shows that a combination of CFD with the Markov chain technique has the potential to provide accurate and fast-than-real-time information of spatial and temporal particle concentrations. Therefore, this chapter aimed to develop and validate a combined CFD and Markov chain method for quickly predicting transient particle transport in enclosed environments.

### 4.1 Development of the Method

#### 4.1.1 Markov chain model

There are two assumptions in the first-order homogeneous Markov chain technique (Ross, 1996):

- 1) Any future state depends only on the present state as well as the probabilities of the state's changing;
- 2) These probabilities of the state's changing are time-independent (or fixed).

To satisfy these assumptions of the Markov chain technique, one should assume the inertial effect of particles to be negligible, which holds well for particles with a diameter smaller than 3  $\mu\text{m}$  (Zhao et al., 2009a; Yin et al., 2011). For particles with a diameter larger than 3  $\mu\text{m}$ , if they are transported by an impinging jet with an extremely high velocity, the inertial impaction may significantly affect the particle transport (Chen et al., 2012). In such scenarios, the first-order homogeneous Markov chain method could have a large error. However, since most of the airflow in enclosed environment does not have strong impinging jets, this method still can be used for particles with a diameter larger than 3  $\mu\text{m}$ . Since the coarse particles intend to rapidly deposit onto the floor, they may be less important in term of airborne infectious diseases transmission.

The first step is to divide the target enclosed environment into  $n-1$  zones. The zone  $n$  can be assigned to represent the space to where the particles are removed. Then the probabilities of the state's changing can form an  $n \times n$  transition probability matrix,  $p_{ij}$ :

$$P = (p_{ij})_{(n \times n)} = \begin{pmatrix} p_{11} & p_{12} & \cdots & p_{1n} \\ p_{21} & p_{22} & \cdots & p_{2n} \\ \vdots & \vdots & & \vdots \\ p_{n1} & p_{n2} & \cdots & p_{nn} \end{pmatrix} \quad (4.1)$$

where  $p_{ij}$  is the probability of a particle's moving from zone  $i$  to zone  $j$  in a certain time step,  $\Delta t$ . The most important property of the transition probability matrix is:

$$\sum_{j=1}^n p_{ij} = 1, \quad p_{ij} \geq 0 \quad (4.2)$$

If we assume that the removed particles cannot re-enter the space, which corresponds to the scenario of a completely fresh-air ventilation system, then:

$$p_{nj} = (0 \ 0 \ \cdots \ 0 \ 1) \quad (4.3)$$

For a fixed airflow field, it is expected that the transition probability matrix is also fixed, because the movement of the particles normally does not have a notable impact on the airflow field.

Assuming that a particle has a probability vector at the present state (state  $k$ ):

$$\pi_k = (\pi_{k,1} \ \pi_{k,2} \ \cdots \ \pi_{k,n}) \quad (4.4)$$

then, after one time step (state  $k+1$ ), the probability of this particle's moving to zone  $j$  can be calculated by:

$$\pi_{k+1,j} = \pi_{k,1}p_{1,j} + \pi_{k,2}p_{2,j} + \cdots + \pi_{k,n}p_{n,j} \quad (4.5)$$

Thus, the probability vector for the particle at state  $k+1$  can be calculated by:

$$\pi_{k+1} = \pi_k P \quad (4.6)$$

If the particle is initially released from zone  $m$ , the probability vector of the particle at the initial state (state 0) is:

$$\pi_{0,i} = \begin{cases} 1, & i = m \\ 0, & i \neq m \end{cases} \quad (4.7)$$

If we calculate the particle transport from state 0, the probability vector of the particle at state  $k+1$  can be calculated by:

$$\pi_{k+1} = \pi_0 P^{k+1} \quad (4.8)$$

If the zones are of the same size, the resulting probability vector versus time can be regarded as the normalized particle concentrations (or normalized number of particles) versus the time in the zones. Therefore, the Markov chain technique can be used for predicting transient particle transport in enclosed environments. Moreover, for a fixed airflow, when the source location is changed, Eq. (4.8) can be used with an updated  $\pi_0$  to quickly calculate the updated particle concentrations versus time. Note that the fixed airflow could be a problem if the source could change the airflow pattern, such as a powerful sneezing without covering the mouth. However, the experimental measurements and then computer simulation of airflow in an airliner cabin by Gupta et al. (2011a) indicated that even a cough without covering mouth can have limited affect on the local airflow field but not the whole airflow field. If a mouth is covered when coughing or sneezing as people would usually do, the influence of coughing and sneezing on the airflow field

would be minimal. Therefore, the assumption that airflow field was fixed should be valid for most of cases.

#### 4.1.2 Calculating the transition probability matrix using CFD

The key point in applying the Markov chain technique to the prediction of indoor particle transport is to obtain the transition probability matrix,  $p_{ij}$ . This study calculated the airflow field using CFD. Next, this investigation uniformly released a certain amount of particles in zone  $i$ , and used Lagrangian stochastic tracking to calculate the percentage of particles that moved from zone  $i$  to zone  $j$  in a certain time,  $\Delta t$ , which can be regarded as the  $p_{ij}$ . Repeating this process for all the zones, the whole transition probability matrix can be obtained. The following paragraphs detail the CFD model used in this study.

The Re-Normalization Group (RNG)  $k-\varepsilon$  model (Choudhury, 1993) was applied to calculate the airflow field. It has the best overall performance among all RANS models for enclosed environments (Zhang et al., 2007). A detailed discussion of the RNG  $k-\varepsilon$  model can be found in Fluent (2005).

The Lagrangian model was adopted to calculate the particle movements in  $\Delta t$ . Using the momentum equation based on Newton's law, the trajectory of each particle can be calculated by:

$$\frac{d\vec{u}_p}{dt} = F_D(\vec{u}_a - \vec{u}_p) + \frac{\vec{g}(\rho_p - \rho_a)}{\rho_p} + \vec{F}_a \quad (4.9)$$

where  $\vec{u}_p$  is the velocity vector of the particle;  $\vec{u}_a$  the velocity vector of the air;  $\vec{g}$  the gravitational acceleration vector;  $\rho_p$  and  $\rho_a$  the particle and air density, respectively; and  $\vec{F}_a$  Brownian motion and the Saffman lift force. The Saffman lift force was included because it may be relatively large near a room's wall for fine indoor particles (Zhao et al., 2004). The drag force is calculated by:

$$F_D(\vec{u}_a - \vec{u}_p) = \frac{18\mu}{\rho_p d_p^2} \frac{C_D Re}{24} (\vec{u}_a - \vec{u}_p) \quad (4.10)$$

where  $\mu$  is fluid viscosity,  $C_D$  the drag coefficient,  $Re$  the Reynolds number, and  $d_p$  the particle diameter. The transient process from a droplet to a droplet nucleus due to evaporation is negligible for particles with a diameter smaller than 3  $\mu\text{m}$  (Chen and Zhao, 2010).

The Discrete Random Walk (DRW) model (Fluent, 2005) is used to calculate the turbulence dispersion:

$$u'_i = \zeta_i \sqrt{2k/3} \quad (4.11)$$

where  $\zeta_i$  is a normal random number.

Note that the time step of the Markov chain,  $\Delta t$ , is an important parameter that needs to be determined based on the ventilation rate of the space and the size of the divided zones. The  $\Delta t$  can be neither too short nor too long. If the  $\Delta t$  is too short, the particles may have no chance to “escape” from the current zone. If the  $\Delta t$  is too long, the particles may move across the adjacent zones so that the fact that they had appeared in these adjacent zones would be missed. Thus, the  $\Delta t$  should allow the particles to move only to the adjacent zones. In addition, to ensure the  $\Delta t$  to be suitable for all the zones, the sizes and dimensions of the zones should be similar. In this study, different time steps of the Markov chain method were tested for each case and the appropriate ones were then used. The specific formulas for determining the time step are not yet available. However, there may be two rules. First, the larger the air change rate is, the smaller the time step intends to be. Second, the smaller the size of the zones becomes, the smaller the time step intends to be. It would take less time for the particles to move across the adjacent zones when the size of the zones is smaller or the air change rate is larger.

## 4.2 Validation

This study used three cases, particle transport in an isothermal clean room (Murakami et al., 1992), a room with an Under-Floor Air-Distribution (UFAD) system (Zhang and Chen, 2006), and the first-class cabin of an MD-82 airliner (Chen et al., 2013), to validate the combined CFD and Markov chain method. This section discusses the validation results.

### 4.2.1 Particle transport in an isothermal clean room

The first study was the case of particle transport in a ventilated clean room as addressed by Murakami et al. (1992), who conducted detailed measurements of particle distributions in a room. Figure 4-1(a) shows the configuration of the clean room with two ceiling supply diffusers and four exhausts located on the lower walls of the room. The total air exchange rate was 40 ACH. The thermo-fluid boundary conditions were defined according to the measurements. The details of the measured boundary conditions can be found in Murakami et al. (1992). The particle diameter used was 1  $\mu\text{m}$ . The review by Lai (2002) indicated that the deposition velocity of the particles with a diameter of 1  $\mu\text{m}$  ranged from  $8 \times 10^{-6}$  to  $2 \times 10^{-5}$  m/s in indoor environments. Thus, the deposition rate for such particles in this room ranged from 0.048 to 0.12 per hour. This was much lower than the air change rate in this room. Therefore, the influence of particle deposition on the results can be neglected. Furthermore, the particle resuspension was also negligible due to the low resuspension rate associated with 1  $\mu\text{m}$  particles (Zhu et al., 2012). As shown in Figure 4-1(b), we divided the room into six zones and labeled the “removal zone” as zone 7.

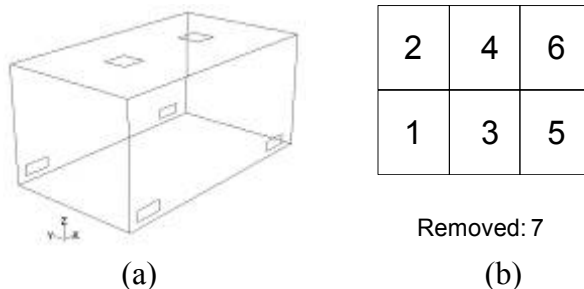


Figure 4-1 (a) Configuration of the clean room studied by Murakami et al. (1992) and (b) the zones of the clean room on a horizontal plane.

Based on the calculated airflow field and Lagrangian particle tracking, the transition probability matrix can be obtained:

$$P = \begin{pmatrix} 0.61 & 0.01 & 0.07 & 0.00 & 0.00 & 0.00 & 0.31 \\ 0.04 & 0.63 & 0.00 & 0.01 & 0.00 & 0.00 & 0.32 \\ 0.08 & 0.00 & 0.69 & 0.10 & 0.13 & 0.00 & 0.00 \\ 0.00 & 0.15 & 0.04 & 0.70 & 0.00 & 0.10 & 0.00 \\ 0.00 & 0.00 & 0.03 & 0.00 & 0.70 & 0.02 & 0.25 \\ 0.00 & 0.00 & 0.00 & 0.03 & 0.02 & 0.67 & 0.27 \\ 0.00 & 0.00 & 0.00 & 0.00 & 0.00 & 0.00 & 1.00 \end{pmatrix} \quad (4.12)$$

The time step of the Markov chain,  $\Delta t$ , was set as 15 s for this case, which ensures that particles move only to the adjacent zones within the  $\Delta t$ . Two scenarios, in which the particle source was located in zone 3 and zone 6, respectively, were used to validate the Markov chain method. The initial probability vector was:

$$\begin{aligned} \pi_0 &= (0 \ 0 \ 1 \ 0 \ 0 \ 0 \ 0), \quad \text{source in zone 3} \\ \pi_0 &= (0 \ 0 \ 0 \ 0 \ 0 \ 1 \ 0), \quad \text{source in zone 6} \end{aligned} \quad (4.13)$$

Using Eq. (4.8), the probability vectors versus time of particle transport can be calculated.

The experiment measured only the steady-state airflow field and particle distributions. Validation of the Markov chain model would require transient particle distributions. However, our earlier study (Wang et al. 2012) validated the RNG  $k-\varepsilon$  – Eulerian drift flux model for this case with a good result. The model can be used to generate transient distributions of particle concentrations as the basis for validating the Markov chain model. Because steady-state and transient particle dispersion are governed by the same physics, this approach would not compromise accuracy.

Figures 4-2 and 4-3 compare the trends of the normalized particle concentrations versus time, as obtained by the Markov chain method and CFD simulations with a source in zones 3 and 6, respectively. The CFD simulation results were obtained by averaging the particle concentrations in each zone. Furthermore, all of the particle concentrations were normalized by the maximum concentration observed in the room. Figure 4-2 shows that both the Markov chain and CFD methods predicted higher particle concentrations in zones 1, 4, and 5 as compared with that in zones 2 and 6. This occurred because zones 1, 4, and 5 were adjacent to zone 3, where the source was located. A comparison of Figures 4-2 and 4-3 shows that both the Markov chain and CFD methods predicted higher particle concentrations with a source in zone 3 than with a source in zone 6. The results make sense because a large portion of particles were directly removed through the exhaust located in zone 6, which resulted in low concentrations in other zones for the case with source in zone 6. In general, the trends of transient particle transport predicted by the Markov chain method agree well with the results of the CFD simulations.

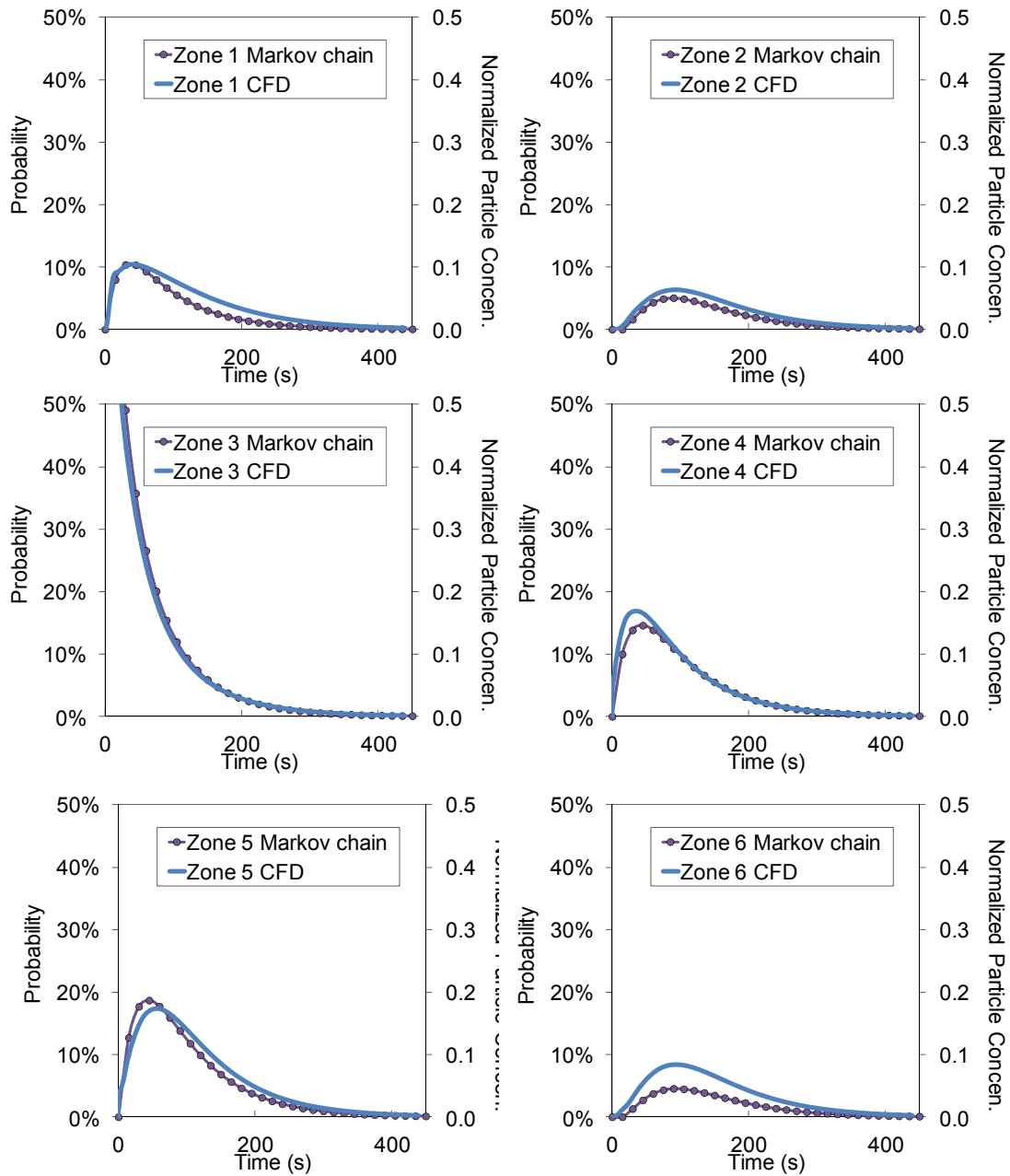


Figure 4-2 Comparison of the trends of the normalized particle concentrations versus time as obtained by the Markov chain method and CFD simulation with a source in zone 3 for the isothermal clean room.

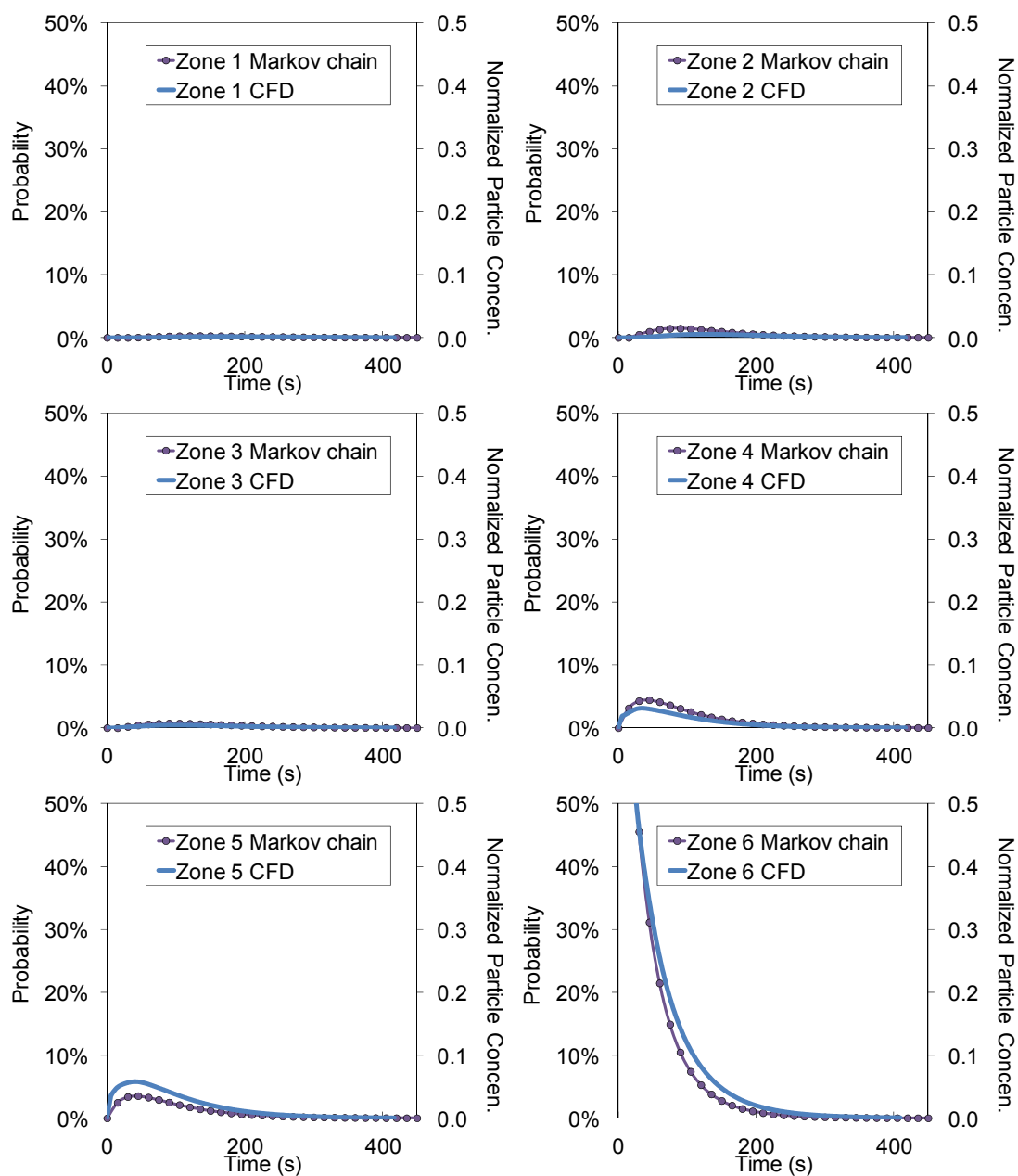


Figure 4-3 Comparison of the trends of the normalized particle concentrations versus time as obtained by the Markov chain method and CFD simulation with a source in zone 6 for the isothermal clean room.

#### 4.2.2 Particle transport in a room with a UFAD system

The second case was a room with a UFAD system, as shown in Figure 4-4(a) and used by Zhang and Chen (2006) for measuring particle distributions. They used four heated boxes to simulate occupants in the room. The air was supplied through two floor inlets and exited through the exhaust at the ceiling. The total air exchange rate was 5.5 ACH. The thermo-fluid boundary

conditions were defined according to the measurements. The detailed measured boundary conditions can be found in Zhang and Chen. (2006). The studied particle diameter was 1  $\mu\text{m}$ . The deposition rate for such particles in this room ranged from 0.046 to 0.116 per hour. This was much lower than the air change rate in this room. Therefore, the influence of particle deposition was negligible. In addition, the particle resuspension was also neglected for this case. As shown in Figure 4-4(b), our investigation divided the room into six zones, with zone 7 as the “removal zone.”

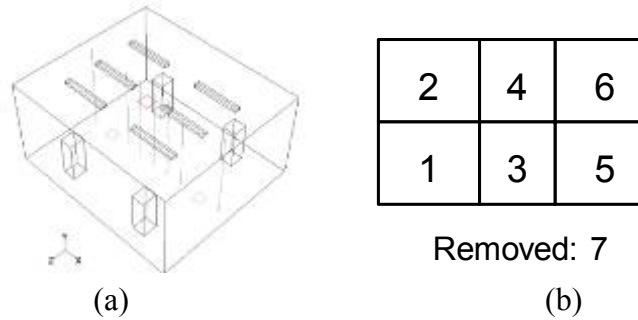


Figure 4-4 (a) Configuration of the room with the UFAD system studied by Zhang and Chen (2006) and (b) the zones of the room on a horizontal plane.

Based on the calculated airflow field and Lagrangian particle tracking, the transition probability matrix is:

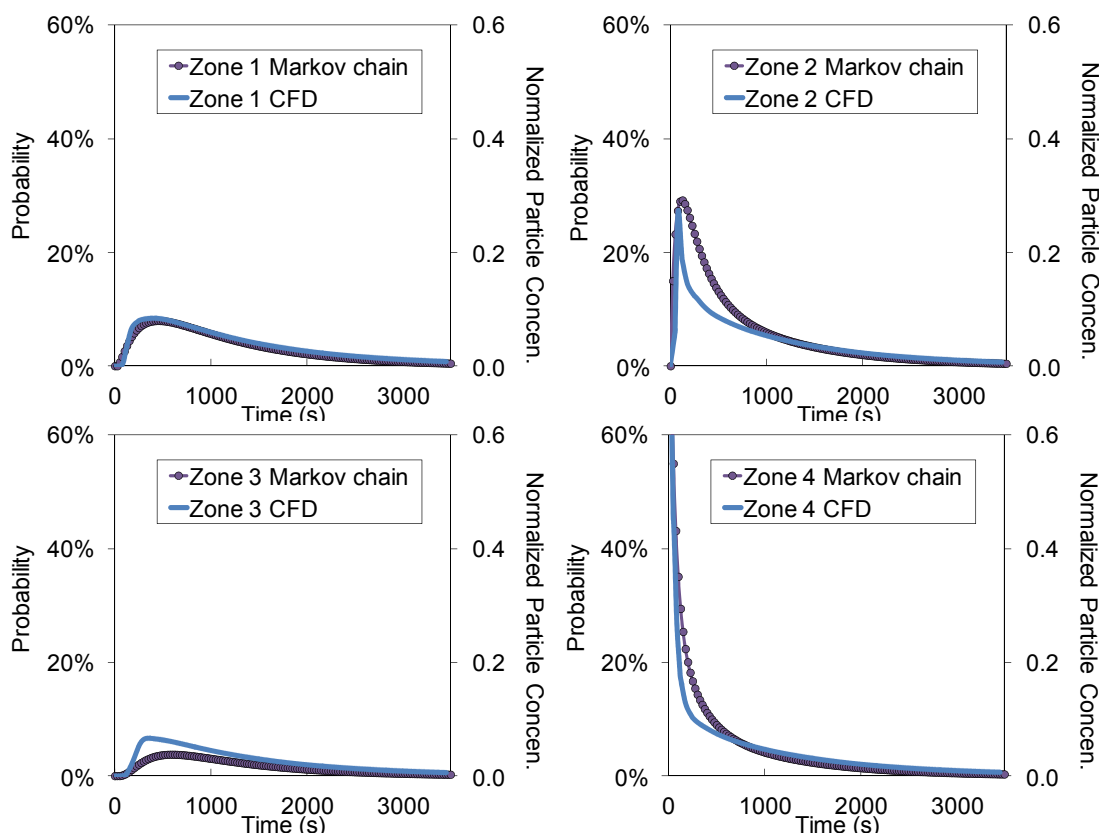
$$P = \begin{pmatrix} 0.85 & 0.04 & 0.11 & 0.00 & 0.00 & 0.00 & 0.00 \\ 0.05 & 0.82 & 0.00 & 0.13 & 0.00 & 0.00 & 0.00 \\ 0.15 & 0.00 & 0.78 & 0.07 & 0.00 & 0.00 & 0.00 \\ 0.00 & 0.15 & 0.00 & 0.73 & 0.00 & 0.00 & 0.12 \\ 0.00 & 0.00 & 0.14 & 0.00 & 0.77 & 0.09 & 0.00 \\ 0.00 & 0.00 & 0.00 & 0.09 & 0.07 & 0.84 & 0.00 \\ 0.00 & 0.00 & 0.00 & 0.00 & 0.00 & 0.00 & 1.00 \end{pmatrix} \quad (4.14)$$

The time step of the Markov chain,  $\Delta t$ , was set as 25 s for this case. The size of the zones of the isolation room was close to that of the room with UFAD system, while the air change rate of the isolation room was much larger than that of the room with UFAD system. Therefore, the time step used for the room with UFAD system (25 s) was larger than that for the isolation room (15 s).

Two scenarios, in which the source was located in zone 4 and zone 6, respectively, were used to validate the Markov chain method. The initial probability vector was:

$$\begin{aligned} \pi_0 &= (0 \ 0 \ 0 \ 1 \ 0 \ 0 \ 0), & \text{source in zone 4} \\ \pi_0 &= (0 \ 0 \ 0 \ 0 \ 0 \ 1 \ 0), & \text{source in zone 6} \end{aligned} \quad (4.15)$$

Because of the lack of experimental data for transient particle concentrations, this study again used the CFD results as a benchmark for this study. The CFD simulation was again validated by steady-state experimental data, with good agreement between them. Figures 4-5 and 4-6 compare the trends of the normalized particle concentrations versus time as obtained by the Markov chain method and CFD simulations with a source in zone 4 and zone 6, respectively. The CFD simulation results were again obtained by averaging the particle concentrations in each zone. A comparison of Figure 4-5 with Figure 4-6 shows that both methods predicted lower concentrations in the room with a source in zone 4 than that with a source in zone 6. This occurred because a considerable portion of the particles released from zone 4 tended to be removed directly by the exhaust located in zone 4. It can be seen that the discrepancies between Markov chain and CFD method were larger in some zones than other zones. Note that the particles were uniformly released in each zone when calculating the transition probability matrix. Thus, the uniformities of the particle concentrations in the zones for a real case might influence the accuracy of the Markov chain method. Since the uniformities of the particle concentrations in the zones were different, the accuracies of the Markov chain method in different zones might be also different. Generally speaking, the trends of the normalized particle concentration distributions predicted by the Markov chain method again agreed reasonably well with the CFD simulations. However, because this case is more complicated than the isothermal clean-room case, the agreement tends to be somewhat worse than that for the clean room.



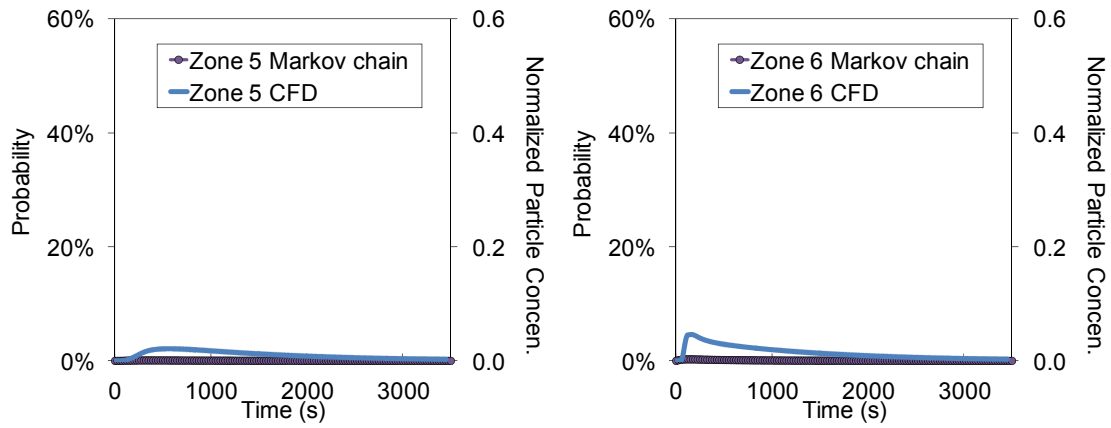
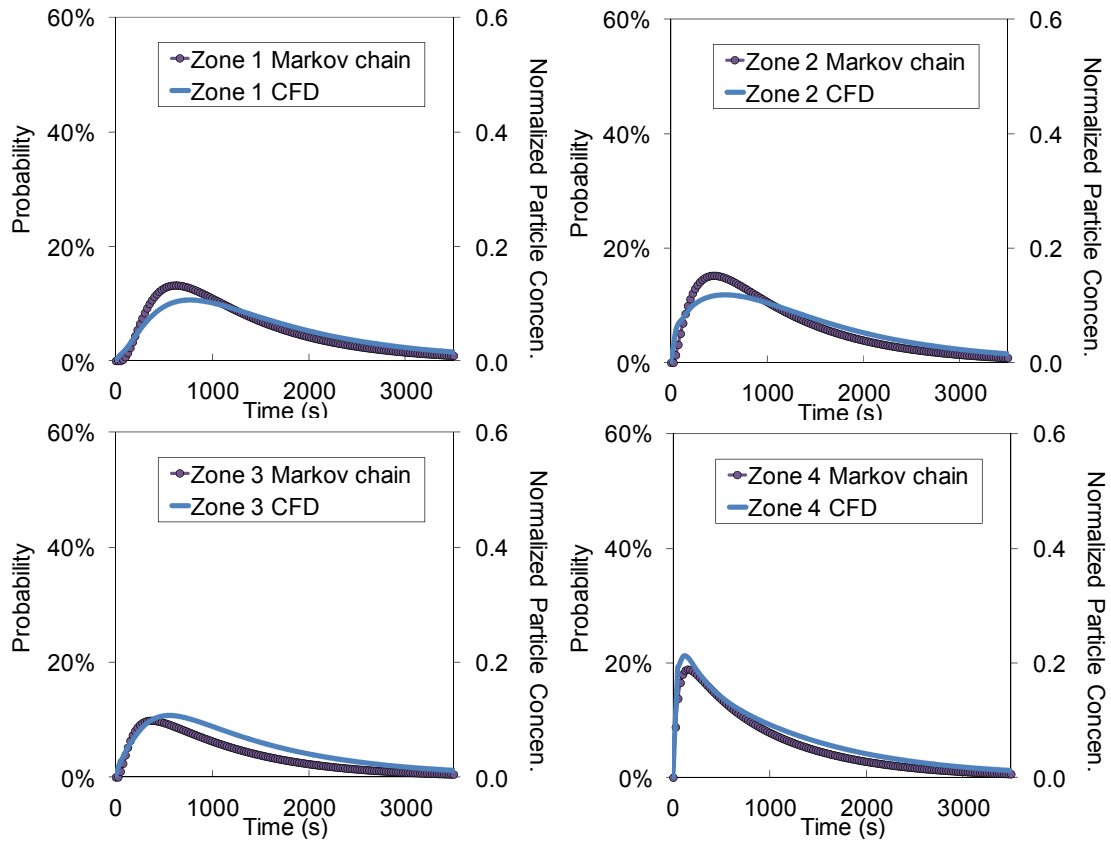


Figure 4-5 Comparison of the trends of the normalized particle concentration distributions versus time as obtained by the Markov chain method and CFD simulation with a source in zone 4 for the room with the UFAD system.



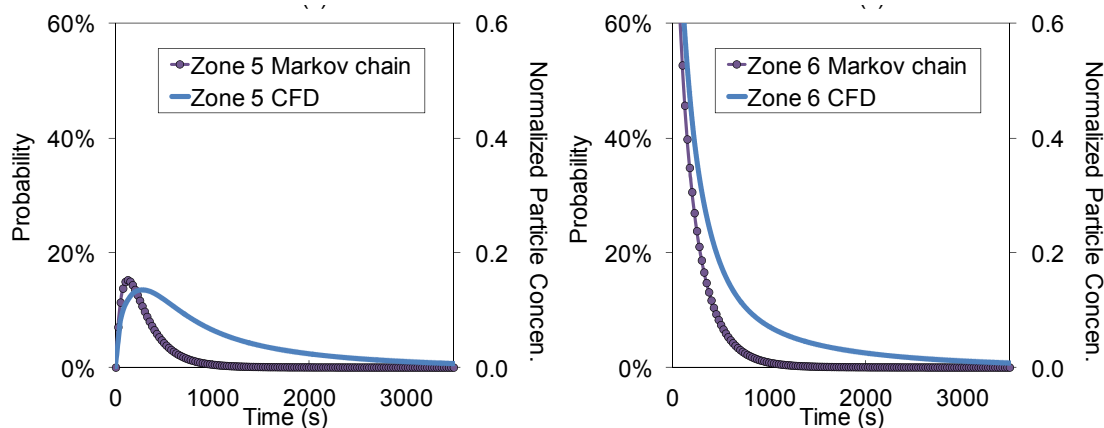


Figure 4-6 Comparison of the trends of the normalized particle concentration distributions versus time as obtained by the Markov chain method and CFD simulation with a source in zone 6 for the room with the UFAD system.

#### 4.2.3 Particle transport in an MD-82 aircraft cabin

The third case was the first-class cabin of a functional MD-82 commercial airliner, as shown in Figure 4-7. Liu et al. (2012) provided a detailed description of the cabin and aircraft and detailed measurements of the thermo-fluid boundary conditions. The cabin had three rows of seats, and each row contained four seats as numbered in Figure 4-7. Manikins were used to simulate passengers. The sensible heat production of each heated manikin was 75 Watt. At the mouth of the manikin in Seat 2C, we released particles with a diameter of  $3\ \mu\text{m}$  into the cabin air for 20 s. The particle concentrations versus time at the breathing zones were measured in front of each passenger's mouth. A detailed description of the experimental procedure and data analysis can be found in Chen et al. (2013). Both the experimental data for the transient particle concentration distributions and the CFD simulation results were used to validate the Markov chain method. You and Zhao (2013) calculated the particle deposition rates in this aircraft cabin. They found that the deposition rate of particles with a diameter of  $3\ \mu\text{m}$  was 1.0 per hour, which was much lower than the air change rate in the aircraft cabin (33 ACH). Therefore, the influence of particle deposition was negligible. Furthermore, the particle resuspension was also neglected (Zhu et al., 2012). As shown in Figure 4-7, we divided the cabin into fifteen zones, with zone 16 as the "removal zone."

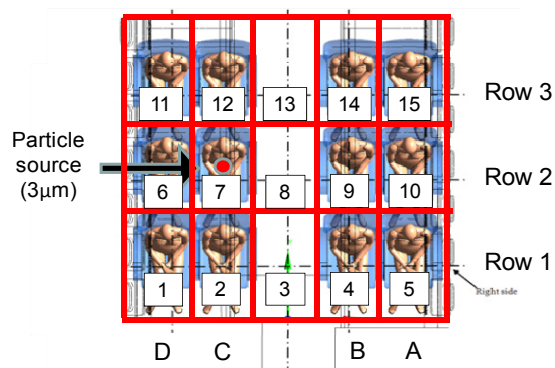


Figure 4-7 The zones of the cabin in a horizontal plane.

Based on the calculated airflow field and Lagrangian particle tracking, the transition probability matrix can be obtained:

$$P = \begin{pmatrix} 0.63 & 0.24 & 0.00 & 0.00 & 0.00 & 0.01 & 0.00 & 0.00 & 0.00 & 0.00 & 0.00 & 0.00 & 0.00 & 0.00 & 0.00 & 0.11 \\ 0.25 & 0.63 & 0.10 & 0.00 & 0.00 & 0.00 & 0.02 & 0.00 & 0.00 & 0.00 & 0.00 & 0.00 & 0.00 & 0.00 & 0.00 & 0.00 \\ 0.00 & 0.33 & 0.37 & 0.29 & 0.00 & 0.00 & 0.00 & 0.01 & 0.00 & 0.00 & 0.00 & 0.00 & 0.00 & 0.00 & 0.00 & 0.00 \\ 0.00 & 0.00 & 0.11 & 0.75 & 0.14 & 0.00 & 0.00 & 0.00 & 0.00 & 0.00 & 0.00 & 0.00 & 0.00 & 0.00 & 0.00 & 0.00 \\ 0.00 & 0.00 & 0.00 & 0.26 & 0.64 & 0.00 & 0.00 & 0.00 & 0.00 & 0.02 & 0.00 & 0.00 & 0.00 & 0.00 & 0.00 & 0.07 \\ 0.13 & 0.00 & 0.00 & 0.00 & 0.00 & 0.39 & 0.19 & 0.00 & 0.00 & 0.00 & 0.11 & 0.00 & 0.00 & 0.00 & 0.00 & 0.17 \\ 0.00 & 0.14 & 0.00 & 0.00 & 0.00 & 0.22 & 0.41 & 0.20 & 0.00 & 0.00 & 0.00 & 0.02 & 0.00 & 0.00 & 0.00 & 0.00 \\ 0.00 & 0.00 & 0.56 & 0.00 & 0.00 & 0.00 & 0.11 & 0.13 & 0.09 & 0.00 & 0.00 & 0.00 & 0.11 & 0.00 & 0.00 & 0.00 \\ 0.00 & 0.00 & 0.00 & 0.11 & 0.00 & 0.00 & 0.00 & 0.23 & 0.51 & 0.07 & 0.00 & 0.00 & 0.00 & 0.09 & 0.00 & 0.00 \\ 0.00 & 0.00 & 0.00 & 0.00 & 0.00 & 0.00 & 0.00 & 0.00 & 0.14 & 0.59 & 0.00 & 0.00 & 0.00 & 0.00 & 0.19 & 0.08 \\ 0.00 & 0.00 & 0.00 & 0.00 & 0.00 & 0.01 & 0.00 & 0.00 & 0.00 & 0.00 & 0.70 & 0.20 & 0.00 & 0.00 & 0.00 & 0.09 \\ 0.00 & 0.00 & 0.00 & 0.00 & 0.00 & 0.00 & 0.19 & 0.00 & 0.00 & 0.00 & 0.03 & 0.64 & 0.14 & 0.00 & 0.00 & 0.00 \\ 0.00 & 0.00 & 0.00 & 0.00 & 0.00 & 0.00 & 0.00 & 0.40 & 0.00 & 0.00 & 0.00 & 0.28 & 0.27 & 0.05 & 0.00 & 0.00 \\ 0.00 & 0.00 & 0.00 & 0.00 & 0.00 & 0.00 & 0.00 & 0.00 & 0.28 & 0.00 & 0.00 & 0.00 & 0.25 & 0.30 & 0.18 & 0.00 \\ 0.00 & 0.00 & 0.00 & 0.00 & 0.00 & 0.00 & 0.00 & 0.00 & 0.00 & 0.04 & 0.00 & 0.00 & 0.00 & 0.39 & 0.45 & 0.12 \\ 0.00 & 0.00 & 0.00 & 0.00 & 0.00 & 0.00 & 0.00 & 0.00 & 0.00 & 0.00 & 0.00 & 0.00 & 0.00 & 0.00 & 0.00 & 1.00 \end{pmatrix} \quad (4.16)$$

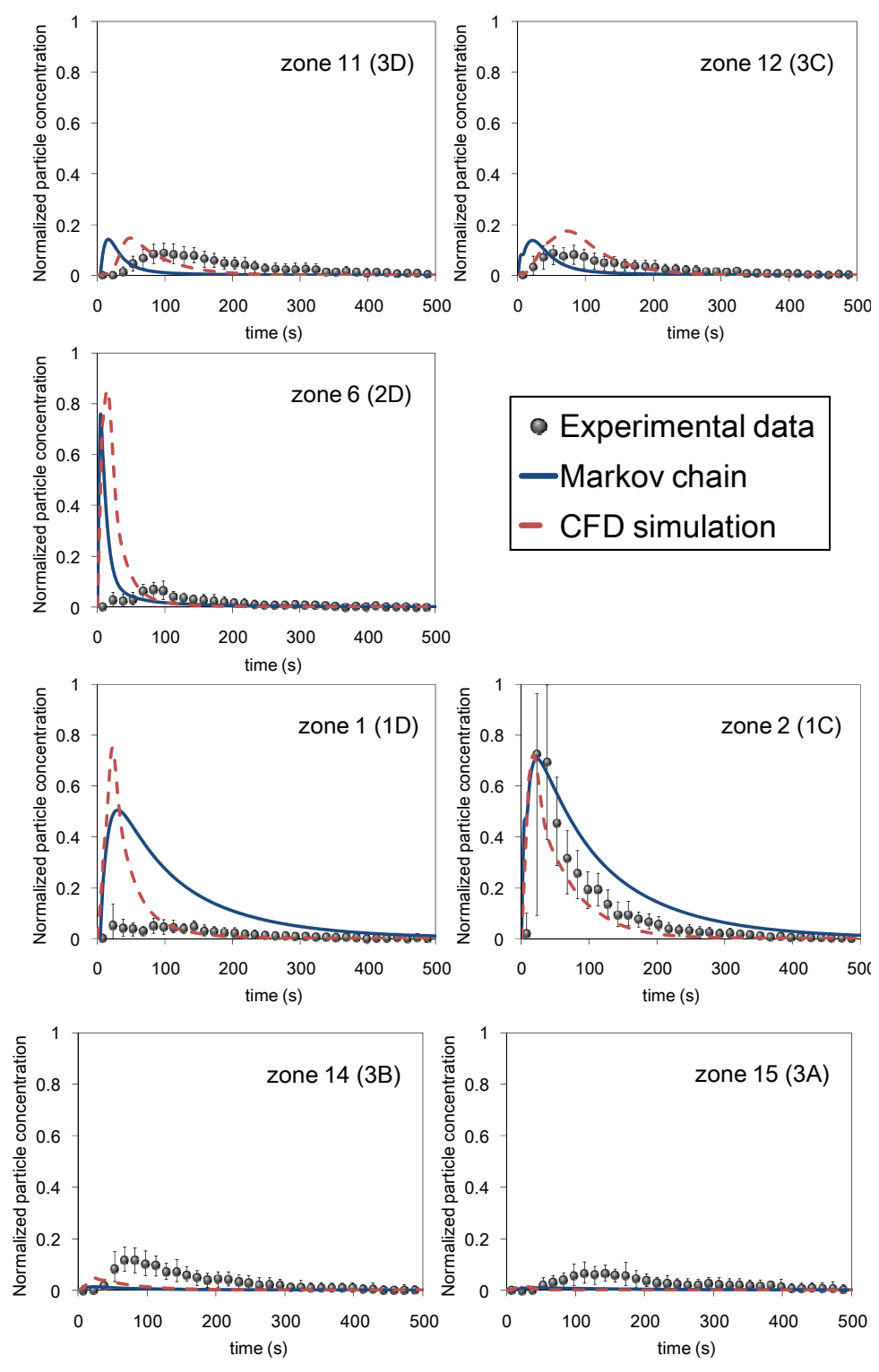
The time step of the Markov chain,  $\Delta t$ , was set as 4 s for this case. The air change rate of the aircraft cabin was close to that of the isolation room, while the size of the zones of the aircraft cabin was much smaller than that of the isolation room. Therefore, the time step used for the aircraft cabin (4 s) was smaller than that for the isolation room (15 s).

To better match the experimental setup, the particles were released only from the mouth of the manikin instead of the whole space of zone 7, where the source was located. The initial probability vector was:

$$\pi_0 = (0 \ 0 \ 0 \ 0 \ 0 \ 0 \ 1 \ 0 \ 0 \ 0 \ 0 \ 0 \ 0 \ 0 \ 0 \ 0) \quad (4.17)$$

Figure 4-8 compares the trends of the normalized particle concentration distribution versus time as obtained by the Markov chain method, CFD simulation, and experimental measurement. The Markov chain method correctly predicted relatively high peak concentrations at Seats 1B and 1C and low concentrations at most of the other seats. However, the Markov chain method over-predicted the concentrations at Seats 1D and 2D. The discrepancies could be attributed to two factors. First, the differences between the simulated and measured airflow fields were significant (Chen et al., 2013), which can cause a large discrepancy in particle concentration distribution. Second, the Markov chain method calculated the average particle concentrations in each zone, while the experiment measured the particle concentration only in the breathing zones. We have further calculated the average particle concentrations in each zone by CFD as shown in Figure 4-8. The CFD simulation also over-predicted the concentrations at Seats 1D and 2D, which confirms the validity of the second factor above. Generally speaking, the Markov chain method

can predict the general trends of the particle concentrations versus time for such a complex case, and it may be used for engineering applications.



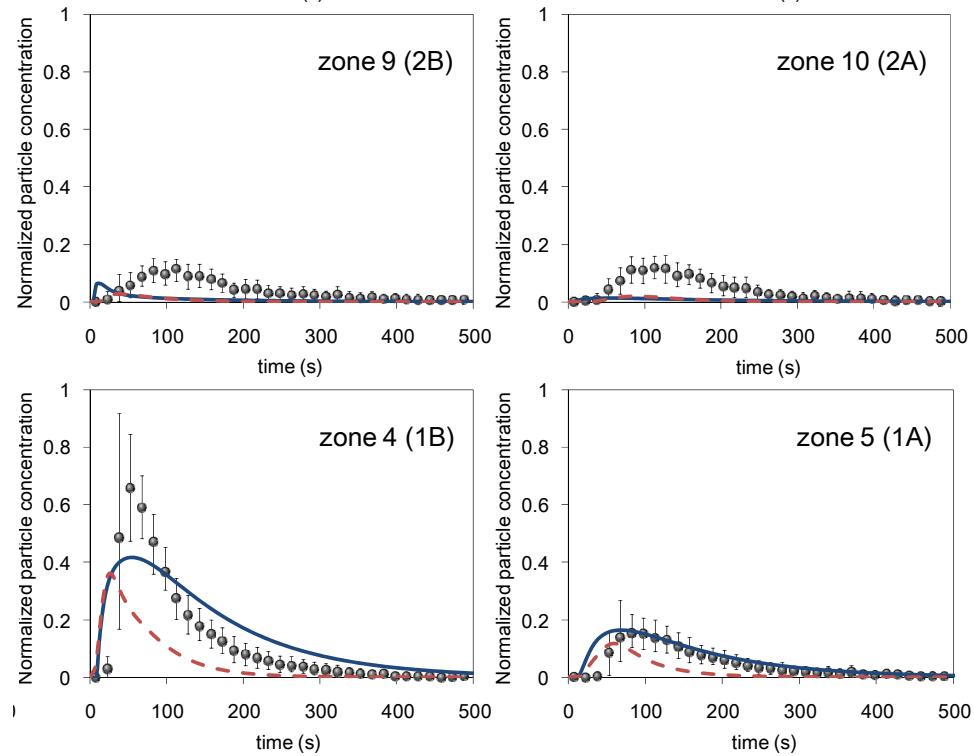


Figure 4-8 Comparison of the trends of the normalized particle concentration distribution versus time for the aircraft cabin as obtained by the Markov chain method, CFD simulation and experimental data (Chen et al., 2013).

### 4.3 Discussion

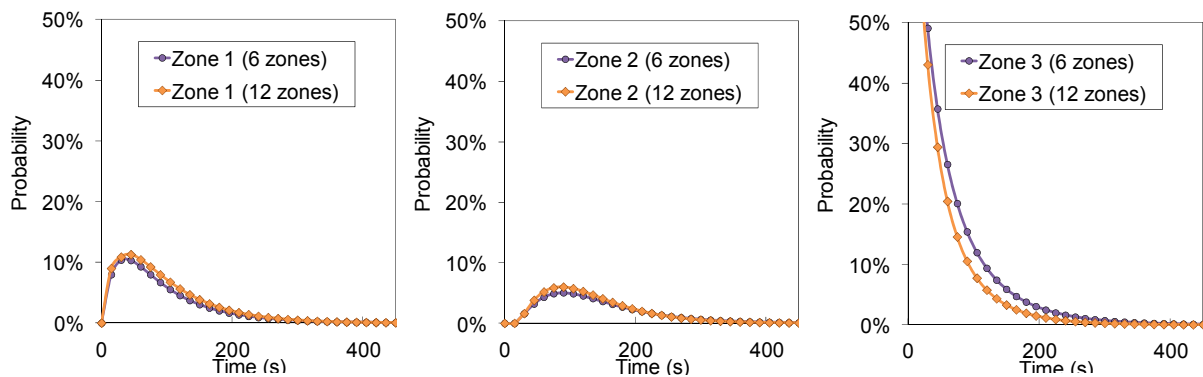
Quickly obtaining information about airborne infectious disease transmission in enclosed environments is crucial for reducing infection risk to the occupants. For an application of the Markov chain method, the airflow field and the transition probability matrix for an enclosed environment can be calculated in advance. For predicting infectious disease transmission, either the CFD or Markov chain method can be used for calculating the transient particle transport. Table 4-1 compares the computing time by the CFD method using the previous calculated airflow field and Markov chain method using the previous calculated transition probability matrix for the three cases. It took only seconds for the Markov chain method to calculate the transient particle transport, while hours or even days were needed for the CFD simulations. This was because the Markov chain method requires only simple matrix multiplications while the CFD requires a lot of numerical iteration for a large amount of grids. It can be seen that the Markov chain method can provide faster-than-real-time information about particle transport in enclosed environments. In other words, for a fixed airflow field, when the index patient or the source location is changed, the Markov chain method can be used to avoid recalculation of the particle transport equation and thus reduce computing costs. This capability has been validated by comparing with the CFD simulations in this study. It is meaningful since the accuracy of CFD simulations has been experimentally validated previously (e.g. Zhang and Chen, 2007; Zhao et al., 2009a; Chen et al., 2013).

Table 4-1 Comparison of the computing time by the CFD method using the previous calculated airflow field and Markov chain method using the previous calculated transition probability matrix.

Case	CFD method (hr)	Markov chain method (s)
Isolation clean room	4	<1
Room with UFAD system	15	<1
Aircraft cabin	75	5

There may be some disadvantages of the proposed combined CFD and Markov chain method. First, the Markov chain method may be not as accurate as the normal CFD methods as shown in the comparison results above. Second, one may concern that the calculation of the transition probability matrix may take even longer time than the re-calculation of the particle equations. Note that, to obtain each  $p_{ij}$ , only one time step,  $\Delta t$ , calculation of particle tracking is needed. Thus, as long as the number of the zones (or the number of the  $p_{ij}$ ) is less than the number of the time steps, the calculation of the transition probability matrix would still take less time than the re-calculation of the particle equations for the whole time period. Therefore, it may not be suitable to use the Markov chain method for obtaining results with very high resolutions.

In addition, the number of the divided zones in the Markov chain method may also affect the results. In principle, the number of the divided zones depends on the required resolution. However, as discussed above, if the size of the zones is unreasonably large, the time step also needs to be very large. Such a large time step may not be able to reflect the transient characteristics of the particle transport. To assess how the results depend on the number of the divided zones, this study further compared the results of transient particle transport when the clean room was divided into 6 and 12 zones, as shown in Figure 4-9. The particle source was located in zone 3. It can be found that the differences between the results for 6 and 12 divided zones are insignificant. Thus, 6 divided zones are sufficient enough to capture the transient characteristics of the particle transport in the clean room.



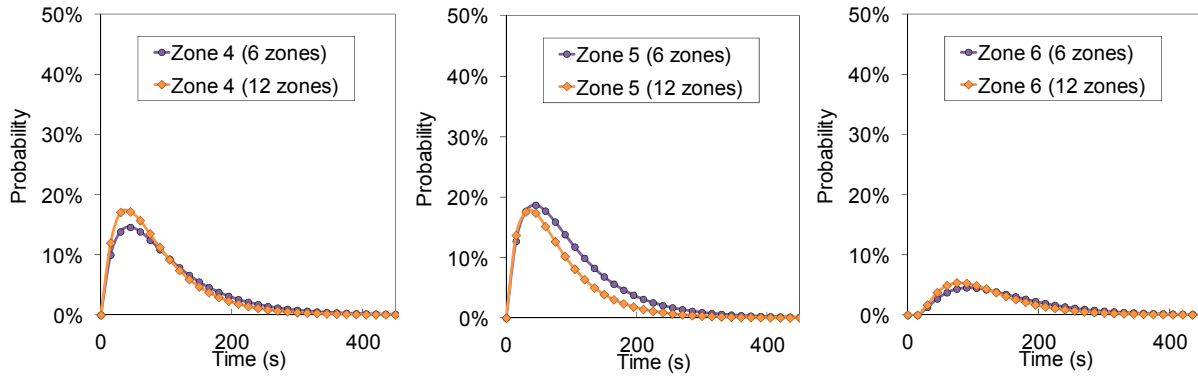


Figure 4-9 Comparison of the trends of the normalized particle concentrations versus time as obtained by the Markov chain method when the clean room was divided into 6 and 12 zones.

Currently, either deterministic or probabilistic approaches can be used for risk assessment of airborne infectious disease transmission (Gupta et al., 2012). In the deterministic approaches, the risk or probability of infection cannot be quantified. In the probabilistic approaches, because the quantities exhaled cannot be directly determined, their accuracy has been debated (Sze To and Chao, 2010). The Markov chain method predicts the probability of a particle's appearing in a zone at a certain point in time. Because the movements of indoor particles tend to be independent, the calculated probabilities should be independent probabilities. Through simple calculations of the joint probability and the probability of either event's occurring, we can calculate the probability of a certain number of particles appearing in the breathing zone of the receptor. For instance, if the index patient exhales 100 particles, we can calculate the probability that 10 out of these 100 particles appear in the breathing zone. Thus, the Markov chain with probability calculations has the potential to account for both deterministic and probabilistic information.

In addition, the Markov chain method has the potential to account for other influencing factors in infectious disease transmission. For instance, compared with completely fresh-air ventilation systems assumed in this study, ventilation systems with return air are more widely used in actual engineering. In these cases, the particles can re-enter the space through the return air. To take this factor into account, we can simply modify the transition probability matrix by rewriting Eq. (4.3):

$$p_{nj} = (r_1 \ r_2 \ \cdots \ r_i \ \cdots \ r_{n-1} \ (1-r_1-r_2-\cdots-r_i-\cdots-r_{n-1})) \quad (4.18)$$

where

$$r_i = f_i(1-\eta)\beta \quad (4.19)$$

where  $f_i$  is the ratio of the supply airflow rate in zone  $i$  to the total airflow rate,  $\eta$  is the particle removal efficiency of filter, and  $\beta$  is the ratio of the return airflow rate to the total airflow rate. Then the effect of contaminated return air and filter can be easily assessed using Eq. (4.8) with the updated transition probability matrix. The effectiveness of wearing masks and the effects of temperature and humidity on virus survival can also be investigated using a similar approach.

## 4.4 Conclusions

This chapter developed a combined CFD and Markov chain method for predicting transient particle transport in enclosed environments. From the results presented in this chapter, the following conclusions can be drawn:

- (1). The proposed combined CFD and Markov chain method can predict the general trends of the particle concentrations versus time in enclosed environments.
- (2). The Markov chain method can provide faster-than-real-time information about particle transport in enclosed environments.
- (3). For a fixed airflow field, when the source location is changed, the Markov chain method can be used to avoid recalculation of the particle transport equation and thus reduce computing costs.

## 5. SYSTEMATIC STUDY OF PERSON-TO-PERSON CONTAMINANT TRANSPORT

The review in Chapter 2 shows that it is worthwhile to systematically investigate the influences of ventilation mode, ventilation rate and person-to-person distance on person-to-person contaminant transport. This chapter details the development of database and the discussion on these influencing factors.

### 5.1 Methods

#### 5.1.1 Developing a database from the literature

This study first collected the cases available in the literature to create a database. Note that different studies used different units or normalization methods for the exposure data. Thus, the selected studies must be comparative so that the relative effects of the target factors on person-to-person contaminant transport can be calculated for each individual study. In this investigation, the relative effect of ventilation mode on exposure was calculated for each study by:

$$E^*_{\text{mod}} = \frac{E}{E_{\text{mixing}}} \quad (5.1)$$

where  $E$  is the exposure for a particular case, and  $E_{\text{mixing}}$  is the average exposure for mixing ventilation in that study. Thus, the relative effects of ventilation mode on exposure could be compared among different studies. The database from the literature included 32, 34, and 4 cases for mixing ventilation, displacement ventilation, and UFAD systems, respectively.

Because all the collected studies included at least one case with a ventilation rate of 6 ACH, the relative effect of ventilation rate was calculated by:

$$E^*_{\text{ACH}} = \frac{E}{E_{6\text{ACH}}} \quad (4.2)$$

where  $E_{6\text{ACH}}$  is the average exposure at a ventilation rate of 6 ACH for each study. The database from the literature contained 23, 20, 15, and 15 cases for 4, 6, 9, and 10 ACH, respectively.

Because all the collected studies included at least one case with a person-to-person distance of 1.1 m, the relative effect of person-to-person distance was calculated by:

$$E^*_{\text{dis}} = \frac{E}{E_{1.1\text{m}}} \quad (4.3)$$

where  $E_{1.1\text{m}}$  is the average exposure of the cases with a person-to-person distance of 1.1 m for each study. There are 40 cases for different person-to-person distances available in the literature.

### 5.1.2 Adding necessary cases to the database

As discussed in the introduction, the effect of the UFAD system on controlling person-to-person contaminant transport has not been thoroughly studied. Thus, this study added 24 UFAD system cases with different ventilation rates and person-to-person distances to the database. The ventilation rate varied from 3 to 9 ACH, which is a reasonable range for common indoor environments. The person-to-person distance varied from 0.5 to 1.8 m, which corresponds to common scenarios in a two-person office. Because only comparative data could be used for the database, 12 mixing ventilation and 12 displacement ventilation cases were also set up for comparison with the UFAD systems. Table 5-1 lists detailed information about ventilation mode, ventilation rate, and person-to-person distance for the cases added to the database.

Table 5-1 Case setup for this study.

Case	Mode	ACR (ACH)	Dis. (m)	Exp.	CFD	Case	Mode	ACR (ACH)	Dis. (m)	CFD
1	UFAD	3	0.5	√	√	25	Mixing	3	0.5	√
2	UFAD	3	0.8		√	26	Mixing	3	1.1	√
3	UFAD	3	1.1	√	√	27	Mixing	5	0.5	√
4	UFAD	3	1.8		√	28	Mixing	5	1.1	√
5	UFAD	5	0.5		√	29	Mixing	6	0.5	√
6	UFAD	5	0.8		√	30	Mixing	6	1.1	√
7	UFAD	5	1.1		√	31	Mixing	7	0.5	√
8	UFAD	5	1.8		√	32	Mixing	7	1.1	√
9	UFAD	6	0.5	√	√	33	Mixing	8	0.5	√
10	UFAD	6	0.8		√	34	Mixing	8	1.1	√
11	UFAD	6	1.1	√	√	35	Mixing	9	0.5	√
12	UFAD	6	1.8		√	36	Mixing	9	1.1	√
13	UFAD	7	0.5		√	37	Displace	3	0.5	√
14	UFAD	7	0.8		√	38	Displace	3	1.1	√
15	UFAD	7	1.1		√	39	Displace	5	0.5	√
16	UFAD	7	1.8		√	40	Displace	5	1.1	√
17	UFAD	8	0.5		√	41	Displace	6	0.5	√
18	UFAD	8	0.8		√	42	Displace	6	1.1	√
19	UFAD	8	1.1		√	43	Displace	7	0.5	√
20	UFAD	8	1.8		√	44	Displace	7	1.1	√
21	UFAD	9	0.5	√	√	45	Displace	8	0.5	√
22	UFAD	9	0.8		√	46	Displace	8	1.1	√
23	UFAD	9	1.1	√	√	47	Displace	9	0.5	√
24	UFAD	9	1.8		√	48	Displace	9	1.1	√

In addition, the literature assessed the effect of ventilation rate on the transport of contaminants exhaled only by reclining patients, which may not be representative of normal scenarios such as

working in an office. Although the patient room settings are more likely to a concern for infectious disease transmission, numerous studies have focused on the contaminant transport in hospital environments (Chen et al., 2010; Chen et al., 2011; Ching et al., 2008; Nielsen et al., 2010; Qian et al., 2006; Yin et al., 2011; Zhao et al., 2009b). The office settings where people spend considerable time are also important, since the cross infections occurring in the offices are strongly related to working efficiency and productivity. Therefore, this study investigated person-to-person contaminant transport in an office with different ventilation rates to extend the knowledge in this area. The schematic of the office is depicted in Figure 5-1(a). There were two seated persons with a height of 1.2 m, two personal computers, and two desks in the office. The following section details the strategy for obtaining person-to-person contaminant exposure data.

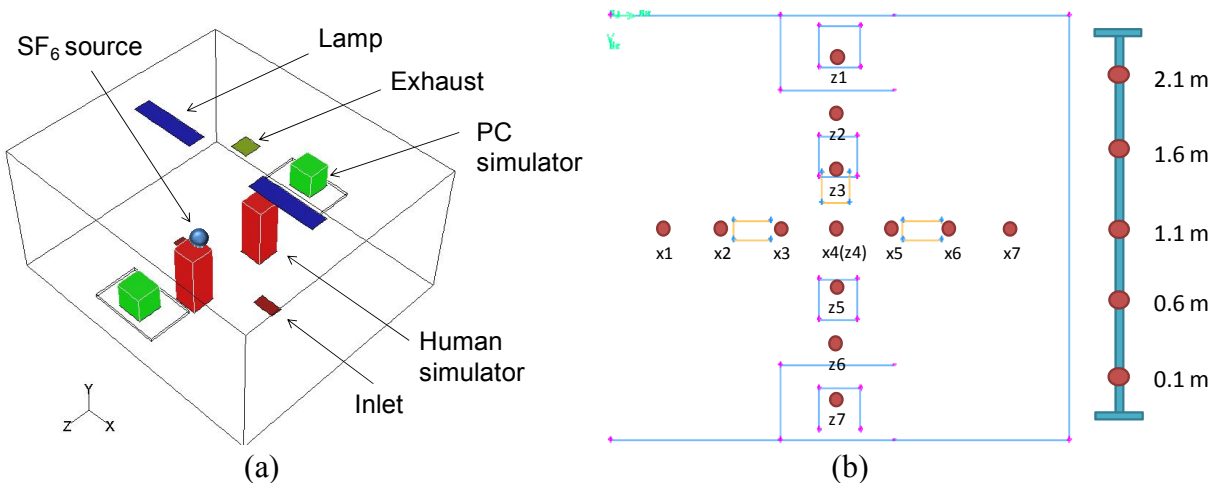


Figure 5-1 (a) Schematic of the office and (b) measuring locations and heights for air velocity, temperature and SF<sub>6</sub> concentration.

### 5.1.3 Obtaining person-to-person contaminant exposure data

#### 5.1.3.1 Strategy for obtaining the exposure data

Compared with experimental measurements, Computational Fluid Dynamics (CFD) modeling is more cost-effective for obtaining person-to-person contaminant exposure data. However, the reliability of the CFD modeling should be verified. Thus, this study first conducted experimental measurements in the office to validate the model, and then applied the model to obtain the exposure data for all the cases listed in Table 5-1.

Because the UFAD system has not been well studied, the experiment was conducted for this system. Furthermore, because ventilation rate and person-to-person distance are the target parameters in this study, different ventilation rates and person-to-person distances were included in the experiment. Ventilation rates of 3, 6, and 9 ACH correspond to low, medium, and high ventilation, respectively, in normal indoor environments. Person-to-person distances of 0.5 and 1.1 m correspond to close and normal distances, respectively, for common scenarios. Table 5-1 also illustrates the measurement cases identified.

#### 5.1.3.2 Experimental setup

This investigation built a full-scale office using an environmental chamber with dimensions of 4.8 m in length, 4.3 m in width, and 2.4 m in height, as shown in Figure 5-1(a). There were two inlets installed at floor level, and the exhaust was located at ceiling level. Figure 5-2 shows the linear type of diffusers used in the experiment. The environmental chamber could provide a controlled air supply at various airflow rates. The enclosures were well insulated so that the chamber could maintain a stable thermal condition.



Figure 5-2 Linear diffuser used in the UFAD system.

The ventilation rate was set at 3, 6, and 9 ACH, and the person-to-person distance was set at 0.5, 1.1, and 1.8 m, as shown in Table 5-1. This study used sulfur hexafluoride, SF<sub>6</sub>, as a tracer gas to simulate the exhaled contaminants. The SF<sub>6</sub> source was located in the breathing zone of one of the human simulators, as shown in Figure 5-1. Before each measurement, this investigation operated the HVAC system for 6 to 8 hours to reach a thermally steady-state condition. The measurement started after a steady-state concentration distribution of SF<sub>6</sub> was reached.

The air velocity, temperature, and SF<sub>6</sub> concentration distributions were measured in the experiment. As depicted in Figure 5-1(b), the air velocity, temperature, and SF<sub>6</sub> concentration were measured in two sections at 13 locations in the plane. At each location the measurements were conducted at five different heights along a pole. The experiment used 30 hot-sphere anemometers to measure the air velocity and air temperature. The hot-sphere anemometers had an accuracy of 0.02 m/s for velocity and 0.2 K for air temperature. A photo-acoustic multi-gas analyzer (INNOVA model 1312) with a multipoint sampler (INNOVA model 1309) was employed to measure the SF<sub>6</sub> concentration with an accuracy of 0.001 ppm. The measurement duration of air velocity, air temperature, and SF<sub>6</sub> at each point was five minutes. Moreover, the air velocity magnitude and direction at the inlets were measured using ultrasonic anemometers. All the surface temperatures were measured using thermocouples as shown in Table 5-2.

Table 5-2 Measured boundary conditions.

Boundary	Temp. (°C)	Boundary	Temp. (°C)	Heat Power (W)
North wall (-X)	24.7	Lamps (north)	-	87
South wall (+X)	23.6	Lamps (south)	-	70
East wall (-Z)	24.8	Human simulator (east)	27.7	84

West wall (+Z)	24.3	Human simulator (west)	28	93.3
Ceiling (+Y)	24.8	PC simulator (east)	31.4	105
Floor (-Y)	24.3	PC simulator (west)	30.8	90
Supply air (north)	21.1	Supply air (south)	20.2	

### 5.1.3.3 Modeling approach

This study applied CFD modeling to obtain the person-to-person exposure data in the office. A RANS model with the Eulerian method for steady-state was used in this study because of the reasonable accuracy and low computing cost associated with the model (Wang et al., 2012). The renormalization group (RNG) k- $\epsilon$  model (Choudhury, 1993) was applied to calculate the airflow and turbulence because it has the best overall performance among all RANS models for enclosed environments (Wang and Chen, 2009). For contaminant modeling, because the mean diameter of the droplets exhaled through breathing was 0.4  $\mu\text{m}$  (Gupta et al., 2010), the effect of gravitational settling on droplet dispersion was negligible (Zhao et al., 2009a). Furthermore, Chen and Zhao (2010) have indicated that the transient process from a droplet to a droplet nucleus due to evaporation is also negligible for particles with a diameter of 0.4  $\mu\text{m}$ . Thus, modeling the exhaled droplets as gaseous contaminants is reasonable. From the perspective of contaminant transport, the major difference between coughing, sneezing and breathing is the influence of exhaled air velocity on contaminant transport. The experimental measurements and then computer simulation of airflow in an aircraft cabin by Gupta et al. (2011) indicated that even a cough without covering mouth can have limited affect on the local airflow field but not the whole airflow field. Moreover, if a mouth is covered when coughing or sneezing as people would usually do, the influence of coughing and sneezing on the airflow field would be minimal. Therefore, exhalation with zero exhaled velocity was assumed in this study.

Numerical simulations were conducted using the CFD program, ANSYS Fluent 12.1 (ANSYS 2010). A user-defined function (UDF) was implemented to realize the Eulerian model. Three grid resolutions (101,709, 729,304, and 1,476,360) were tested for CFD grid independence. The 729,304 grid resolution was sufficiently fine to capture such a turbulent flow in the office mockup.

Using the RANS-Eulerian model, this investigation calculated the contaminant concentration at the breathing zone of the receptor for the 48 cases shown in Table 5-1. The relative effects of ventilation mode, ventilation rate, and person-to-person distance were calculated by Eqs. (5.1) – (5.3). Combining the cases from the literature and this study, we assessed the effect of ventilation mode, ventilation rate, and person-to-person distance on person-to-person contaminant transport.

## 5.2 Validation of the CFD Model

To ensure that the CFD model could produce high-fidelity results for the database, this study first validated the model. Figure 5-3 compares the measured and calculated air velocity profiles for the six validation cases. The lower and upper bounds of the error bars represent the 10<sup>th</sup> and 90<sup>th</sup> percentiles of the measurement data, respectively. There was a large quantity of data; therefore,

in order to keep the paper concise, this study shows only representative results at poles x1 and x3. It can be seen in Figure 5-3 that both the measured and calculated air velocities were higher at the lower region of pole x3, which was near an inlet. At that location, the model predicted higher air velocities when the ventilation rate increased, which agrees well with the measurements. At the locations that were far away from the inlets, such as pole x1, both the measurements and the modeling results show relatively low air velocities. For all the cases, the average relative error of air velocity was 45%.

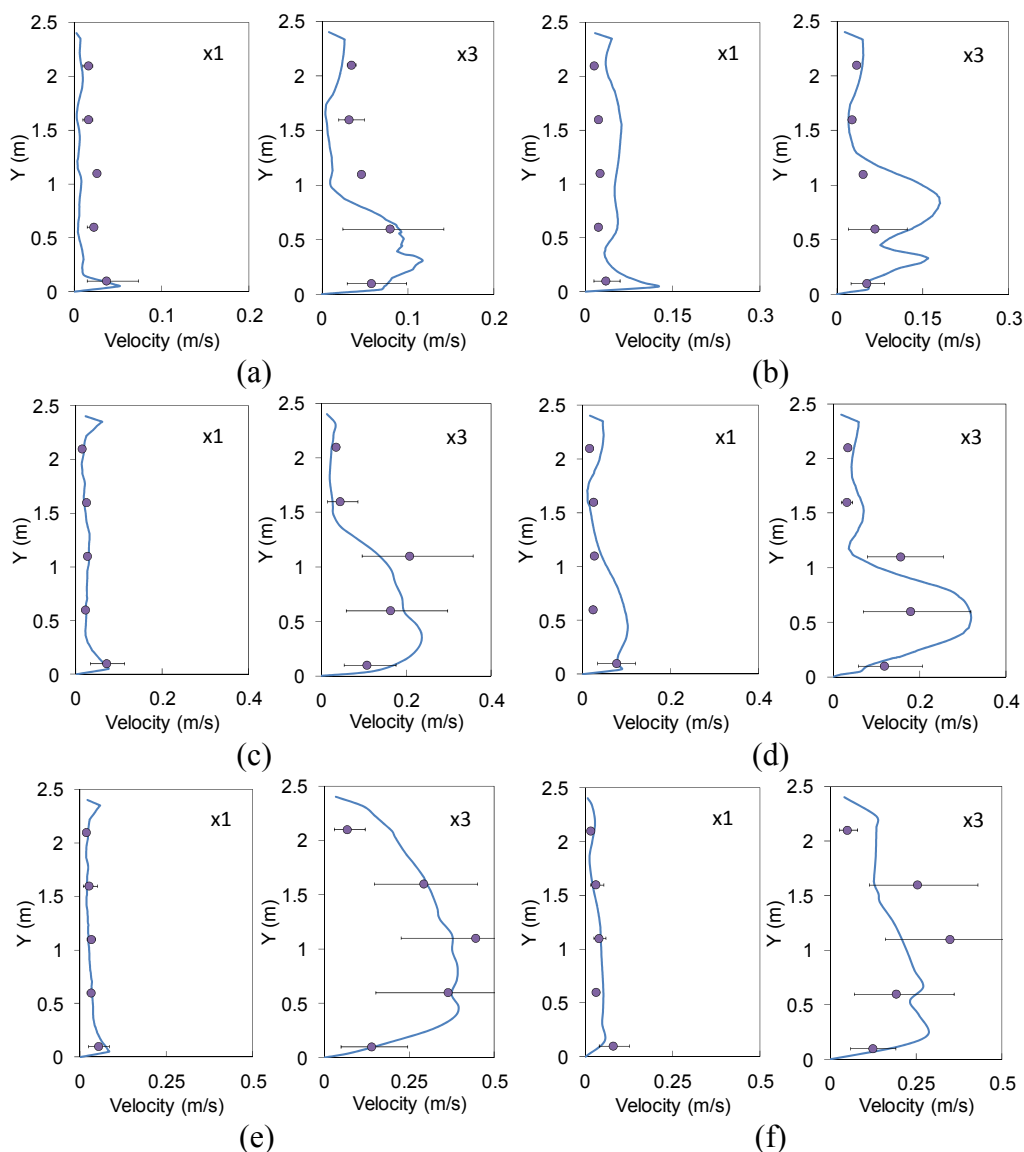


Figure 5-3 Comparison of the measured and calculated air velocity profiles for (a) Case 1: 3 ACH and 0.5 m distance; (b) Case 3: 3 ACH and 1.1 m distance; (c) Case 9: 6 ACH and 0.5 m distance; (d) Case 11: 6 ACH and 1.1 m distance; (e) Case 21: 9 ACH and 0.5 m distance; and (f) Case 23: 9 ACH and 1.1 m distance.

Figure 5-4 shows a comparison of the measured and calculated air temperature profiles at poles x3 and z2. The air temperature was normalized by

$$\theta = \frac{T - T_{in}}{T_{out} - T_{in}} \quad (5.4)$$

where  $T$  is the local temperature, and  $T_{in}$  and  $T_{out}$  are the temperatures at the inlets and exhaust, respectively. Both the measured and calculated results show positive vertical temperature gradients for all the cases. At pole x3, which was close to an inlet, the temperature gradients tended to be small when the ventilation rate was increased to 9 ACH. The reason was that such high air velocities near the inlet caused mixing and destroyed the stratification. The model can predict such a phenomenon in good agreement with the measurements. For all the cases, the average relative error of air temperature was 31%.

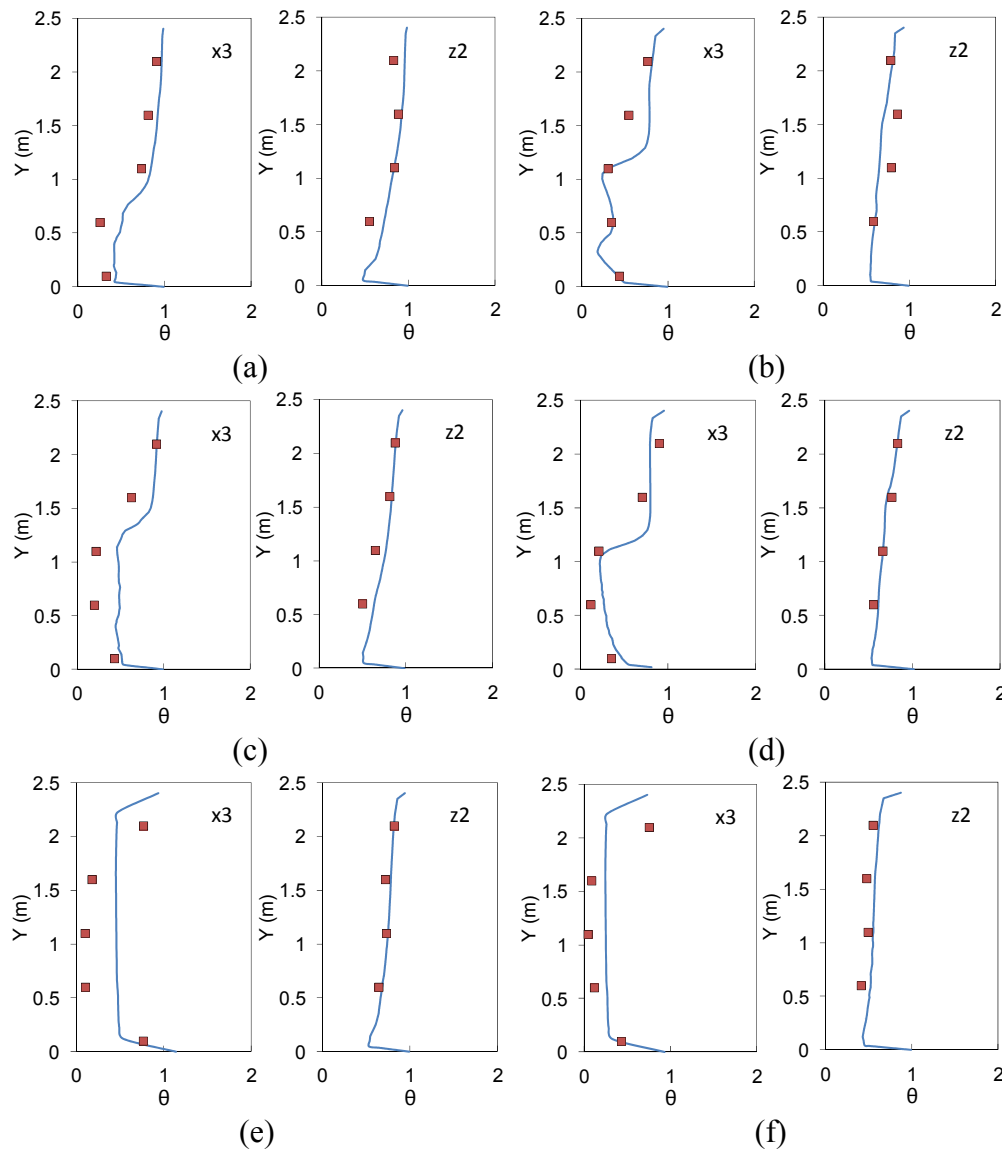


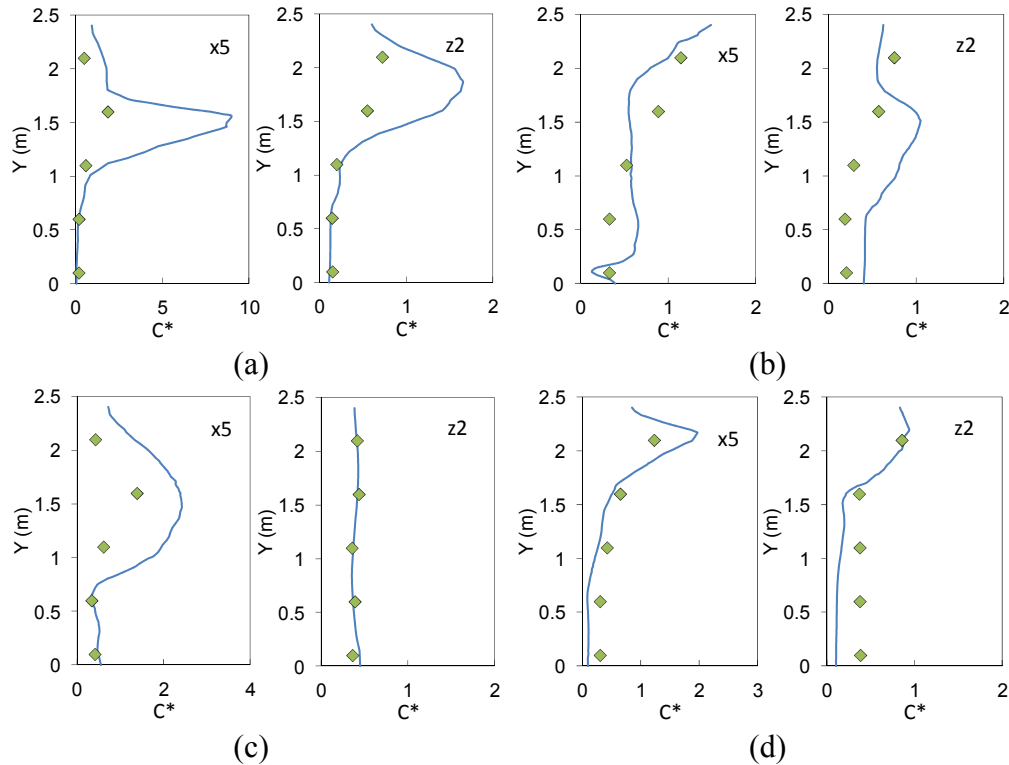
Figure 5-4 Comparison of the measured and calculated air temperature profiles for (a) Case 1: 3 ACH and 0.5 m distance; (b) Case 3: 3 ACH and 1.1 m distance; (c) Case 9: 6 ACH and 0.5 m

distance; (d) Case 11: 6 ACH and 1.1m distance; (e) Case 21: 9 ACH and 0.5 m distance; and (f) Case 23: 9 ACH and 1.1 m distance.

Figure 5-5 compares the measured and calculated SF<sub>6</sub> concentration profiles for the six cases. Again, the SF<sub>6</sub> concentration was normalized by

$$C^* = \frac{C - C_{in}}{C_{out} - C_{in}} \quad (5.5)$$

where  $C$  is the local concentration, and  $C_{in}$  and  $C_{out}$  are the concentrations at the inlets and exhaust, respectively. When the ventilation rate was 3 and 6 ACH, both the measured and calculated results show that the SF<sub>6</sub> concentration had a positive vertical gradient. This confirmed that the UFAD system could create a stratified air distribution. With a high ventilation rate of 9 ACH, the SF<sub>6</sub> concentration was uniform. The high air velocities near the inlets caused the mixing type of air distribution at pole x3. In Figure 4(a), remarkable differences existed between measurement and simulation. For pole x5, the simulation shows that there was a sudden change of concentrations at the height between 1.6 to 1.7 m. A single measurement point here was difficult to capture such a sudden change of concentrations. This might be the major reason for the remarkable difference between measurement and simulation. However, it can be seen that the measured data at 1.6 m matches well with the calculated data at 1.7 m. The measured data did fell in the range of calculated results at the height between 1.6 to 1.7 m. The similar explanation may apply to the remarkable difference at pole z2. For all the cases, the average relative error of SF<sub>6</sub> was 44%.



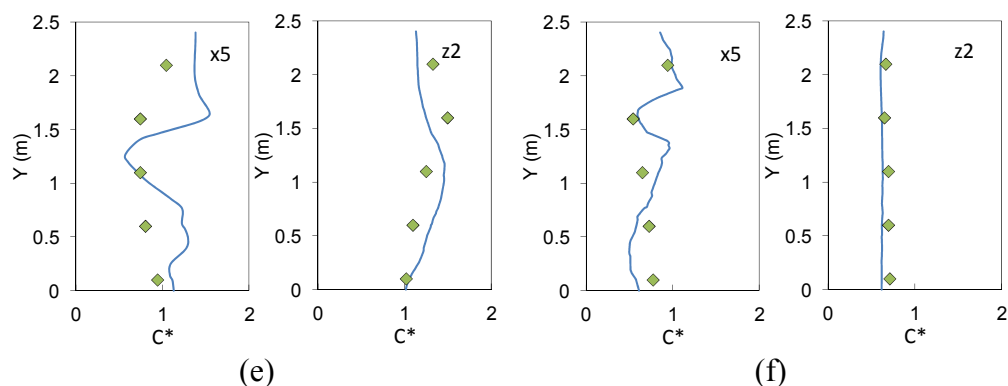


Figure 5-5 Comparison of the measured and calculated SF<sub>6</sub> concentration profiles for (a) Case 1: 3 ACH and 0.5 m distance; (b) Case 3: 3 ACH and 1.1 m distance; (c) Case 9: 6 ACH and 0.5 m distance; (d) Case 11: 6 ACH and 1.1m distance; (e) Case 21: 9 ACH and 0.5 m distance; and (f) Case 23: 9 ACH and 1.1 m distance.

Generally speaking, the calculated results agree reasonably well with the experimental data in terms of air velocity, temperature, and contaminant concentration distributions. Thus, the RANS - Eulerian model was then used to produce data for the 48 cases shown in Table 5-1 for establishing the database with confidence. By combining these cases with the cases from the literature, this investigation created a database of 118 cases for studying ventilation mode, 124 cases for ventilation rate, and 88 cases for person-to-person distance.

## 5.3 Results

### 5.3.1 Effect of ventilation mode

Using the 118 cases in the database that address ventilation mode, it is possible to study the effect of ventilation mode on person-to-person contaminant transport. Figure 5-6 compares the median value of the relative effect of mixing ventilation, displacement ventilation, and the UFAD system on person-to-person contaminant exposure. The lower and upper bounds of the error bars represent the 10<sup>th</sup> and 90<sup>th</sup> percentiles of the data from the database, respectively.

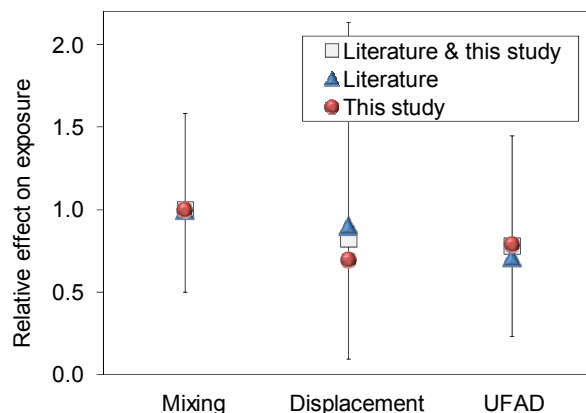


Figure 5-6 Relationship between ventilation mode and person-to-person contaminant exposure.

The median value of the relative effect from the literature and from this study is also shown separately in the figure. Because the reference for the relative effect was the person-to-person contaminant exposure under mixing ventilation, the median values of the relative effect for mixing ventilation from the literature and from this study were both close to 1.0. The median value of the relative effect for displacement ventilation from the literature was 0.91, while the median value from this study was 0.70. The difference may be attributed to the differences in scenarios. For instance, some cases from the literature were for the scenario of contaminant transport between reclining patients (Qian et al., 2006; Yin et al., 2011). The thermal plumes from the reclining patients tended to be weaker than those from the standing or seated persons in our study. Thermal plumes from the human body play an important role in the distribution of exhaled contaminants (Gao et al., 2012a). Weaker thermal plumes may reduce the chance of removal of exhaled contaminants by fresh air. When the relative effects from the literature and this study were combined, the median value of the relative effect for displacement ventilation was 0.82. The median values of the relative effect for the UFAD system from the literature and from this study were in good agreement. The median value from the combination of the literature and this study for the UFAD system was 0.78. It can be seen that the deviation in the performance of displacement ventilation was larger than in that of mixing ventilation. The high exposure cases of displacement ventilation were the measurement cases by Olmedo et al. (2012) when the person-to-person distance was 0.35 m. Their measurements showed that, when the person-to-person distance was 0.35 m, the exposure under displacement ventilation was much higher than that under mixing ventilation.

Generally speaking, the performances of displacement ventilation and UFAD systems in controlling person-to-person contaminant transport were quite similar. They were about 20% better than mixing ventilation in reducing person-to-person contaminant exposure. Displacement ventilation and UFAD systems can be categorized as stratified air-distribution systems. The cool, fresh air from the inlets remains in the lower region of the room and then moves directly into the occupied zone because of thermal buoyancy. Thus, these systems have the potential to reduce person-to-person contaminant exposure and provide better indoor air quality, as compared with mixing ventilation. This finding is consistent with the results of many previous studies (Chen and Glicksman, 2003; Lau and Chen, 2006). However, Olmedo et al. (2012) pointed out that displacement ventilation may have poorer performance than mixing ventilation in controlling person-to-person exposure under certain circumstances. The large error bars shown in Figure 5-6 also indicate significant variations in the relative effects for different ventilation modes. The median value of the relative effect was 1.0 for mixing ventilation and around 0.8 for the displacement ventilation and UFAD systems. A factor of 1.25 may represent the general effect of ventilation mode on person-to-person contaminant transport in mechanically ventilated spaces.

### 5.3.2 Effect of ventilation rate

Similarly, a total of 124 cases in the database could be used to study the effect of ventilation rate on person-to-person contaminant transport. Figure 5-7 shows the relationship between person-to-person contaminant exposure and ventilation rate. Each symbol represents the median value of the relative effect for the corresponding ventilation rate. The lower and upper bounds of the error bars represent the 10<sup>th</sup> and 90<sup>th</sup> percentiles of the data, respectively. The median values of the relative effect from the literature and from this study are also shown separately in the figure.

Because the reference for the relative effect was the person-to-person contaminant exposure under a ventilation rate of 6 ACH, the median values of the relative effect for 6 ACH from the literature and from this study were both close to 1.0. The trends of the relative effects on contaminant exposure versus ventilation rate in Figure 5-7 show that the results of this study matched well with those from the literature. However, the relative effect for 4 ACH from the literature seems to be lower than the general trend. The reason is unknown, but the difference is not significant. Combining the relative effects from the literature and from this study, a linear regression was performed for the median value of the relative effect with the corresponding ventilation rates. The correlation between ventilation rate and person-to-person contaminant transport is significant, with an  $R^2$  of 0.87.

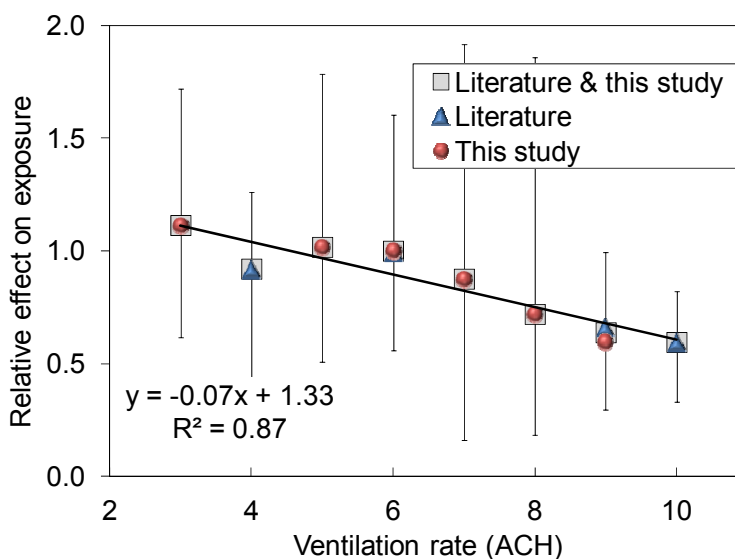


Figure 5-7 Relationship between ventilation rate and person-to-person contaminant exposure.

The database shows that the exposure was negatively associated with ventilation rate for all the ventilation modes. This finding makes sense because higher ventilation rate corresponds to higher dilution rate, which can reduce contaminant concentration in the breathing zone of the receptor. ASHRAE (2008) and CDC (2005) guidelines recommend a minimum ventilation rate of 12 ACH for hospital isolation rooms. These guidelines are evidence that ventilation rate is important in controlling person-to-person contaminant transport. Gao et al. (2012b) also indicated that increasing ventilation rate together with household isolation could be as effective as school closure for influenza transmission control in schools. However, the large error bars shown in Figure 5-7 imply significant variations in the relative effects of ventilation rate on person-to-person contaminant transport. Thus, other factors may modify the effect of ventilation rate. In addition, the median values of the relative effect on person-to-person contaminant exposure were 1.1 and 0.6 for ventilation rates of 3 and 10 ACH, respectively. This implies that an increase in ventilation rate by a factor of 3.3 resulted in a decrease of person-to-person contaminant transport by a factor of only 1.8. Memarzadeh and Xu (2012) also indicated that although increasing ventilation rate diluted concentrations more effectively when the contaminant source was constant, it did not necessarily increase the ventilation effectiveness.

Thus, controlling person-to-person contaminant transport by increasing ventilation rate may have certain limitations.

### 5.3.3 Effect of person-to-person distance

Very similarly to the previous subsections, 88 cases in the database were available for studying the effect of person-to-person distance on person-to-person contaminant transport. Figure 5-8 shows the relationship between person-to-person contaminant exposure and person-to-person distance. Each symbol represents the median value of the cases at the corresponding person-to-person distance. The lower and upper bounds of the error bars represent the 10<sup>th</sup> and 90<sup>th</sup> percentiles of the data, respectively. The median values of the relative effect from the literature and from this study are also shown separately in the figure. Because the reference for the relative effects was the person-to-person contaminant exposure at a distance of 1.1 m, the median values of the relative effect for 1.1 m from the literature and from this study should be close to 1.0, as confirmed in the figure. Most of the median values of the relative effect from the literature were close to those from this study, except at distances of 0.5 and 0.8 m. It is difficult for us to articulate the reason for these differences because there were many unknown factors. The differences are acceptable for our analysis in this investigation. Combining the relative effects from the literature and from this study, a power regression was performed for the median values of the relative effect with the corresponding person-to-person distances. An  $R^2$  of 0.94 implies a strong correlation between person-to-person contaminant transport and person-to-person distance.

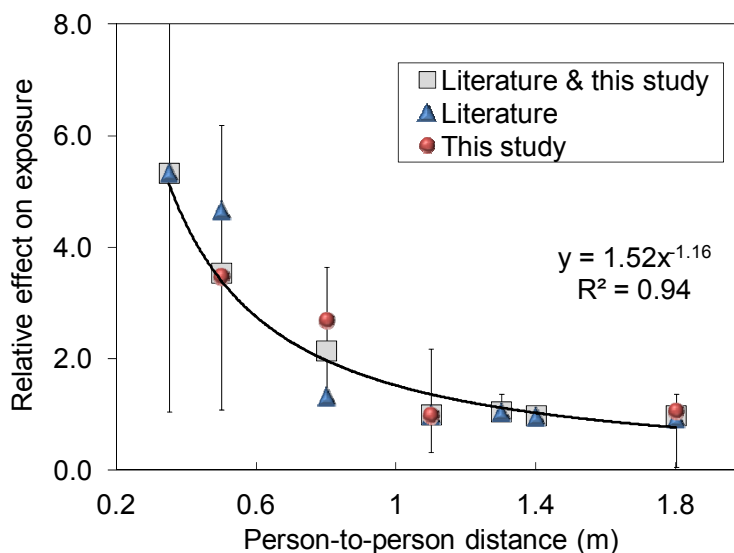


Figure 5-8 Relationship between person-to-person distance and person-to-person contaminant exposure.

It can be seen that when the person-to-person distance was smaller than 1.1 m, the relative effect on person-to-person contaminant exposure increased rapidly with the decrease in distance. However, when the person-to-person distance was larger than or equal to 1.1 m, the curve tended

to be rather flat. This was because the contaminant concentration gradient was larger near the source than in other locations. Thus, when the person-to-person distance increased to some extent, the influence of concentration gradient became insignificant. In this study, 1.1 m can be regarded as a cut-off person-to-person distance in terms of person-to-person contaminant transport. The median value of the relative effect on contaminant exposure was 5.3 for a distance of 0.35 m, and around 1 for a distance of 1.8 m. A factor of 5.3 indicates that person-to-person distance is a rather important parameter in terms of controlling person-to-person contaminant transport, when compared with ventilation mode and ventilation rate.

## 5.4 Discussion

This study compared mixing, displacement, and UFAD ventilation systems, which are the most commonly-used systems in residential or commercial buildings. However, other ventilation modes may also affect person-to-person contaminant transport. For instance, downward ventilation has been widely used in hospital wards or clean rooms. Qian et al. (2006) reported that downward and mixing ventilation had similar performance in a multi-bed hospital ward. Moreover, personalized ventilation has become a popular ventilation mode. He et al. (2011) concluded that personalized ventilation could increase contaminant concentration in the breathing zone of the receptor as well as provide clean personalized airflow. Whether person-to-person exposure could be reduced depends on the balance of the pros and cons of personalized ventilation.

Although the cases collected from the literature included both breathing and coughing cases, this study did not quantitatively assess the differences between breathing and coughing. The peak exhaled velocity of coughing is much higher than that of breathing. Thus, the contaminant exhaled by a cough tends to travel more quickly than by a breath. The model used in this study was for breathing cases, which can be regarded as a steady-state condition. If the transient particle transport resulting from a cough were investigated, the hybrid model developed and validated in our previous study could be used (Chen et al., 2013).

The key factor in contaminant transport is the “path” of airflow (Memarzadeh and Xu, 2012). The perfect “path” should be that the fresh air firstly goes through the receptor, then reaches to the source, and finally removes the contaminant to the exhaust. However, it is difficult to use a single parameter to describe the “path”. The “path” depends on ventilation mode, ventilation rate, person-to-person distance, and other parameters. At the first stage of design, a designer needs to make a decision on what kind of ventilation mode should be used, how much ventilation is needed, and how far the person-to-person distance (e.g. desk-to-desk distance in an office) should be designed. The statistical results in this study can be a general guideline to support the designers’ decisions at this stage. After that, if possible, the designer can use CFD technique to investigate the “path” in detail.

In addition to ventilation mode, ventilation rate, and person-to-person distance, which are among the ones that mostly related to HVAC design, other factors may influence person-to-person contaminant transport. Previous studies have reported that air cleaners have the potential to reduce person-to-person contaminant transport in hospital wards (Chen et al., 2010). Wearing masks has been identified as an effective method to reduce the risk of exposure to exhaled

contaminants (Gupta et al., 2012; Lai et al., 2012). The use of air curtains may also reduce contaminant transport between two zones (Ching et al., 2008; Chen et al., 2011). Moreover, the use of upper-room ultraviolet germicidal irradiation (UVGI) has been proven effective in disinfecting exhaled airborne pathogens and reducing the risk of person-to-person exposure (Yang et al., 2012). Furthermore, the orientations of persons relative to one another (Olmedo et al., 2012) and the gestures of the persons (Zhao et al., 2009b) can also influence person-to-person contaminant exposure.

## 5.5 Conclusions

This chapter presents a systematic study of the effect of ventilation mode, ventilation rate, and person-to-person distance on person-to-person contaminant transport. This investigation collected a large quantity of data from the literature and used a validated CFD model to generate additional data in order to establish a database. From this database, the following conclusions can be drawn:

- (1). The overall performances of displacement ventilation and a UFAD system were similar in terms of reducing exposure to person-to-person contaminant transport, and the two systems were about 20% better than mixing ventilation.
- (2). The data show that person-to-person contaminant exposure tended to be reduced with an increase in ventilation rate.
- (3). When the person-to-person distance was less than 1.1 m, person-to-person contaminant exposure increased rapidly with distance. At a distance larger than 1.1 m, the effect of distance was insignificant.
- (4). Person-to-person distance is more important than ventilation mode and ventilation rate in controlling person-to-person contaminant transport.

## 6. SIMPLIFIED MODELS FOR PREDICTING THE EXHALED AIRFLOW BY A COUGH WITH A MOUTH COVERING

The review in Chapter 2 shows that there are no valid approaches for modeling the airflow by a cough with a mouth covering available in the literature. Since coughing with a mouth covering is quite common in civilized societies, this chapter aims to develop simplified models for predicting the exhaled airflow by a cough with a mouth covering.

### 6.1 Visualization of exhaled airflow by a cough with a mouth covering

#### 6.1.1 Experimental methods

To understand the characteristics of exhaled airflow by a cough with a mouth covering, this study conducted smoke tests to visualize the exhaled airflow by 16 human subjects. The exhaled flows were visualized through moderate-speed photography with a frequency of 80 Hz. Cigarette smoke was used as seeding fluid, since the exhaled smoke jet can closely follow the cough air jet profile (Gupta et al., 2009). The recordings were performed over 16 normal healthy subjects who are smokers with an approval from the Institutional Review Board for human subject experimentation. The subjects were informed about the objectives of the research and the associated risk. Every subject signed a consent form before proceeding for the experiments. Five types of mouth covering including covering with a tissue, a cupped hand, a fist and an elbow with a sleeve and without a sleeve as well as uncovered cough were investigated. Each test was repeated at least twice for each subject. The subjects were asked to exhale smoke out through a single cough. For ensuring the quality of flow visualization, a light source along with a dark background was used in the experiments.

#### 6.1.2 Characterizing exhaled airflow by a cough with a mouth covering

Figure 6-1 shows the representative images of a cough covered with a tissue obtained from the experiments. The images can show the transient exhaled airflow profiles in detail. As shown in the figure, there was a front jet penetrating the tissue and an upward jet escaping from the upside leakage between the tissue and the face. Figure 6-2 shows more visualization results of a cough covered with a tissue. In Figure 6-2(a), the subjects exhaled both a front and an upward jet, while in Figure 6-2(b) and (c), there was only a front jet and only an upward jet existing, respectively. Generally speaking, when a subject coughs with covering a tissue, there may be a front air jet penetrating the tissue and an upward air jet escaping from the upside leakage.

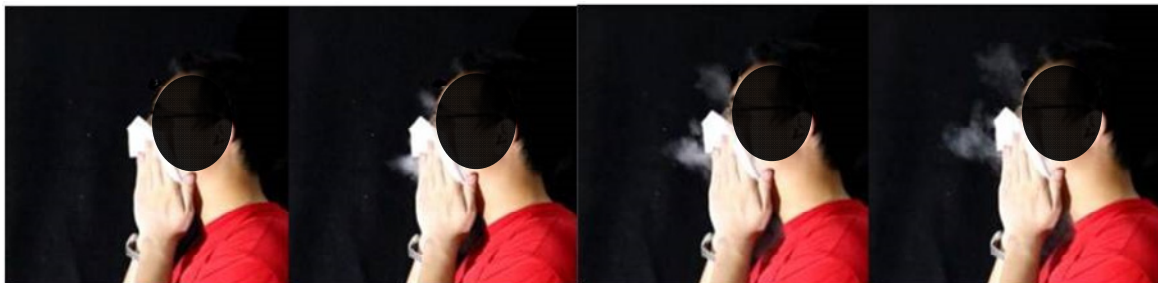
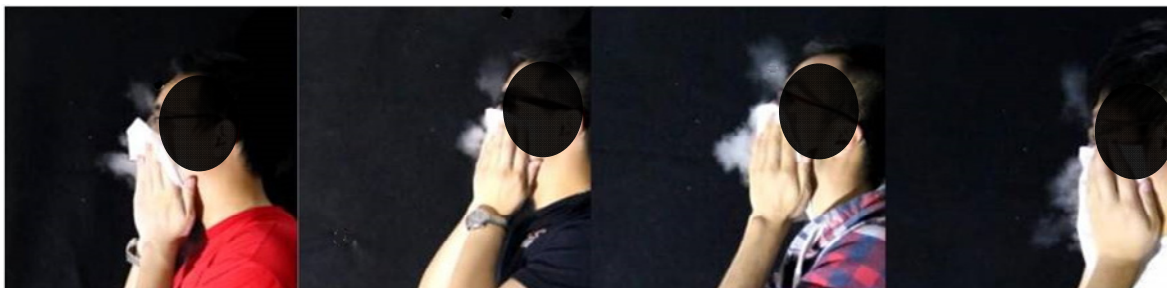


Figure 6-1 Representative images of a cough covered with a tissue.



(a)



(b)



(c)

Figure 6-2 Visualization of a cough covering with a tissue (a) both front and upward jets, (b) only front jet, (c) only upward jet.

The representative images of a cough with covering a cupped hand are shown in Figure 6-3. There was an upward and a downward jet escaping from the upside and downside leakage between the hand and the face, respectively. Moreover, the upward jet tended to move forward to some extent. Figure 6-4 shows more visualization results of a cough with covering a cupped hand. In Figure 6-4(a), the subjects had both an upward and a downward jet, while in Figure 6-4(b) and (c), there was only an upward jet and only a downward jet existing, respectively. In summary, when a subject coughs with covering a cupped hand, there may be an upward and a downward air jet escaping from the upside and downside leakages.

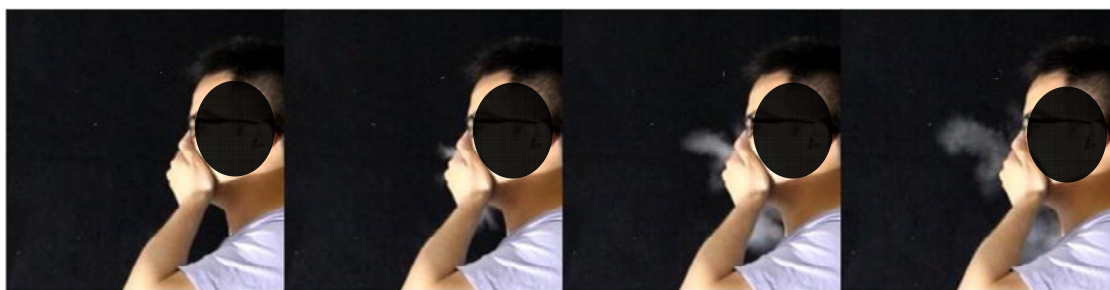


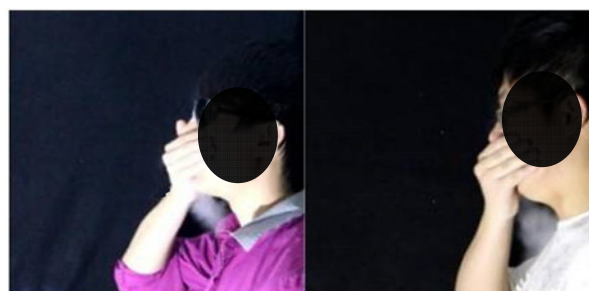
Figure 6-3 Representative imagines of a cough with covering a cupped hand.



(a)



(b)



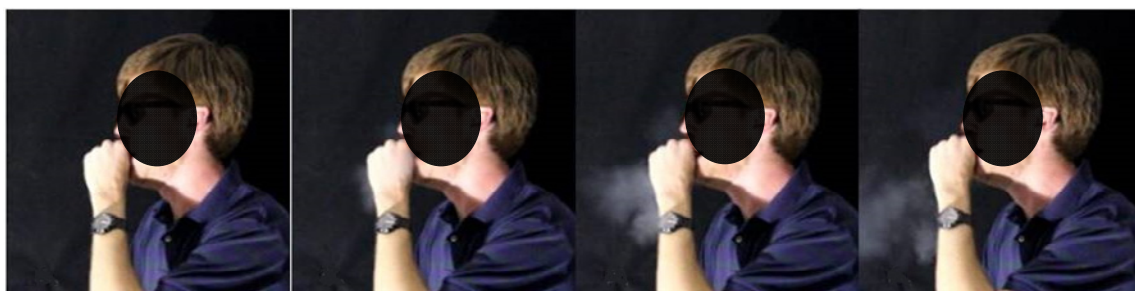
(c)

Figure 6-4 Visualization of a cough covering with a cupped hand (a) both upward and downward jets, (b) only upward jet, (c) only downward jet.

Figure 6-5 shows the representative imagines of a cough with covering a fist. In Figure 6-5(a), there was a strong front jet moving through the hole of the subject's fist, while in Figure 6-5(b), the jets moved forward through the side leakages between the fist and face. In this case, the subject's fist was tight without a hole. Thus, the characteristics of exhaled airflow of a cough with covering a fist depend on the tightness of the subject's fist. Figure 6-6 shows more visualization results of a cough with covering a fist. In Figure 6-6(a), the subjects exhaled only a front jet through the hole of the fist, while in Figure 6-6(b), the jets moved forward through the side leakages between the fist and face. In Figure 6-6(c), both types of the jets existed. Generally speaking, when a subject coughs with covering a fist, there may be a jet moving through the hole of fist and jets moving forward through the side leakages between the fist and face.



(a)



(b)

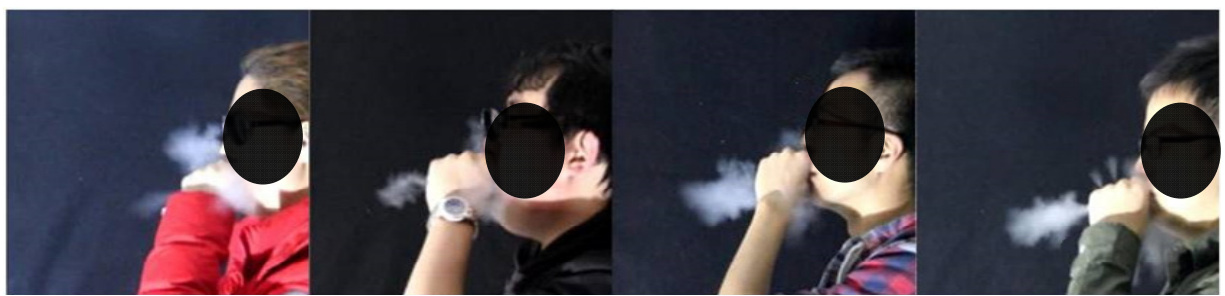
Figure 6-5 Representative images of a cough with covering a fist, (a) front jet through the hole of fist, (b) jets through the leakages between the face and fist.



(a)



(b)



(c)

Figure 6-6 Visualization of a cough covering with a fist (a) front jet through the hole of fist, (b) jets through the leakages between the face and fist, (c) both jets.

The representative imagines of a cough covered with an elbow with a sleeve are shown in Figure 6-7. It can be found that there was a relatively strong upward jet and a relatively weak downward jet through the leakages between the face and the elbow. Figure 6-8 shows more visualization results of a cough covered with an elbow with a sleeve. The patterns of the airflows for these subjects are similar to that in Figure 6-7. Clearly, the elbow with a sleeve can significantly redirect the exhaled airflow.



Figure 6-7 Representative imagines of a cough covered with an elbow with a sleeve.





Figure 6-8 Visualization of a cough covering with an elbow with a sleeve.

Figure 6-9 shows representative images of a cough covered with an elbow without a sleeve. Similar to the cases for covering an elbow with a sleeve, there was an upward jet and a downward jet through the leakages between the face and elbow. However, without a sleeve, the jet can move further than that with a sleeve. Figure 6-10 shows more visualization results, whose patterns are somewhat similar to that in Figure 6-7. The effectiveness of covering coughs with an elbow without a sleeve is worse than that with a sleeve. This may be because the sleeve enhances the area of the blockage which is beneficial for redirecting the exhaled airflow.



Figure 6-9 Representative images of a cough covered with an elbow with a sleeve.





Figure 6-10 Visualization of a cough covering with an elbow with a sleeve.

## 6.2 Simplified models for the airflow by a cough with a mouth covering

Based on the images captured in the experiments, it is possible to determine the jet velocity and direction for the studied mouth covering approaches. The information of jet velocity and direction of a cough with a mouth covering can be used as boundary conditions when modeling person-to-person contaminant transport in ventilated spaces. This section details the determination of jet velocity and direction.

### 6.2.1 Methods for determining the jet velocity, direction and flow ratio

Figure 6-11 shows an example of the first image after exhalation, i.e. the image is at the time,  $\Delta t$ , of 0.0125 s, since the image capture frequency was 80 Hz. The distance that the jet travels along is shown in the Figure labeled as  $\Delta s$ . This study used a digit color model called Y'UV model to distinguish the white smoke and the black background. The Y' value of a cell in the image can represent the brightness of that cell, which ranges from 0 (pure black) to 255 (pure white). A criteria was set to distinguish the smoke and background, i.e. if  $Y'_{\text{cell}} \leq Y'_{\text{back}} + \Delta Y'$ , the cell is not smoke, where  $Y'_{\text{cell}}$  is the Y' value of the cell and  $Y'_{\text{back}}$  is the average Y' value of the background.  $\Delta Y'$  represents the error of distinguishing the brightness caused by the human eyes. This investigation randomly chose 10 images to test this error and the results show that the average  $\Delta Y'$  is equal to 8.3. Using this method, the  $\Delta s$  can be quantitatively determined. Based on the images, it was found that the peak velocity occurred at the very beginning of the exhalation. Thus, the peak velocity of the jet can be calculated by

$$V = \frac{\Delta s}{\Delta t} \quad (6.1)$$



Figure 6-11 An example of the first image after exhalation.

The direction of the jet central line was roughly determined as shown in Figure 6-12. Two angles,  $\theta_1$  and  $\theta_2$ , were used to describe the direction of the jets. Since there were two jets for a lot of cases, the ratio of these two flows,  $R$ , is another important parameter. It was calculated by

$$R = \frac{A_1 L_1 (Y'_1 - Y'_{back})}{A_2 L_2 (Y'_2 - Y'_{back})} \quad (6.2)$$

where the subscript 1 and 2 represents the flow\_1 and flow\_2, respectively, as shown in Figure 6-12.  $A$  and  $L$  is the area from the side view and the horizontal spread distance from the front view of the smoke flow, respectively.  $Y'$  and  $Y'_{back}$  is the average  $Y'$  value of the smoke flow and the background, respectively.

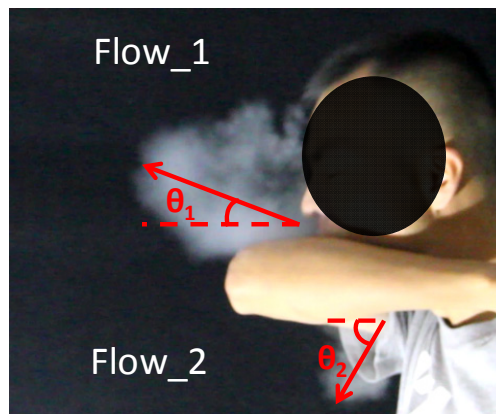


Figure 6-12 The direction of the jet central line.

### 6.2.2 Verification of the jet velocity

In addition to the airflow by a cough with a mouth covering, this investigation also visualized the airflow by an uncovered cough and used the proposed method to calculate the peak velocity. Then the calculated results were compared with the detailed measurement data by Gupta et al. (2009) to verify the method. Gupta et al. (2009) used 25 human subjects to measure the flow rate versus time of uncovered coughs with a frequency of 330 Hz. The peak velocities were collected as a reference in this study. Figure 6-13 compares the average peak velocity of uncovered coughs by this study and Gupta et al. (2009). The upper and lower bound of the error bar in the figure represents the 10<sup>th</sup> and 90<sup>th</sup> percentile point, respectively. The calculated peak velocity of uncovered coughs reasonably agrees with the measurement data by Gupta et al. (2009). Thus, this method can be used to determine the jet velocity of a cough with a mouth covering.

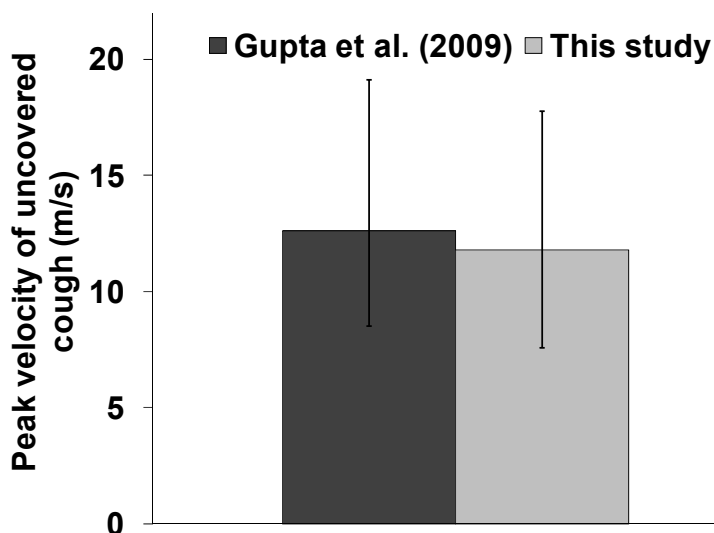


Figure 6-13 Comparison of the peak velocity of uncovered cough in this study and the detailed measurement data by Gupta et al. (2009).

### 6.2.3 Results of the jet velocity, direction and flow ratio

The average, 10<sup>th</sup> and 90<sup>th</sup> percentile point of the jet velocity, direction and flow ratio for tissue, cupped hand, fist and elbow with and without a sleeve as well as uncovered cough are shown in Figure 6-14. Since a cough with covering a fist and an uncovered cough generates only one branch of jet, the flow ratios for them are not applicable. The average jet velocity of the front and upward jet for the tissue cases was 2.6 and 3.8 m/s, respectively, which are lower than that for other mouth coverings. Furthermore, since using a tissue can avoid the infectious diseases transmission through indirect contacts of the hands, covering coughs with a tissue should be among the best approach. Covering coughs with a cupped hand is the second best approach with an average upward jet velocity of 6.3 m/s and an average angle of 59.2°. Comparing with covering coughs with an elbow with and without a sleeve, although the average jet velocity was similar, covering coughs with an elbow with a sleeve has larger angles than that without a sleeve. Thus, the sleeve is beneficial for re-directing the exhaled airflow and reducing the risk of horizontal transport of the droplets. Covering coughs with a fist is the worst approach with a relatively high velocity of 8.5 m/s and relatively small angle of 25.8°. These detailed results can be used as boundary conditions when modeling person-to-person contaminant transport in ventilated spaces.

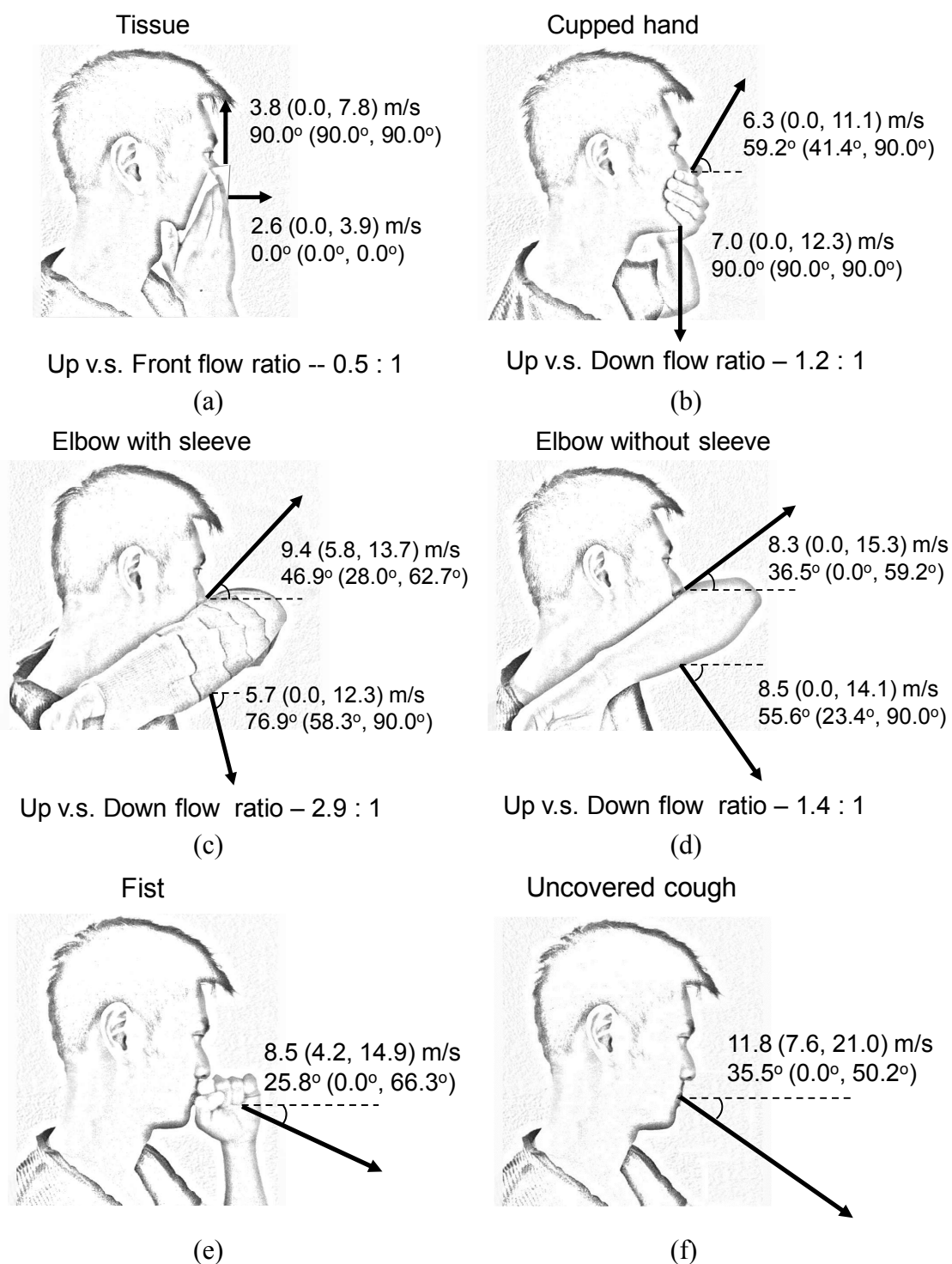


Figure 6-14 Average jet velocity, direction and flow ratio for (a) tissue, (b) cupped hand, (c) elbow with sleeve, (d) elbow without sleeve, (e) fist and (f) uncovered cough. The number in the parentheses is the 10<sup>th</sup> and 90<sup>th</sup> percentile point.

### 6.2.4 Simplified models

As discussed in Chapter 2, one option of modeling the airflow by a cough with a mouth covering is to directly build the realistic geometry of the mouth coverings. However, the difficulties in indentifying the air leakages and the significant consumption of computing time due to the large amount of grids associated with the complicated mouth coverings make this method challenging. Thus, this study proposes simplified models of the boundaries in CFD simulations for predicting the airflow by a cough with a mouth covering. In the simplified models, the mouth was equally separated into four parts, as shown in Figure 6-15, with a total area of  $8 \text{ cm}^2$ . The jet velocity and direction was defined at two of them and the other two was defined as solid walls. Thus, the area of the opening can remain at  $4 \text{ cm}^2$ , which is the actual area of the mouth opening (Gupta et al., 2009). Figure 6-15 shows the definition methods for different mouth coverings. The rule is that, if the angle was larger than  $45^\circ$ , the jet was defined at the upper or lower part of the mouth, while, if the angle was smaller than  $45^\circ$ , the jet was defined at the upper-front or lower-front part of the mouth. This simplification avoids the complicated geometries of the mouth coverings and makes the models easier to use for engineering application.

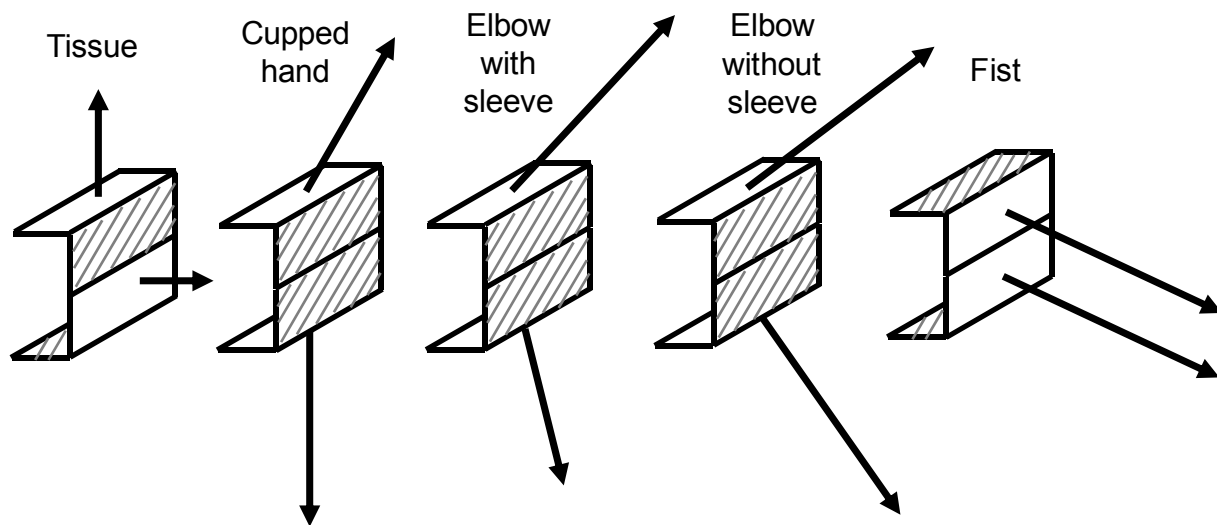


Figure 6-15 the definition methods for different mouth coverings in CFD simulations.

### 6.3 Model verification and case study

This investigation set up a case and applied the proposed simplified models to calculate the droplet concentration distribution versus time. The CFD simulation results were then qualitatively compared with the images of smoke flow obtained from the experiments to verify the models to some extent. Finally, this study explored the influence of mouth coverings on the dispersion of coughed droplets and the receptor's exposure. Note that the influence of mouth coverings on the transmission of coughed droplets consists of two parts. The first part is that the mouth coverings can reduce the exhaled air velocity and re-direct the exhaled airflow. The second part is that the mouth coverings can remove a portion of the coughed droplets. This section only discusses the first part, while the second part will be discussed in the next section.

### 6.3.1 Case setup

Figure 6-16 illustrates the configuration of the simulated room. The dimensions are 3.0 m in length, 3.0 m in width and 2.3 m in height. There are two persons sitting face to face with a distance of about 1.0 m between their noses. The person on the left is assumed to be the index person who coughed out with droplets, while the one on the right is the receptor. The room is ventilated with a mixing ventilation system with an air change rate of 6 ACH. The temperature of supplied air is 21 °C and the surface temperature of the persons is 32 °C. All the walls are assumed to be adiabatic. Eight cases were investigated, including droplets emission with zero momentum, covering a cough with a tissue, a cupped hand, a fist, an elbow with a sleeve, an elbow without a sleeve, uncovered cough with an average velocity and uncovered cough with a maximum velocity. The baseline of comparison is that the total droplet emission rates are exactly the same for all the cases. The exhaled velocity and direction depends on the mouth covering approach as shown in Figure 6-14. The duration of exhalation was assumed at 0.15 s based on the measurements by Gupta et al. (2009). The droplet size was assumed at 1.0  $\mu\text{m}$  to represent fine droplets.

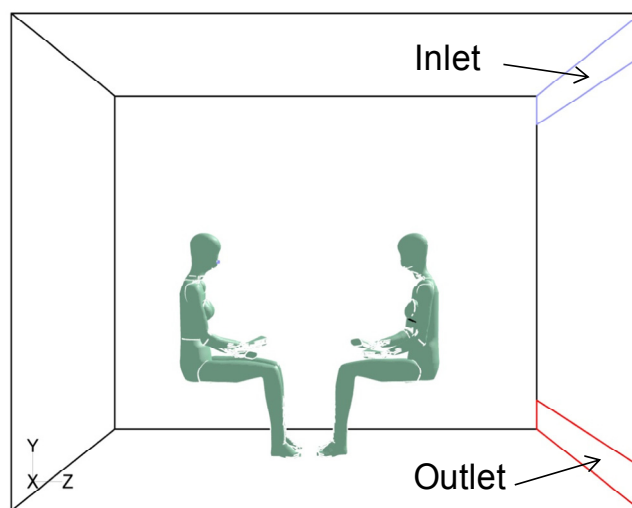


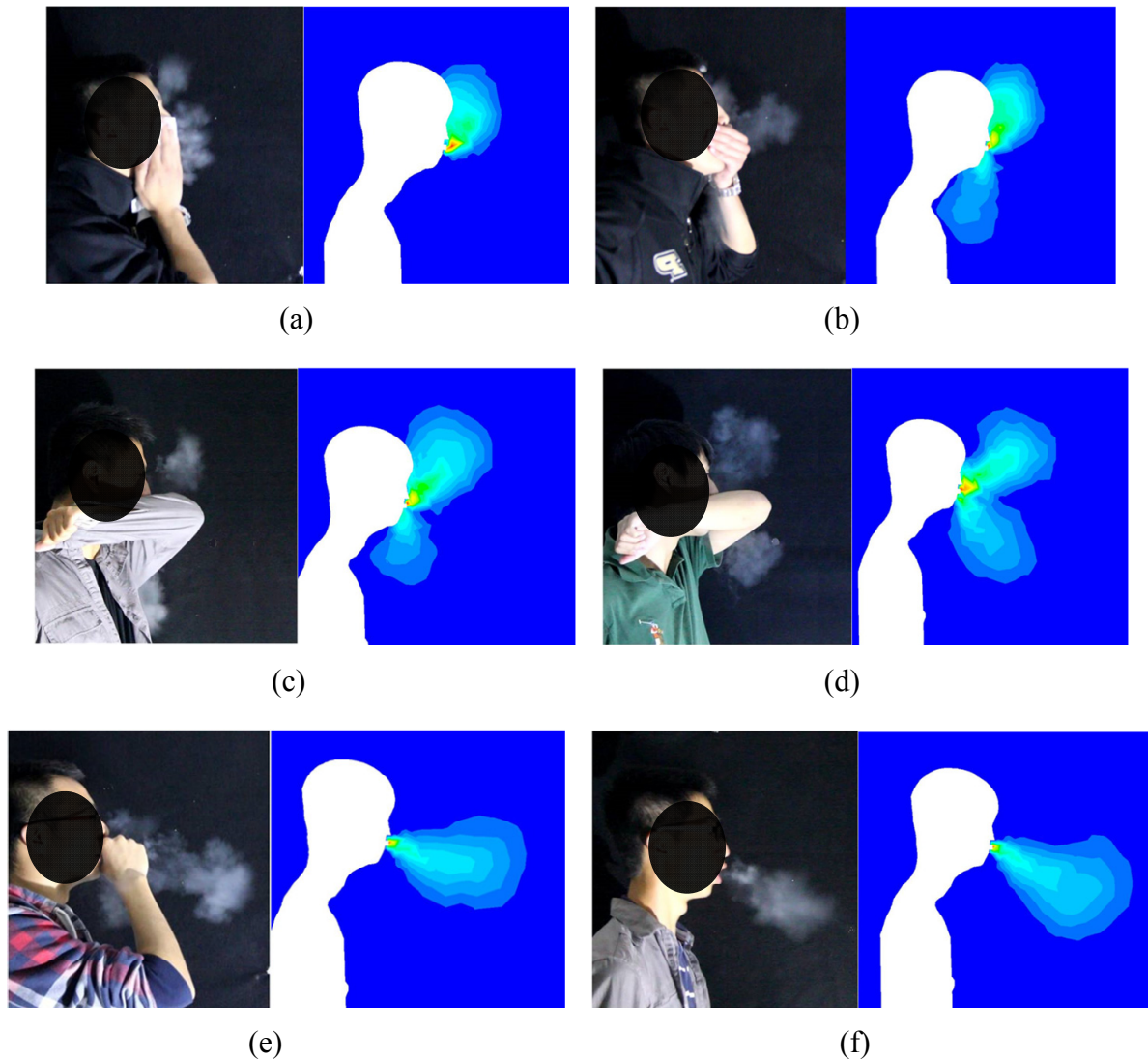
Figure 6-16 Configuration of the simulated room.

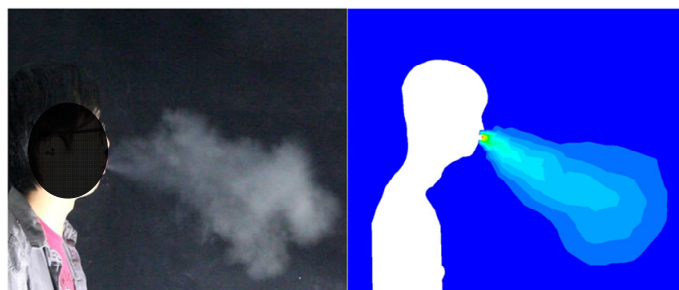
### 6.3.2 Simulation models

The renormalization group (RNG)  $k\text{-}\epsilon$  model (Choudhury 1993) is applied to calculate the airflow and turbulence, which was recommended by Wang and Chen (2009). Standard logarithmic law wall functions (Launder and Spalding, 1974) are adopted to show the connection of the solution variables at the near-wall cells and the corresponding quantities on the wall. Boussinesq assumption is used in the momentum equations to account for the effect of thermal plume. The Eulerian drift-flux model is used to calculate the dispersion of exhaled droplet. The effect of droplet deposition onto the walls was negligible at a droplet size of 1.0  $\mu\text{m}$  (Zhao et al., 2009). Three grid resolutions (669,109, 1,446,790 and 2,937,128) were tested for CFD grid independence. The 1,446,790 grid resolution was sufficiently fine to capture such a turbulent flow in the simulated room.

### 6.3.3 Verification of the simplified models

Figure 6-17 qualitatively compares the CFD simulation results (at 0.05 s) with the images of smoke flow obtained from the experiments to verify the models to some extent. As shown in the figure, the proposed simplified models can reasonably predict the general trend of airflow by a cough with a mouth covering. For instance, the simplified model can predict the relatively weak jet generated by a cough covered with a tissue. For covering a cough with a cupped hand and an elbow, the model correctly predicted an upward and a downward jet. Furthermore, the model can reflect the fact that covering a cough with an elbow with a sleeve can re-direct the airflow more significantly than that without a sleeve. In addition, the predicted horizontal jet generated by a cough with covering a fist was the strongest among the mouth covering approaches, which agrees with the experiments. Thus, these simplified models can be used to predict the airflow by a cough with a mouth covering.



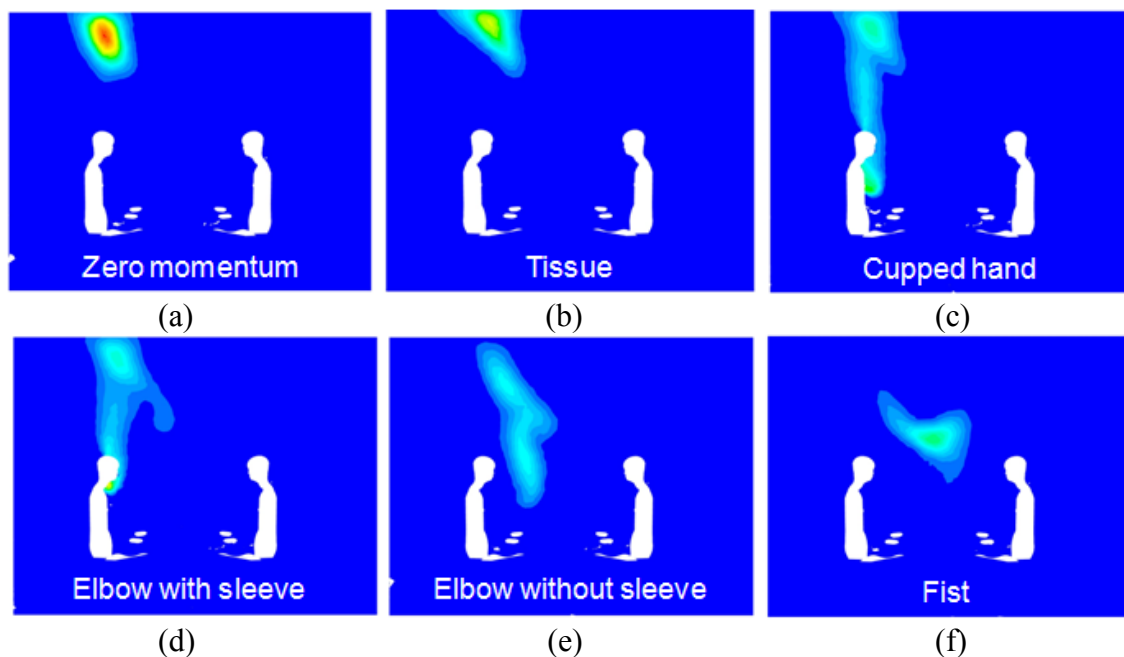


(g)

Figure 6-17 Qualitative comparison of the airflow by a cough with a mouth covering by the simplified models in CFD simulations and images from the experiments: (a) tissue, (b) cupped hand, (c) elbow with a sleeve, (d) elbow without a sleeve, (e) fist, (f) uncovered cough with an average velocity, (g) uncovered cough with a maximum velocity.

#### 6.3.4 Influence of mouth coverings on droplet dispersion and receptor's exposure

Figure 6-18 compares the droplet concentration distribution at 5.0 s for the eight cases. For droplet emission with zero momentum, covering a cough with a tissue, a cupped hand and an elbow, the exhaled droplets moved upward with the human thermal plume. For covering a cough with a fist and uncovered cough with an average velocity, the droplets penetrated the human thermal plume and moved forward to some extent. For uncovered cough with a maximum velocity, the droplets directly entered the breathing zone of receptor through the strong cough jet. The results indicates that the mouth coverings except for a fist can significantly reduce the horizontal exhaled air velocity and make the droplets move upward with the human thermal plume. Furthermore, when the horizontal exhaled air velocity is high enough, or the person-to-person distance is small enough, the droplets can directly enter the breathing zone of receptor and result in serious exposure.



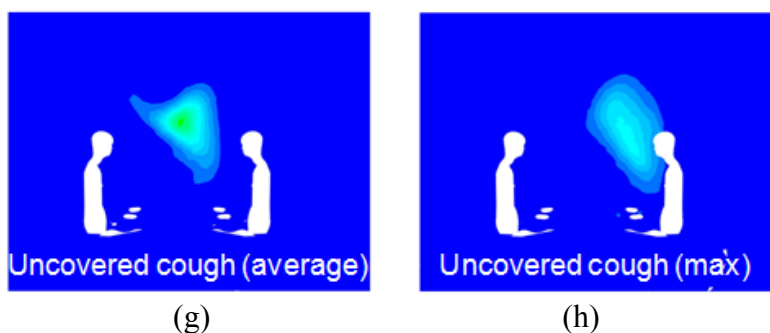


Figure 6-18 Comparison of droplet concentration field at 5.0 s for (a) zero momentum, (b) tissue, (c) cupped hand, (d) elbow with a sleeve, (e) elbow without a sleeve, (f) fist, (g) uncovered cough with an average velocity and (h) uncovered cough with a maximum velocity.

Figure 6-19 compares the normalized droplet concentration versus time in the breathing zone of receptor for the eight cases. The reference concentration is the highest concentration observed in the breathing zone of receptor among all the cases. It can be seen that there were two stages of exposure for uncovered cough cases. The first stage was that the exhaled droplets directly entered the breathing zone of receptor. The second stage is that the droplets dispersed in the room and then reached to the receptor again. However, for covering a cough with a mouth covering cases, there were only the exposures at the second stage. This reflects the fact that the mouth coverings can significantly reduce the horizontal exhaled air velocity and then avoid the exposure at the first stage.

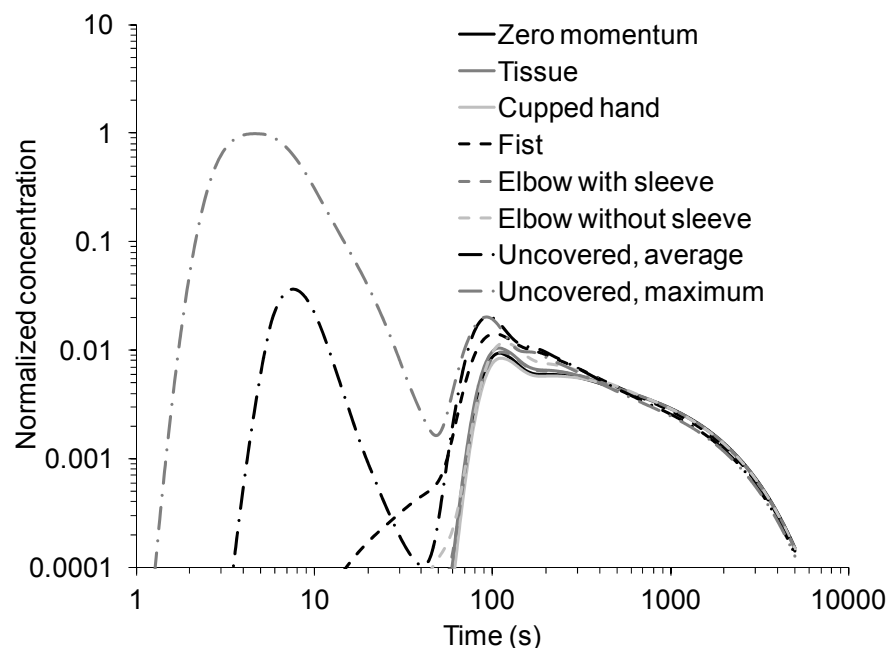


Figure 6-19 Comparison of droplet concentration versus time in the breathing zone of receptor for the eight cases.

In addition to the droplet concentration versus time, the total exposure of receptor may be more important in term of estimating the risk of infection. This study used an index called inhaled dose to represent the total exposure which has been recommended by Li et al. (2012). The inhaled dose, ID, was calculated by

$$ID = \frac{\int_{t=0}^{t'} C(t)dt \cdot q}{\dot{S} \cdot t_{cough}} \quad (6.3)$$

where  $C(t)$  is the droplet concentration in the breathing zone of receptor,  $t$  is the time,  $q$  is the breathing flow rate which is equal to  $0.00014 \text{ m}^3/\text{s}$  (Huang 1977),  $\dot{S}$  is the droplet emission rate and  $t_{cough}$  is the duration of exhalation. The inhaled dose was further separated into two parts. The first part is the exposure from 0 to 50 s, while the second part is the exposure from 50 to 5000 s. The results show that, for uncovered cough with a maximum velocity, the exposure at the first stage was 44.7% of the total exposure. For the other cases, the exposure at the first stage was all below 5% of the total exposure. Furthermore, the exposures at the second stage for all the cases were similar. That is to say covering a cough with a mouth covering can reduce about 45% of total exposure compared with uncovered cough with a maximum velocity for this case.

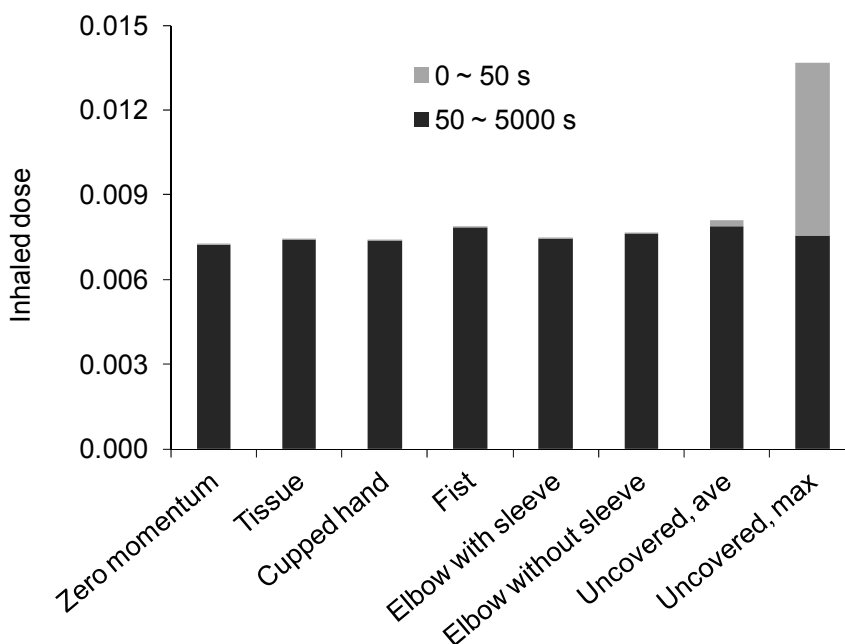


Figure 6-20 Comparison of the inhaled dose for the eight cases.

### 6.3.5 Influence of turning head on receptor's exposure

The results above indicate that the benefit of using a mouth covering is that it can avoid the direct exposure at the first stage. Thus, it is possible that turning head when coughing can also reduce the exposure at the first stage. This sub-section tests this hypothesis using numerical simulations. This study assumed the person on the left turned her head for  $90^\circ$  when coughed.

Three turning head cases were calculated, including uncovered coughed with an average velocity and a maximum velocity and covered a cough with an elbow with a sleeve. Figure 6-21 compares the normalized droplet concentration versus time in the breathing zone of receptor for the turning head cases with the cases of droplet emission with zero momentum and face-to-face uncovered cough. It can be found that there were only the exposures at the second stage for the turning head cases. That is understandable because the cough air jet was re-directed and the direct exposure could be avoided. Figure 6-22 is analogous to Figure 6-20, which shows that the exposures at the second stage for all the cases were similar. Moreover, the total exposures for the turning head cases were similar to that of droplet emission with zero momentum. Note that although turning head without a mouth covering can also avoid the exposure at the first stage, it cannot remove a portion of coughed droplets as using a mouth covering can do. Therefore, using a mouth covering is still the better choice than turning head without a mouth covering. Possibly, turning head with a mouth covering may be the best way to reduce the risk of infection.

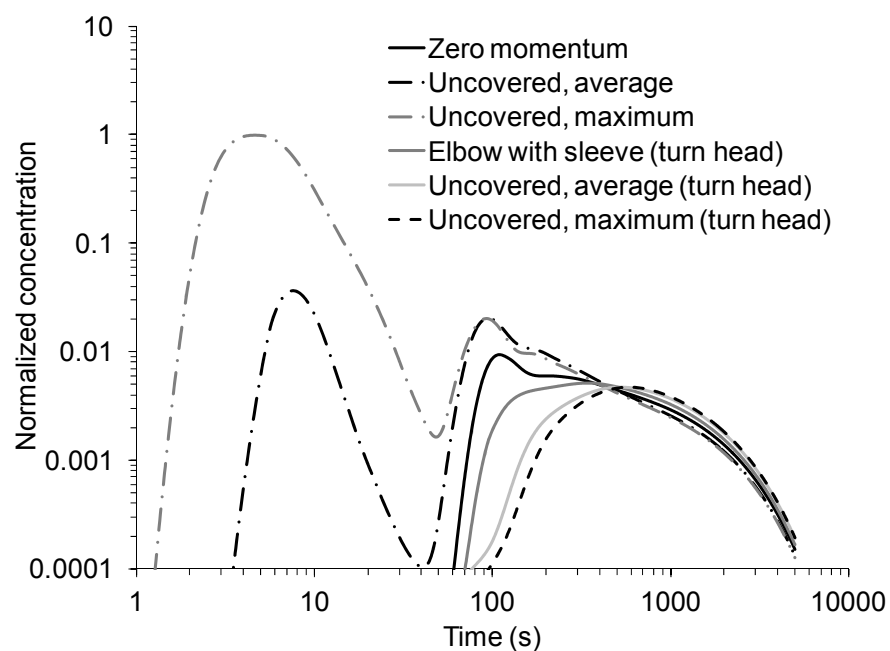


Figure 6-21 Comparison of droplet concentration versus time in the breathing zone of receptor for the turning head cases with zero momentum and face-to-face uncovered cough cases.

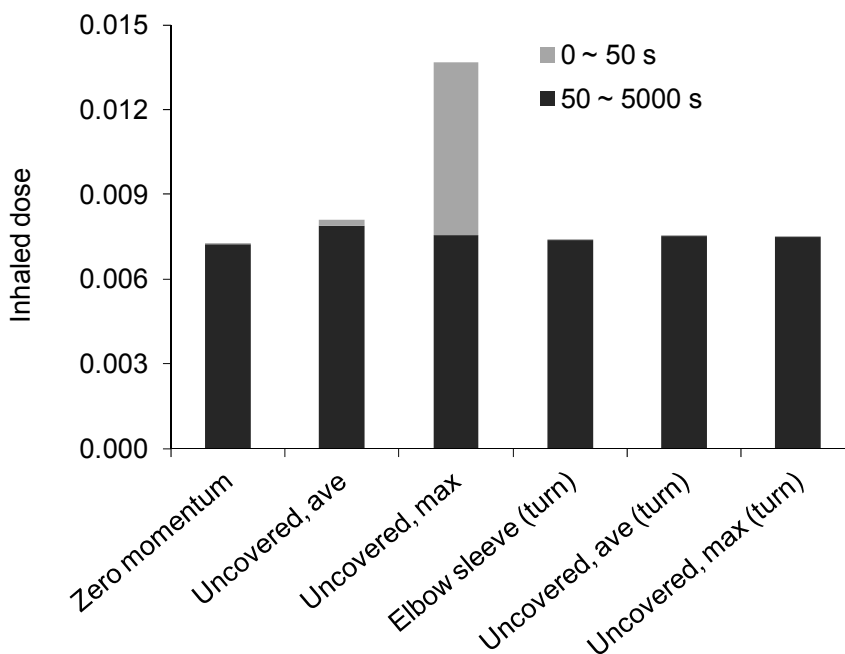


Figure 6-22 Comparison of the inhaled dose for the turning head cases with zero momentum and face-to-face uncovered cough cases.

### 6.3.6 Possibility in further simplifying the model

The above results show that the total exposures of the mouth covering cases were close to that of the zero momentum case. Thus, it is possible to use the zero momentum assumption for these cases to calculate reasonable results of the total exposure of receptor. Table 6-1 shows the relative errors of using the zero momentum assumption for the mouth covering cases. The relative error was defined by

$$\varepsilon = \frac{|ID_{\text{zero}} - ID_{\text{covering}}|}{ID_{\text{covering}}} \times 100\% \quad (6.4)$$

where  $ID_{\text{zero}}$  is the inhaled dose of the zero momentum case and  $ID_{\text{covering}}$  is the inhaled dose of the mouth covering cases. It was found that the relative errors of using the zero momentum assumption were all below 3% for covering a cough with a tissue, a cupped hand and an elbow with a sleeve. Using the zero momentum assumption for covering a cough with a fist resulted in the largest relative error of 7.9%. It was because the exhaled droplets by a cough with covering a fist penetrated the human thermal plume while the droplets moved upward with the human thermal plume if assuming emission with zero momentum. It should be noticed that the relative errors shown in the table were obtained based on this particular case. Other settings may result in either higher or lower relative errors. In principle, as long as the mouth coverings can make the exhaled droplets move with the human thermal plume, the relative error of using the zero momentum assumption can be minimized.

Table 6-1 Relative errors of using the zero momentum assumption for the mouth covering cases.

Mouth covering approach	Relative error
Tissue	2.4%
Cupped hand	2.1%
Fist	7.9%
Elbow with a sleeve	2.8%
Elbow without a sleeve	5.3%

## 6.4 Estimation of droplet removal by mouth coverings

As discussed in the section above, covering a cough can re-direct the exhaled air jet and avoid the exposure at the first stage. In addition, the mouth coverings may remove a portion of coughed droplets. Thus, this chapter further estimates the droplet removal by the mouth coverings using theoretical analyses. The exhaled droplets can deposit onto the surface of a mouth covering by several mechanisms, such as Brownian and turbulent diffusion, gravitational settling, inertial impaction etc. Since inertial impaction is quite different from other mechanisms, this study investigated them separately.

### 6.4.1 Droplet removal due to diffusion and gravitational settling

Lai (2002) reviewed and collected the particle deposition velocity associated with Brownian and turbulent diffusion, gravitational settling and other mechanisms such as thermophoresis measured in indoor environments. The deposition velocity,  $V_d$ , has a magnitude of  $10^{-6}$  to  $10^{-3}$  m/s (Lai, 2002). The deposition area i.e. the surface area of mouth covering,  $A_d$ , has a magnitude of  $10^{-2}$  m<sup>2</sup>. Thus, the droplet deposition “flow rate”,  $V_d A_d$ , has a magnitude of  $10^{-8}$  to  $10^{-5}$  m<sup>3</sup>/s. However, the cough airflow rate has a magnitude of  $10^{-3}$  m<sup>3</sup>/s, which is much larger than the deposition “flow rate”. Thus, the droplet deposition onto the surface of mouth covering is negligible. Li et al. (2012) also found that the droplet removal by a mouth covering due to diffusion and gravitational settling was negligible.

### 6.4.2 Droplet removal due to inertial impaction

For droplet deposition due to inertial impaction, this study referred to the impactor theory (Hinds, 1999). The particle removal efficiency is a function of the square root of Stokes number as shown in Figure 6-23 (Marple and Liu, 1974). The Stokes number is expressed as (Hinds, 1999)

$$Stk = \frac{\rho_p d_p^2 U C_c}{9 \mu h} \quad (6.5)$$

where  $\rho_p$  is the particle density,  $d_p$  is the particle diameter,  $U$  is the cough air velocity,  $C_c$  is the Cunningham coefficient caused by slippage which can be calculated by Eq. (3.6),  $\mu$  is the dynamic viscosity of air and  $h$  is the height of mouth opening. Furthermore, the relationship between the particle removal efficiency and the square root of Stokes number depends on the

Reynolds number. Since the average cough air velocity is 11.8 m/s and the height of mouth opening is about 0.02 m (Gupta et al. 2009), the Reynolds number is equal to 15,051. Thus, the curve for the Reynolds number of 25,000 in the Figure 6-23 should be used.

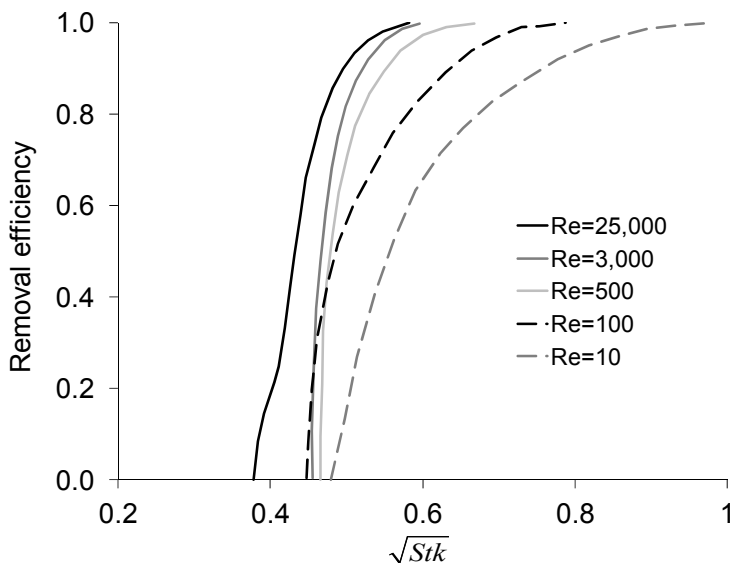


Figure 6-23 Relationship between particle removal efficiency and the square root of Stokes number (Marple and Liu, 1974).

As reviewed in Chapter 2, the original size distribution and concentration of sub-micrometer coughed droplets is available (Morawska et al., 2009). For super-micrometer droplets, Chao et al. (2009) measured the size distribution and estimated the concentration using four different methods based on some unverified assumptions. This study combined their results to obtain the size distribution of coughed droplets for the entire size range as shown in Figure 2-7. The estimated concentrations for super-micrometer droplets by the first method in Chao et al. (2009) were used. Figure 6-24 shows the size distribution of the coughed droplets at the original site, after removed by the mouth covering and after evaporation. The droplet nuclei size was calculated by Eq. (2.1) which was proposed by Nicas et al. (2005). It was found that the droplets with a diameter larger than 10  $\mu\text{m}$  could be removed by the mouth covering. However, fine droplets could move with the airflow and escape from the leakages between the face and the mouth covering. After removed by the mouth covering, the representative diameter reduces from 13.5 to 5.4  $\mu\text{m}$ . When the remaining droplets were completely evaporated, the representative diameter further reduces to 2.4  $\mu\text{m}$ . Previous studies indicated that particles with a diameter smaller than 3  $\mu\text{m}$  can follow the airflow very well (Yin et al., 2011). Regarding the total removal efficiency, the mouth covering can remove 64.8% of the total number of coughed droplets. Assuming the droplets are spherical and share the same density, the mouth covering can remove 99.99% of the total mass of coughed droplets. It should be noticed that the uncertainty in the concentrations of super-micrometer droplets may lead to a certain error in the total removal efficiency. For instance, if the estimated concentrations for super-micrometer droplets by the four different methods in Chao et al. (2009) were used, respectively, the removal efficiency of

total number of coughed droplets would vary from 58.6% to 64.8%. Thus, the size distribution and concentration for super-micrometer coughed droplets deserves further detailed study.

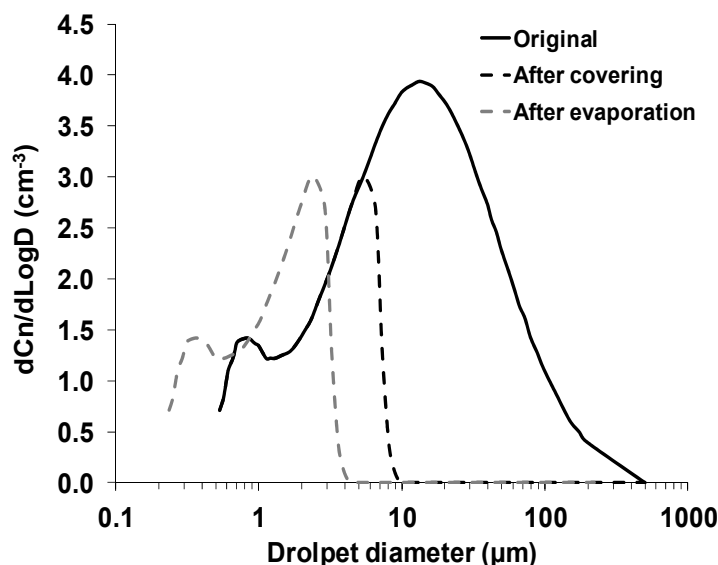


Figure 6-24 Size distribution of the coughed droplets at the original site, after removed by the mouth covering and after evaporation.

## 6.5 Conclusions

This chapter firstly conducted smoke tests to visualize exhaled airflow by a cough with a mouth covering by 16 human subjects. Based on the experimental data, this study developed simplified models for predicting the airflow by a cough with a mouth covering. Finally, the influence of mouth coverings on the dispersion of coughed droplets and receptor's exposure was discussed. The following conclusions can be drawn:

- (1). The proposed simplified models can be used to predict the airflow by a cough with a mouth covering.
- (2). Covering a cough with a tissue, a cupped hand and an elbow can significantly reduce the horizontal velocity and make the droplets move upward with the human thermal plume.
- (3). Covering a cough or turning head can avoid the receptor's direct exposure at the first stage.
- (4). In term of inhaled dose, it is reasonable to use the zero momentum assumption for covering a cough with a mouth covering.
- (5). Based on the available emission data in the literature and theoretical analysis, the mouth coverings can remove about 60% of total number of coughed droplets.

## 7. CONCLUSIONS AND FUTURE DIRECTION

### 7.1 Conclusions

Firstly, this study developed a hybrid DES-Lagrangian and RANS-Eulerian model for investigating transient particle transport in enclosed environments. The estimation methods of how to estimate the two key time constants for the model,  $t_1$  and  $t_2$ , were proposed. The estimated  $t_1$  and  $t_2$  were verified by an office and an aircraft cabin case. Furthermore, this investigation conducted experimental measurements of transient particle distributions in the first-class cabin of an MD-82 aircraft cabin to validate the hybrid model. The results show that the model can predict the trend of the transient particle concentration distribution when compared with the experimental data. The proposed hybrid DES-Lagrangian and RANS-Eulerian model can be used for investigating transient particle transport in enclosed environments with relatively high accuracy, while the computing time can be reduced by 80%.

Furthermore, this study developed a combined CFD and Markov chain method for predicting transient particle transport in enclosed environments. The validation results show that the proposed combined CFD and Markov chain method can predict the general trends of the particle concentrations versus time in enclosed environments. Moreover, the Markov chain method can provide faster-than-real-time information about particle transport in enclosed environments. In addition, for a fixed airflow field, when the source location is changed, the Markov chain method can be used to avoid recalculation of the particle transport equation and thus reduce computing costs.

This study further systematically investigated several influencing factors on person-to-person contaminant transport in enclosed environments. This investigation firstly collected a large quantity of data from the literature and used a validated CFD model to generate additional data in order to establish a database. This study then investigated the influence of ventilation mode, ventilation rate and person-to-person distance. The results show that the overall performances of displacement ventilation and a UFAD system were similar in terms of reducing exposure to person-to-person contaminant transport, and the two systems were about 20% better than mixing ventilation. The person-to-person contaminant exposure tended to be reduced with an increase in ventilation rate. When the person-to-person distance was less than 1.1 m, person-to-person contaminant exposure increased rapidly with distance. At a distance larger than 1.1 m, the effect of distance was insignificant. Generally speaking, person-to-person distance is more important than ventilation mode and ventilation rate in controlling person-to-person contaminant transport.

Finally, this study developed simplified models for predicting the airflow by a cough with a mouth covering. This investigation firstly conducted smoke tests to visualize the exhaled airflow by a cough with a mouth covering by 16 human subjects. Then the simplified models were proposed and verified by the images obtained from the experiments. It was found that covering a cough with a tissue, a cupped hand and an elbow can significantly reduce the horizontal velocity and make the droplets move upward with the human thermal plume. Furthermore, covering a cough or turning head can avoid the receptor's direct exposure at the first stage. In term of inhaled dose, it is reasonable to use the zero momentum assumption for covering a cough with a

mouth covering. In addition, based on the available emission data in the literature and theoretical analysis, the mouth coverings can remove about 60% of total number of coughed droplets.

## **7.2 Future direction**

The models developed in this study calculate the steady-state or transient exhaled contaminant concentration at the receptor's breathing zone. The next step should be assessing the risk of acquiring infection based on the information of concentration. Currently, either deterministic or probabilistic approaches can be used for risk assessment of airborne infectious disease transmission. In the deterministic approaches, the risk or probability of infection cannot be quantified. In the probabilistic approaches, because the quantities exhaled cannot be directly determined, their accuracy has been debated. Thus, it is essential to develop a method accounting for both deterministic and probabilistic information for reasonably predicting the risk of infection.

The Markov chain method introduced in this study predicts the probability of a particle's appearing in a zone at a certain point in time. Because the movements of indoor particles tend to be independent, the calculated probabilities should be independent probabilities. Through simple calculations of the joint probability and the probability of either events occurring, we can calculate the probability of a certain number of particles appearing in the breathing zone of the receptor. For instance, if the index patient exhales 100 particles, we can calculate the probability that 10 of these 100 particles appear in the breathing zone. Thus, the Markov chain with probability calculations has the potential to account for both deterministic and probabilistic information for risk assessment. This is a future direction for person-to-person infectious disease transmission in ventilated spaces.

## REFERENCES

- ANSYS, 2010. *Fluent 12.1 Documentation*. Fluent Inc., Lebanon, NH.
- ASHRAE/ASHE Standard, 170-2008. 2008. *Ventilation of Health Care Facilities*. Atlanta: American Society of Heating, Refrigerating, and Air-conditioning Engineers.
- Balazy, A., Toivola, M., Adhikari, A., Sivasubramani, S.K., Reponen, T. and Grinshpun, S.A., 2006. Do N95 respirators provide 95% protection level against airborne viruses, and how adequate are surgical masks? *American Journal of Infection Control* 34, 51-7.
- Bloch, A.B., Orenstein, W.A., Ewing, W.M., Spain, W.H., Mallison, G.F., Herrmann, K.L. and Hinman, A.R., 1985. Measles outbreak in a pediatric practice: airborne transmission in an office setting. *Pediatrics* 75, 676-683.
- CDC. 2005. Guidelines for preventing the transmission of mycobacterium tuberculosis in health-care settings, 2005. *Morbidity and Mortality Weekly Report (MMWR)* 54 (17): 1-141.
- Chao, C.Y.H., and Wan, M.P., 2006. A study of the dispersion of expiratory aerosols in unidirectional downward and ceiling-return type airflows using multiphase approach. *Indoor Air* 16, 296-312.
- Chao, C.Y.H., Wan, M.P., Morawska, L., Johnson, G.R., Ristovski, Z.D., Hargreaves, M., Mengersen, K., Corbett, S., Li, Y., Xie, X. and Katoshevski, D., 2009. Characterization of expiration air jets and droplet size distributions immediately at the mouth opening. *Journal of Aerosol Science* 40, 122-133.
- Chen, C., Zhao, B., 2010. Some questions on dispersion of human exhaled droplets in ventilation room: Answers from numerical investigation. *Indoor Air* 20, 95-111.
- Chen, C., Zhao, B., Cui, W., Dong, L., An, N., Ouyang, X., 2010. The effectiveness of an air cleaner in controlling droplet/aerosol particle dispersion emitted from a patient's mouth in the indoor environment of dental clinics. *Journal of the Royal Society Interface* 7, 1105-1118.
- Chen, C., Zhao, B., Yang, X. and Li, Y., 2011. Role of two-way airflow owing to temperature difference in severe acute respiratory syndrome transmission: revisiting the largest nosocomial severe acute respiratory syndrome outbreak in Hong Kong. *Journal of the Royal Society Interface* 8, 699-710.
- Chen, C., Liu, W., Li, F., Lin, C.-H., Liu, J., Pei, J. and Chen, Q., 2013. A hybrid model for investigating transient particle transport in enclosed environments. *Building and Environment* 62, 45-54.
- Chen, Q. and Glicksman, L., 2003. *System Performance Evaluation and Design Guidelines for Displacement Ventilation*. Atlanta: ASHRAE.

- Chen, Q. 2009. Ventilation performance prediction for buildings: A method overview and recent applications. *Building and Environment* 44, 848-858.
- Chen, F., Yu, S. C. M., and Lai, A. C. K., 2006. Modeling particle distribution and deposition in indoor environments with a new drift-flux model. *Atmospheric Environment* 40, 357–367.
- Choudhury, D., 1993. *Introduction to the Renormalization Group Method and Turbulence Modeling*, Canonsburg, Fluent Inc. Technical Memorandum TM-107.
- Ching, W. H., Leung, M. K. H., Leung, D. Y. C., Li, Y. and Yuen, P. L., 2008. Reducing risk of airborne transmitted infection in hospitals by use of hospital curtains. *Indoor and Built Environment* 17, 252–259.
- Coffey, C.C., Campbell, D.L. and Zhuang Z., 1999. Simulated workplace performance of N95 respirators. *American Industrial Hygiene Association Journal* 60, 613–24.
- Cole, E.C. and Cook, C.E., 1998. Characterization of infectious aerosols in health care facilities: An aid to effective engineering controls and preventive strategies. *American Journal of Infection Control* 26, 453–464.
- Duguid, J.F. 1945. The numbers and the sites of origin of the droplets expelled during expiratory activities. *Edinburgh Medicine Journal* 52, 335–340.
- Dye, C., Scheele, S., Dolin, P., Pathania, V. and Raviglione, MC., 1999. Global burden of tuberculosis: estimated incidence, prevalence, and mortality by country. *Journal of American Medicine Association* 282, 677-68.
- Edwards, D.A., Man, J.C. et al. 2004. Inhaling to mitigate exhaled bioaerosols. *Proceedings of the National Academy of Sciences USA* 101, 17383–17388.
- Fabian, P., McDevitt, J.J., DeHaan, W.H., Fung, R.O.P., Cowling, B.J., Chan, K.H., Leung, G.M. and Milton, D.K., 2008. Influenza virus in human exhaled breath: an observational study. *PLoS ONE* 3, e2691.
- Fabian, P.M., McDevitt, J.J. and Milton, D.K., 2009. Influenza virus in fine particles exhaled during tidal breathing and coughing. In: *Proceedings of the American Thoracic Society Conference*, San Diego.
- Fairchild, C.I., and Stamper, J.F., 1987. Particle concentration in exhaled breath. *American Industrial Hygiene Association Journal* 48, 948.
- FLUENT, 2005. *FLUENT 6.3 Documentation*, Fluent Inc., Lebanon, NH.

Gao, N., He, Q. and Niu, J., 2012a. Numerical study of the lock-up phenomenon of human exhaled droplets under a displacement ventilated room. *Building Simulation* 5, 51–60.

Gao, X., Li, Y., Xu, P. and Cowling, B.J., 2012b. Evaluation of intervention strategies in schools including ventilation for influenza transmission control. *Building Simulation* 5, 29–37.

Grinsphun, S.A., Haruta, H., Eninger, R.M., Reponen, T., McKay R.T. And Lee S., 2009. Performance of an N95 Filtering Facepiece Particulate Respirator and a Surgical Mask During Human Breathing: Two Pathways for Particle Penetration. *Journal of Occupational and Environmental Hygiene* 6, 593-603.

Gupta, J.K., Lin, C.-H., Chen, Q., 2009. Flow dynamics and characterization of a cough. *Indoor Air* 19, 517-525.

Gupta, J.K., Lin, C.-H. and Chen, Q., 2010. Characterizing exhaled airflow from breathing and talking. *Indoor Air* 20, 31-39.

Gupta, J.K., Lin, C.-H., Chen, Q., 2011a. Transport of expiratory droplets in an aircraft cabin. *Indoor Air* 21, 3-11.

Gupta, J.K., Lin, C.-H. and Chen, Q., 2011b. Inhalation of expiratory droplets in aircraft cabin, *Indoor Air* 21, 341–350.

Gupta, J.K., Lin, C.H. and Chen, Q., 2012. Risk assessment of airborne infectious diseases in aircraft cabins. *Indoor Air* 22, 388–395.

He, Q., Niu, J., Gao, N., Zhu, T. and Wu, J. 2011., CFD study of exhaled droplet transmission between occupants under different ventilation strategies in a typical office room. *Building and Environment* 46, 397-408.

Hinds, W.C. 1999. *Aerosol Technology: Properties, Behavior, and Measurement of Airborne Particles*, 2nd edition. New York: Wiley.

Huang, D.Y., 1977. Physical diagnostics. China Commerce Publishing Co.

ISO,-7730. 2005. *Ergonomics of the thermal environment — Analytical determination and interpretation of thermal comfort using calculation of the PMV and PPD indices and local thermal comfort criteria*. Switzerland.

Jones, R.M., Masago, Y., Bartrand, T., Nicas, M. and Rose J.B., 2009. Characterizing the risk of infection from mycobacterium tuberculosis in commercial passenger aircraft using quantitative microbial risk assessment. *Risk Analysis* 29, 355 – 365.

Kenyon, T.A., Valway, S.E., Ihle, W.W., Onorato, I.M., and Castro, K.G., 1996. Transmission of multidrug resistant mycobacterium tuberculosis during a long airplane flight. *New England Journal of Medicine* 334, 933-938.

Kirking, H.L., Cortes, J., Sherry, B., Hall, A.J., Cohen, N.J., Lipman, H., Kim, C., Daly, E.R., and Fishbein, D.B., 2010. Likely Transmission of Norovirus on an Airplane, October 2008. *Clinical Infectious Diseases* 50, 1216-1221.

Klepeis, N.E., Nelson, W.C., Ott, W.R., et al., 2001. The National Human Activity Pattern Survey (NHAPS): a resource for assessing exposure to environmental pollutants. *Journal of Exposure Analysis and Environmental Epidemiology* 11, 231–252.

Ko, G., Thompson, K.M. and Nardell, E.A., 2004. Estimation of tuberculosis risk on a commercial airliner. *Risk Analysis* 24, 379–88.

Lai, A.C.K., 2002. Particle deposition indoors: a review. *Indoor Air* 12, 211-214.

Lai, A.C.K. and Wong, S.L., 2010. Experimental investigation of exhaled aerosol transport under two ventilation systems. *Aerosol Science and Technology* 44, 444–452.

Lai, A.C.K. and Wong, S.L., 2011. Expiratory aerosol transport in a scaled chamber under a variety of emission characteristics: an experimental study. *Aerosol Science Technology* 45, 899–907.

Lai, A.C.K., Poon, C.K.M. and Cheung, A.C.T., 2012. Effectiveness of facemasks to reduce exposure hazards for airborne infections among general populations. *Journal of the Royal Society Interface* 9, 938-948.

Lau, J. and Chen, Q., 2007. Floor-supply displacement ventilation for workshops. *Building and Environment* 42, 1718-1730.

Launder, B.E. and Spalding, D.B. (1974). The numerical computation of turbulent flows. *Computer Methods in Applied Mechanics and Engineering* 3, 269-289.

Li, X., Niu, J. and Gao, N., 2011. Spatial distribution of human respiratory droplet residuals and exposure risk for the co-occupant under different ventilation methods. *HVAC&R Research* 17, 432–445.

Li, X., Niu, J. and Gao, N., 2012. Co-occupant's exposure of expiratory droplets—Effects of mouth coverings. *HVAC&R Research* 18, 575–587.

Li, Y., Huang, X., Yu, I.T., Wong, T.W. and Qian, H., 2005. Role of air distribution in SARS transmission during the largest nosocomial outbreak in Hong Kong. *Indoor Air* 15, 83–95.

- Li, Y., Leung, G.M., Tang, J.W., Yang, X., Chao, C., Lin, J.H., Lu, J.W., Nielsen, P.V., Niu, J.L., Qian, H., Sleigh, A.C., Su, H.J., Sundell, J., Wong, T.W., Yuen, P.L., 2007. Role of ventilation in airborne transmission of infectious agents in the built environment – a multidisciplinary systematic review. *Indoor Air* 17, 2–18.
- Liu, W., Wen, J., Chao, J., Yin, W., Shen, C., Lai, D., Lin, C.-H., Liu, J., Sun, H., and Chen, Q., 2012. Accurate and high-resolution boundary conditions and flow fields in the first-class cabin of an MD-82 commercial airliner. *Atmospheric Environment* 56, 33-44.
- Liu, W., Wen, J., Lin, C.-H., Liu, J., Long, Z., and Chen, Q., 2013. Evaluation of various categories of turbulence models for predicting air distribution in an airliner cabin. *Building and Environment* 65, 118-131.
- Lee, S., Grinshpun, S. and Reponen T., 2008. Respiratory Performance Offered by N95 Respirators and Surgical Masks: Human Subject Evaluation with NaCl Aerosol Representing Bacterial and Viral Particle Size Range. *American Occupational Hygiene* 52, 177-85.
- Loudon, R.G. and Roberts, R.M., 1967. Relation between the airborne diameter of respiratory droplets and the diameter of the stains left after recovery. *Nature* 213, 95–96.
- Mahajan, R.P., Singh, P., Murty, G.E. and Aitkenhead, A.R., 1994. Relationship between expired lung volume, peak flow rate and peak velocity time during a cough manoeuvre. *British Journal of Anaesthesia*, 72, 298-301.
- Mangili, A., Gendreau, M.A., 2005. Transmission of infectious disease during commercial air travel. *Lancet* 365, 989-996.
- Marple, V.A. and Liu, B.Y.H., 1974. Characteristics of laminar jet impactors. *Environmental Science and Technology*, 8, 648-654.
- Mazumdar, S. and Chen, Q., 2009. A one-dimensional analytical model for airborne contaminant transport in airliner cabins. *Indoor Air* 19, 3-13.
- Memarzadeh, F. and Xu, W., 2012. Role of air changes per hour (ACH) in possible transmission of airborne infections. *Building Simulation* 5, 15–28.
- Menzies, D., Fanning, A., Yuan, L. and FitzGerald, J.M., 2000. Hospital ventilation and risk for tuberculous infection in Canadian health care workers. *Annals of Internal Medicine* 133, 779–789.
- Milton, D.K., Fabian, P.M., Angel, M., Perez, D.R. and McDevitt, J.J., 2010. Influenza virus aerosols in human exhaled breath: particle size, culturability, and effect of surgical masks. In: *Proceedings of the American Thoracic Society Conference*, New Orleans.

Morawska, L., 2006. Droplet fate in indoor environments, or can we prevent the spread of infection? *Indoor Air* 16, 335–347.

Morawska, L., Johnson, G.R., Ristovski, Z.D., Hargreaves, M., Mengersen, K., Corbett, S., Chao, C.Y.H., Li, Y., Katoshevski, D. 2009. Size distribution and sites of origin of droplets expelled from the human respiratory tract during expiratory activities. *Journal of Aerosol Science* 40, 256-269.

Moser, M.R., Bender, T.R., Margolis, H.S., Noble, G.R., Kendal, A.P., Ritter, D.G., 1979. An outbreak of influenza aboard a commercial airliner. *American Journal of Epidemiology* 110, 1-6.

Murakami, S., Kato, S., Nagano, S., and Tanaka, S., 1992. Diffusion characteristics of airborne particles with gravitational settling in a convection-dominant indoor flow field. *ASHRAE Transactions* 98, 82–97.

Nicas, M., 2000. Markov modeling of contaminant concentrations in indoor air. *American Industrial Hygiene Association Journal* 61, 484–491.

Nicas, M., Nazaroff, W.W., Hubbard, A., 2005. Toward understanding the risk of secondary airborne infection: Emission of respirable pathogens. *Journal of Occupational and Environmental Hygiene* 2, 143–154.

Nielsen, P.V., Li, Y., Buus, M. and Winther, F.V., 2010. Risk of cross-infection in a hospital ward with downward ventilation. *Building and Environment* 45, 2008–2014.

Oberg, T. and Brosseau, L.M., 2008. Surgical mask filter and fit performance. *American Journal of Infection Control* 36, 276-82.

Olmedo, I., Nielsen, P.V., Ruiz de Adana, M., Jensen, R.L. and Grzelecki, P., 2012. Distribution of exhaled contaminants and personal exposure in a room using three different air distribution strategies. *Indoor Air* 22, 64–76.

Olsen, S.J., Chang, H., Cheung, T.Y., Tang, A.F., Fisk, T.L., Ooi, S.P., Kuo, H., Jiang, D.D., Chen, K., Lando, J., Hsu, K., Chen, T., Dowell, S.F., 2003. Transmission of the severe acute respiratory syndrome on aircraft. *New England Journal of Medicine* 349, 2416-2422

Parianta D, Morawska L, Johnson GR, et al. 2011. Theoretical analysis of the motion and evaporation of exhaled respiratory droplets of mixed composition. *Journal of Aerosol Science* 42, 1–10.

Papineni R.S. and Rosenthal F.S., 1997. The size distribution of droplets in the exhaled breath of healthy human subjects. *Journal of Aerosol Medicine* 10, 105–116.

- Qian, H., Li, Y., Nielsen, P.V., Hyldgaard, C.E., Wong, T.W. and Chwang, A.T.Y., 2006. Dispersion of exhaled droplet nuclei in a two-bed hospital ward with three different ventilation systems. *Indoor Air* 16, 111 – 128.
- Qian Y., Willeke K., Grinshpun S.A., Donnelly J. and Coffey, C.C., 1998. Performance of N95 respirators: Filtration efficiency for airborne microbial and inert particles. *American Industrial Hygiene Association Journal* 59, 128–32.
- Ross, S.M., 1996. *Stochastic Processes*, 2nd Edn. John Wiley & Sons, Inc.
- Seepana, S. and Lai, A.C.K., 2012. Experimental and numerical investigation of interpersonal exposure of sneezing in full-scale chamber. *Aerosol Science and Technology* 46, 485–493.
- Shaman J, and Kohn M., 2009. Absolute humidity modulates influenza survival, transmission, and seasonality. *PNAS* 106, 3243-3248.
- Shur, M., Spalart, P. R., Strelets, M., Travin, A., 1999. *Detached-Eddy Simulation of an airfoil at high angle of attack*. In 4th Int. Symposium on Eng. Turb. Modeling and Experiments, Corsica, France.
- Sze To, G.N. and Chao, C.Y.H., 2010. Review and comparison between the Wells–Riley and dose-response approaches to risk assessment of infectious respiratory diseases. *Indoor Air* 20, 2–16.
- Tang, J.W.-T. and Settles, G.S., 2009. Coughing and Masks. *New England Journal of Medicine* 361, E62-E62.
- US DOT (United States Department of Transportation), 2011. *2010 Traffic Data for U.S Airlines and Foreign Airlines U.S. Flights: Total Passengers up from 2009, Still Below 2008*, Washington DC.
- Viboud, C., Boelle, PY. and Pakdaman K, et al., 2004. Influenza epidemics in the United States, France, and Australia, 1972–1997. *Emergence Infectious Diseases* 10, 32–39.
- Walkinshaw, D.S., 2010. Germs, flying and the truth. *ASHRAE Journal* 52, 70-73.
- Wan, M.P. and Chao, C.Y.H., 2007. Transport characteristics of expiratory droplets and droplet nuclei in indoor environments with different ventilation air flow patterns. *Journal Biomechanical Engineering Transaction ASME* 129, 341–353.
- Wang B., Zhang A., Sun J., Liu H., Hu J. and Xu L., 2005. Study of SARS transmission via liquid droplets in air. *Transactions of the ASME* 127, 32-38A.
- Wang, M., 2011. *Modeling airflow and contaminant transport in enclosed spaces with advanced models*. PhD Thesis. Purdue University.

- Wang, M., Chen, Q., 2009. Assessment of various turbulence models for transitional flows in enclosed environment. *HVAC&R Research* 15, 1099-1119.
- Wang, M., Lin, C.-H., Chen, Q., 2012. Advanced turbulence models for predicting particle transport in enclosed environment. *Building and Environment* 47, 40-49.
- Weber, T.P. and Stilianakis, N.L., 2008. Inactivation of influenza A viruses in the environment and modes of transmission: A critical review. *Journal of Infection* 57, 361-373.
- WHO, 2002. *Bulletin of the World Health Organization*; 80 (3): 261.
- Willeke, K. and Qian, Y., 1998. Tuberculosis control through respirator wear: performance of National Institute for Occupational Safety and Health regulated respirators. *American Journal of Infection Control* 26, 139-142.
- World Bank 2005. <http://web.worldbank.org/WBSITE/EXTERNAL/NEWS/0,,contentMDK:20715408~pagePK:64257043~piPK:437376~theSitePK:4607,00.html>
- Yang, S., Lee, G.W.M., Chen, C.M., Wu, C.C. and Yu, K.P., 2007. The size and concentration of droplets generated by coughing in human subjects. *Journal of Aerosol Medicine* 20, 484-494.
- Yang, Y., Chan, W.Y., Wu, C.L., Kong, R.Y.C. and Lai, A.C.K., 2012. Minimizing the exposure of airborne pathogens by upper-room ultraviolet germicidal irradiation: an experimental and numerical study. *Journal of the Royal Society Interface* 9, 3184-3195.
- Yin, Y., Gupta, J.K., Zhang, X., Liu, J. and Chen, Q., 2011. Distributions of respiratory contaminants from a patient with different postures and exhaling modes in a single-bed inpatient room. *Building and Environment* 46, 75-81.
- You, R. and Zhao, B., 2013. A simplified method for assessing particle deposition rate in aircraft cabins. *Atmospheric Environment* 67, 80-84.
- Xie, X., Li, Y., Chwang, A.T.Y., Ho, P.L. Seto, W.H., 2007. How far droplets can move in indoor environments – revisiting the Wells evaporation–falling curve. *Indoor Air* 17, 211-225.
- Zhang, L. and Li, Y., 2012. Dispersion of coughed droplets in a fully-occupied high-speed rail cabin. *Building and Environment* 47, 58-66.
- Zhang, Z., Chen, Q., 2006. Experimental measurements and numerical simulations of particle transport and distribution in ventilated rooms. *Atmospheric Environment* 40, 3396-3408.
- Zhang, Z. and Chen, Q., 2007. Comparison of the Eulerian and Lagrangian methods for predicting particle transport in enclosed spaces, *Atmospheric Environment* 41, 5236-5248.

- Zhang, Z., Zhai, Z.Q., Zhang, W., Chen, Q., 2007. Evaluation of various turbulence models in predicting airflow and turbulence in enclosed environments by CFD: part 2 - comparison with experimental data from literature. *HVAC&R Research* 13, 871-886.
- Zhang, Z., Chen, X., Mazumdar, S., Zhang, T., Chen, Q., 2009. Experimental and numerical investigation of airflow and contaminant transport in an airliner cabin mockup. *Building and Environment* 44, 85-94.
- Zhao, B., Zhang, Y., Li, X., Yang, X. and Huang, D., 2004. Comparison of indoor aerosol particle concentration and deposition in different ventilated rooms by numerical method. *Building and Environment* 39, 1-8.
- Zhao, B., Zhang, Z. and Li, X., 2005. Numerical study of the transport of droplets or particles generated by respiratory system indoors. *Building and Environment* 40, 1032–1039.
- Zhao, B., Chen, C., and Tan, Z., 2009a. Modeling of ultrafine particle dispersion in indoor environments with an improved drift flux model. *Journal of Aerosol Science* 40, 29–43.
- Zhao, B., Yang, C., Chen, C., Feng, C., Yang, X., Sun, L., Gong, W. and Yu, L., 2009b. How many airborne particles emitted from a nurse will reach the breathing zone/body surface of the patient in ISO class-5 single-bed hospital protective environments?-a numerical analysis. *Aerosol Science and Technology* 43, 990-1005.
- Zhu, S., Kato, S., and Yang, J.H., 2006. Study on transport characteristics of saliva droplets produced by coughing in a calm indoor environment. *Building and Environment* 41, 1691-1702.
- Zhu, Y., Zhao, B., Zhou, B. and Tan, Z., 2012. A particle resuspension model in ventilation ducts. *Aerosol Science and Technology* 46, 222-235.